8-2021

Investigations of elastin recoil on molecular and macroscopic levels.

Nour Mohammad Jamhawi
University of Louisville

INVESTIGATIONS OF ELASTIN RECOIL ON MOLECULAR AND
MACROSCOPIC LEVELS

By

Nour Mohammad Jamhawi

B.Sc., Jordan University of Science and Technology, 2004

M.Sc., Jordan University of Science and Technology, 2010

M.Sc., University of Louisville, 2018

A Dissertation

Submitted to the Faculty of the

College of Arts and Sciences of the University of Louisville

in Partial Fulfillment of the Requirements

for the Degree of

Doctor of Philosophy in Chemistry

Department of Chemistry

University of Louisville

Louisville, KY

August 2021

INVESTIGATIONS OF ELASTIN RECOIL ON MOLECULAR AND
MACROSCOPIC LEVELS

By

Nour Mohammad Jamhawi

B.Sc., Jordan University of Science and Technology, 2004

M.Sc., Jordan University of Science and Technology, 2010

M.Sc., University of Louisville, 2018

A Dissertation Approved on

April 30, 2021

By the following Dissertation Committee

_____

Dissertation Chair

Dr. Richard J. Wittebort

_____

Dr. Muriel C. Maurer

_____

Dr. Eugene G. Mueller

_____

Dr. Michael H. Nantz

_____

Dr. Donghan Lee

To my mother

My father, may his soul rest in peace

And my brothers

ABSTRACT

INVESTIGATIONS OF ELASTIN RECOIL ON MOLECULAR AND
MACROSCOPIC LEVELS

Nour Mohammad Jamhawi

April 30, 2021

Elastin is one of the most hydrophobic proteins, and it is extremely flexible when

hydrated. The driving force for recoil is the decrease in entropy of the protein and/or the

hydrating solvent. This dissertation is a study of both mechanisms. Following an

introduction (Chapter 1), Chapters 2 and 3 investigate the recoil mechanism on the

molecular level in the hydrating solvent and in the protein, respectively. Chapter 4

examines macroscopic properties of recoil by thermomechanics. Conclusions are discussed

in Chapter 5.

Using double quantum NMR, the deuterated water ordering at the elastin surface

was studied quantitatively as a function of stretch and in the presence of solutes known to

modulate the hydrophobic effect: polyethylene glycol (PEG), sulfate ion, a kosmotrope,

and perchlorate ion, a chaotrope. When the purified elastin is stretched, a nearly one order

of magnitude increase in the ordering of water is observed, and this is due to the increase

in water exposed to the hydrophobic surface. When PEG and sulfate ions are added to the

solvent, ordering of the water is significantly decreased due to a more compact protein with

reduced solvent exposed surface area. At concentrations below 0.3 mol/kg perchlorate ion,

only minor changes in the magnitude of the ordered water signal are observed because perchlorate interacts with peptide bonds and does not decrease exposed hydrophobic surface area.

Ordering of elastin was studied using static ^{13}C NMR to assess the amplitude of backbone motions in the mature elastic material. It was found that the residual shielding anisotropy is small, $1 - 3$ ppm and within the experimental resolution of this experiment, no stretch induced ordering was observed. Thus, cross-linked elastin is dynamically disordered much like soluble minielastins.

The thermomechanical experiments show that elastin is stiffer in the presence of PEG, sulfate and high perchlorate concentrations. These solutes do not interact with the protein and decrease the volume and the length of the fiber, confirming the increase in compaction. Also, they decrease the heat liberated, the change in entropy and the internal energy with stretch. Thus, the hydrophobic effect is the major player in elastin recoil.

TABLE OF CONTENTS

LIST OF TABLES

LIST OF FIGURES

CHAPTER 1 INTRODUCTION

1.1   Elastin

Elastin, an extracellular matrix protein, is crucial for elasticity in many vertebrate tissues including arteries, lungs, skin and elastic cartilage. It is a fibrous protein and, in terms of evolution, is a relatively new protein. It provides essential energy storage for the closed circulatory system found in all vertebrates.[1] Unlike rubbers, elastin requires a solvent to recoil. Dry elastin is an insoluble fragile polymer and gains elasticity only when swollen in water.

Tropoelastin is the natural soluble precursor of elastin. It was first isolated in 1969 from copper deficient porcine aorta.[2] It is 60 – 70 kDa in molecular weight and composed of alternating hydrophobic modules (25 – 40 amino acids) and smaller cross-linking modules.[3, 4] The hydrophobic modules are highly repetitive sequences rich in proline (P), alanine (A), valine (V), leucine (L), isoleucine (I) and glycine (G). Typical cross-linking domains have pairs of lysyl residues separated by two or three alanyl residues embedded within P- or A- rich regions.[4]

Elastogenesis is the formation of a mature elastic matrix. It is a complex process, and involves the coordination of intracellular transcription, translation and processing of tropoelastin precursor protein. Following synthesis, tropoelastin is secreted into the extracellular space for microfibrillar assembly.

In addition to other proteins, assembly requires a unique inverse phase transition known as coacervation. Finally, intra- and intermolecular cross-linking results from the action of lysyl oxidase to produce mature insoluble elastin matrix.[3] Lysyl oxidase converts ε-amino groups into aldehyde groups that combine with ε-amino groups to produce ultimately four lysyl side-chains in a pyridyl ring structure known as desmosine or isodesmosine.[5] This crosslinking process is random and results in an unordered network.[6]

1.1.1 Elastic Mechanisms of Elastin

The recoil force behind the elasticity of elastin is believed to be entropic.[7-10] Stretch decreases the entropy of the system and recoil is spontaneous to restore the lost entropy. Two main structure-function groups of models have been proposed to explain the recoil mechanism. [1, 3] But, the precise mechanism has not been elucidated.

Structure-based models are divided into two main groups. The first, introduced by Hoeve and Flory, describes elastin as a network of free, randomly moving chains with high entropy that is reduced by stretch.[9] The fibrillar model relies on the presence of β-turn repeat structures that are less disordered upon stretching.[4, 11] The latter model is widely accepted; however, direct experimental evidence of stable β-turn structures in natural elastin has not been reported.

Function-based models are also divided into two main groups. In "rubber-like" models, the entropy decreases upon stretch due to backbone ordering. This group of models describes elastin as either a network of random chains[9] or a protein with secondary structures; more specifically β-turns.[4, 11] In the second group, entropy decrease upon stretch is from polymer and solvent ordering. The first model of this group, the liquid drop model, was introduced in 1970 by Weis-Fogh and Anderson. In this model, tropoelastin molecules

are hydrophobic globular monomers cross-linked to form the aggregates of elastin. Stretch deforms the globules thereby increasing their surface area and decreasing solvent entropy due to the hydrophobic effect.[8] The oil coiled model is similar to the liquid drop model in regard to decreased entropy of the exposed solvent but considers tropoelastin fibrillar instead of gloubular.[12]

It is widely assumed that recoil in elastin is the same as in rubber, i.e., recoil is driven by an increase in polymer entropy. However, this assumption does not account for two important features of elastin: it is not elastic when water is absent, and elastin has evolved into one of the most hydrophobic proteins known. In this research, both theories were investigated with the focus on the hydrophobic effect model. This was achieved through combining three different approaches. First, water ordering was directly observed using novel Double Quantum Nuclear Magnetic Resonance (2Q NMR) experiments as a function of both stretch and in the presence of Hofmeister ions, polyethylene glycol (PEG) and deuterated solvent that systematically modulate the hydrophobic effect. These are the first experiments in which stretch induced water ordering has been directly observed at the molecular level. Second, the effect of stretch on the amplitude and timescale of the protein dynamics was studied using static solid state natural abundance ^{13}C NMR of backbone carbonyl groups. Third to complement the NMR measurements, the entropy changes from stretching natural elastin were measured in a newly designed and homebuilt apparatus in the presence of Hofmeister ions and PEG. All experiments were performed on highly purified bovine elastin.

Elastin has inspired the design of wide variety of proteins with different functions, including protein purification, matrices for tissue engineering and drug delivery. The

significance of this research is to understand elastin recoil, which is fundamental to the systematic approach of developing and designing new protein-based elastomers.

1.1.2   Elastin Fibers Purification

2Q NMR experiments were performed first on bovine elastin fibers obtained from Elastin Products Company (Owensville, MO). These fibers were prepared by the neutral extraction method.[13] Reproducibility and consistency problems plagued these samples, so elastin fibers from freshly obtained bovine neck ligaments were purified using a recently described protocol optimized by Van Kuppevelt et al. that included several organic and aqueous extraction steps coupled with a short trypsin digestion to ensure intact smooth and uniform pure elastin fibers, (Figure 1.1). [14]

This protocol starts by washing the fibers with sodium chloride solutions over three nights to remove water soluble proteins. Washes with ethanol, chloroform, methanol, acetone and ethyl ether follow to remove lipid-containing molecules. Afterwards, the fibers are treated with cyanogen bromide to cleave proteins at methionine residues, which are present in almost all proteins but are absent in elastin. The fibers are next treated with urea and β-mercaptoethanol. Because trypsin cuts after basic residues and the predominant basic residue in mature elastin are cross-linked lysyl groups, elastin is digested slowly, and digestion with trypsin (4 h at 37 °C) removes remaining microfibrillar components leaving the remaining elastin fibers intact. The fibers were dried using a vacuum desiccator and were stored at –80 °C.
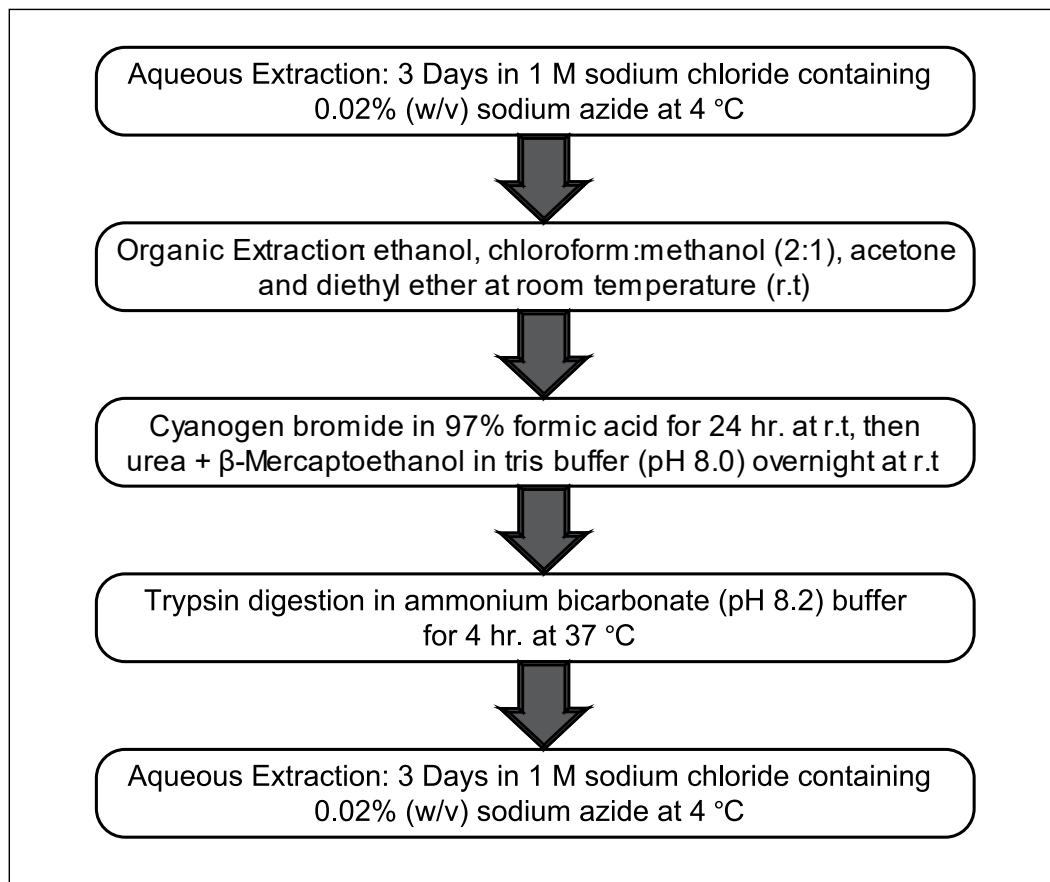
Figure 1.1. Schematic representation of elastin purification procedure from freshly obtained bovine ligamentum nuchae.

The purified elastin fibers were examined using scanning electron microscope (SEM) at the Conn Center for Renewable Energy Research in the University of Louisville with the gracious help of Dr. Jacek B. Jasinski and his coworkers. Dry elastin fibers were sputtered with an ultrathin layer of gold and examined with VEGA3 TESCAN SEM instrument operating at 10 kV. The elastin fibers were pure and intact in agreement with the purification protocol used, (Figure 1.2).[14] Young's modulus was about 0.6 MPa for two different batches of elastin fibers purified using this protocol indicating consistency in the mechanical properties.
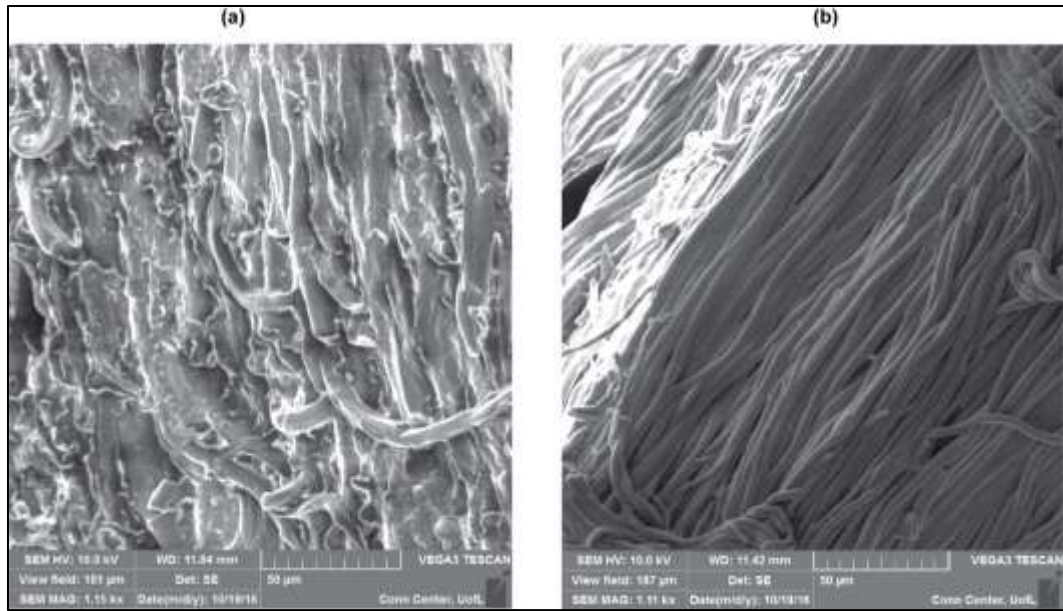
Figure 1.2. SEM micrographs of bovine ligamentum nuchae elastin fiber (a) before purification and (b) after purification.

1.2 Hofmeister ions

In 1888, Franz Hofmeister was the first scientist systematically to study the effect of a series of ions on proteins. He ranked separately the anions and the cations based on their ability to precipitate proteins. [15, 16] This series of ions is known as the Hofmeister ions series, and their effect on proteins is called the Hofmeister effect or the ion-specific effect.

Hofmeister ions fall into two classes: ions that salt-out macromolecules and ions that salt-in macromolecules, (Figure 1.3).[17]

Figure 1.3. Ranking of Hofmeister anions and cations. Ions on the left are referred to as chaotropes and the ones on the right are kosmotropes.

Anions have a more profound effect than cations due to their larger size, polarizability and hydration features. [18, 19] Thus, anions rather than cations were chosen to vary in this research. Hofmeister ions used in this research were sodium salts to unify the cation effect and because the sodium ion is considered the border line between kosmotropes and chaotropes in the cation series.

The Hofmeister effect was primarily explained based on ions interaction with water molecules and their effect on the H-bonding network of water, i.e., the ions water affinity and the hydration characteristics. Ions were classified in two groups, kosmotropes (order-making) and chaotrops (disorder-making). Kosmotropes, like sulfate (SO_4^{2-}) which is a well-known protein precipitant, are small ions with high surface charge density that interact strongly with water molecules. Chaotropes are larger ions with lower charge density and interact with water to a lesser extent. However, a reverse Hofmeister effect was observed with some macromolecules.

The simplified approach did not take into consideration the possibility of the macromolecule interacting with the Hoffmeister ion at its exposed surface. Studies with different surfaces, hydrophilic and hydrophobic or charged and uncharged, confirm the role of ion-surface interaction as either repulsive or attractive to establish the direct Hofmeister

effect or the reverse. [20, 21] Several mechanisms were proposed to describe this ion-specific effect in polymer solutions. [22]

Cremer et al. studied the specific ion effect on different polymers such as poly(N-isopropylacrylamide) (PINPAM), elastin-like polypeptides and others. They proposed three primary mechanisms, (Figure 1.4).[23-27]
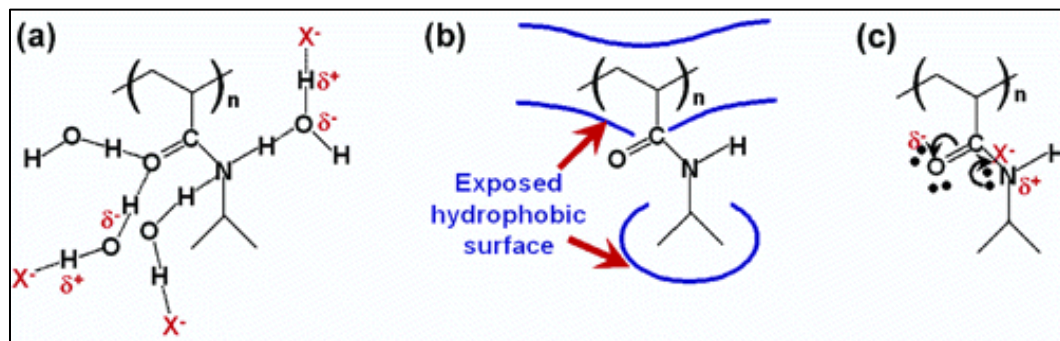
Figure 1.4. Cremer et al. three mechanisms. (a) polarizing water molecule H-bonded to the amide group. (b) modulating the hydrophobic interactions by surface tension effects. (c) direct binding of the anion with the amide group.

In the first mechanism, strongly hydrated anions are suggested to be responsible for polarizing the water molecules that are hydrogen-bonded to the amide groups in the polymer, leading to dehydrating the polymer backbone and eventually salting it out, (Figure 1.4(a)) In the second mechanism, kosmostropic anions interrupt the hydration of the hydrophobic residues of the polymer by increasing the surface tension. This makes it difficult to create the cavity needed to surround those residues causing shrinkage of hydrophobic surface and eventually salting them out, (Figure 1.4 (b)). In the third mechanism, weakly hydrated anions interact directly with the backbone of the polymer, resulting in a salting in effect, (Figure 1.4 (c)). This salting in effect often reaches a turnover point at a certain concentration, after which salting out can be observed. Cremer et al.

hypothesized that this is the result of saturation of the binding sites at the polymer backbone and the salting out effect is due to increased surface tension. The first two mechanisms are based on the anion effect on the hydration of the polymer, whereas the third mechanism is based on the direct interaction between the anion and the polymer. In this context, anions were only discussed rather than salts (anion and shell cation) because only sodium salts were investigated.

Pegram and Record investigated the effect of Hofmeister salts and other nonelectrolyte osmolytes on air-water surface tension, solubility of nonpolar solutes and biopolymer stability in water as a function of salt concentrations. These effects were interpreted using the Solute Partitioning Model (SPM).[28-31] SPM analyzes the interaction between ions and the biopolymer surface in terms of the hydration characteristics of the surface and the partition coefficient of the ions. It assumes two possible thermodynamic states of the surface in the presence of the ions: the unfolded state and the native state.[22] The effect of salts on the conformational change between the two states, as well as any other aqueous process that comes with changes in exposed surface area to water was quantified using an "m-value". The m-value is the first derivative of the standard free energy of transition between the two states with respect to the salt concentration. It is assumed that the changes in free energy are linear and directly related to the changes in the accessible surface area of the biopolymer (ΔASA) through a constant α, which links the surface hydration term as the number of water molecules per surface area and the ion portioning term as the partition coefficient of the salt concentration between the surface and the bulk solution (K_p). The m-values, (ΔASA) and K_p were determined experimentally

and then K_p was used to quantify the accumulation or exclusion of the ions from the surface, (Figure 1.5).[32]
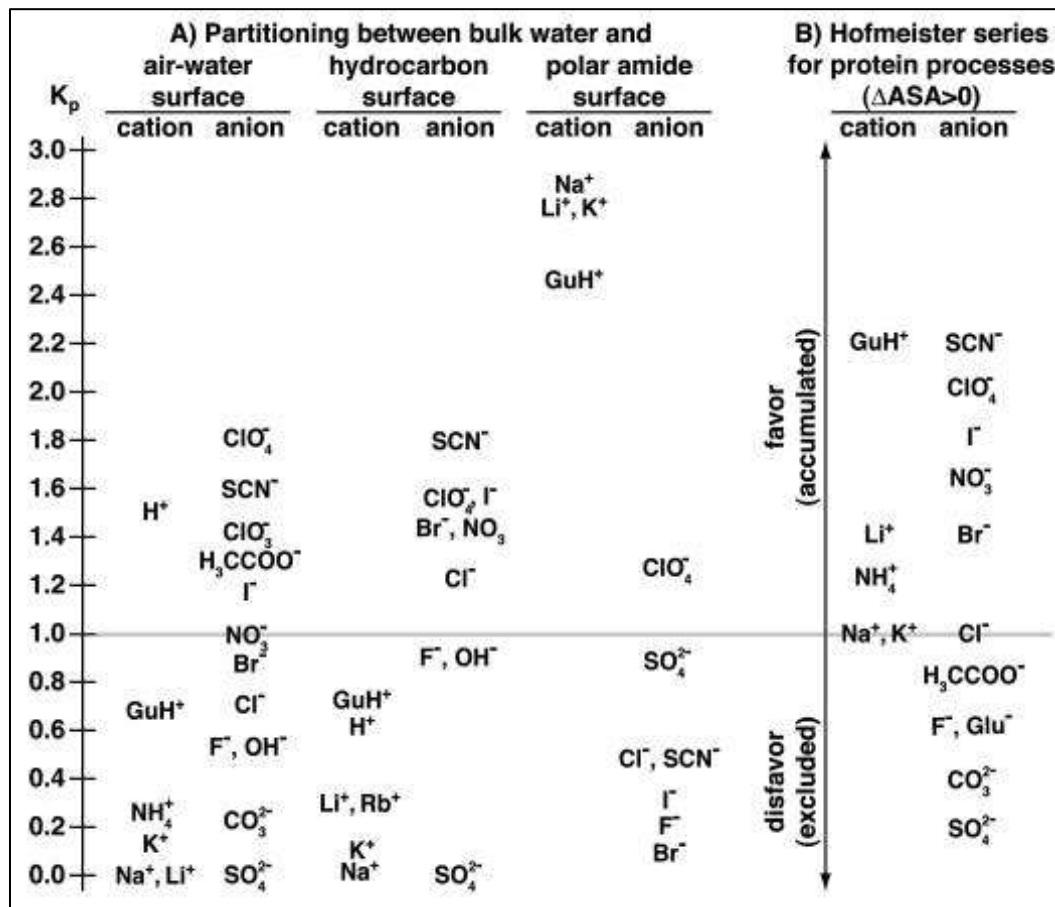
Figure 1.5. Partition coefficients of anions and cations at different model surfaces obtained from SPM.

Poorly hydrated anions accumulate at the air-water surface, whereas strongly hydrated anions are excluded from the surface and almost all cations are excluded. The effect of salts on hydrocarbon model solutes agreed with the ones observed on the air-water surface. This means that weakly hydrated anions have a strong affinity towards the hydrophobic surfaces and accumulate at them. In case of polar amide surfaces, anions are excluded but cations accumulate at the surface. This means that the salt effect is a result of both a cation effect and an anion effect. Pegram and Record concluded that the ordering of the anions is defined

by whether the anions are accumulated or repelled from the nonpolar regions in the biopolymer.

The most recent model, the thermodynamic model, was introduced by Dzubiella and Heyda. It is similar to the SPM and is derived from basic thermodynamic principles. In this approach, two possible thermodynamic states are also assumed, but correction parameters to account for the nonlinear behavior of the weakly hydrated anions (chaotropes) are added.[33] At sufficiently low salt concentration where the linear behavior of the free energy is observed, their model is reduced to the SPM model. Dzubiella et al. were able to fit the experimental data for PNIPAM reported by Cremer et al. to their model and then calculate the thermodynamic parameters. Based on the obtained thermodynamic data, they proposed two different mechanisms to explain the specific ion effects. The first mechanism, the excluded-volume mechanism, is used to explain the linear free energy behavior. Strongly hydrated salts are excluded from the polymer surface and consequently produce depletion volumes around the surface in a manner independent of temperature and concentration. This explains the linear salting out behavior of kosmotropes. The second mechanism is used to interpret the nonlinear behavior of weakly hydrated chaotropes that salt in at low concentration and turnover to salting out at high concentrations. This required second-order corrections to the changes in free energy and entropy that are due to the direct interaction between the salt and the polymer surface. The turnover observed with chaotropes originates from the preferential adsorption of the salt to the globular state (folded) over the coiled state (unfolded) with increasing concentration.[33] Dzubiella and Heyda reported that the nonlinear behavior of added sodium perchlorate ($NaClO_4$) was significant compared to other weakly hydrated salts, so these investigators used molecular

dynamics (MD) simulations to study the swelling and collapse behavior of a model polymer with respect to $NaClO_4$.[34] Dzubiella and Heyda concluded from this study that polymer swelling is maximal if both monomer-monomer and monomer-cosolute are weakly attractive, leading to cosolute density inside the coil that is bulk-like and homogenous. However, the highly attractive polymer-cosolute interactions from added $NaClO_4$ induce the collapsed conformation and display an enhanced density of the cosolute in the globule. Although the collapsed states are similar to the ones observed with kosmotropes, they are a result of a very different mechanism. Dzubiella and Heyda hypothesized that $NaClO_4$ accumulates within the polymer coil and the collapse is driven by "cross-linking-like bridging effects".[34]

1.3   Polyethylene Glycol (PEG)

PEG is a synthetic hydrophilic polymer of repeating units of ethylene glycol ($HO-CH_2-CH_2-OH$). Unlike Hoffmeister ions, PEG is uncharged and is a macromolecule with a molecular weight that can be systematically varied. With increasing molecular weight and concentration, PEG increases the viscosity of water.[35] PEG increases solution density with increased concentration, no relation between solution density and PEG molar mass was observed.[35] PEG has a wide spectrum of functions from industry to medicine. One specific function important in biochemistry and related to my research; its ability to precipitate proteins. PEG is an important precipitating agent widely used to improve crystallization of proteins for x-ray diffraction analysis. [36]

The PEG precipitation mechanism has been explained based on volume exclusion, i.e., the impossibility of both the polymer and the protein, both with high molecular weights, to coexist in the same volume at the same time. So, the polymer is excluded from

the protein surface creating a gradient of osmotic pressure surrounding the protein. When

protein molecules get closer to each other, their depletion areas overlap. This increases the

protein concentration and its chemical potential resulting in higher attractions between the

protein molecules and eventually phase separation (- Figure 1.7).[37]
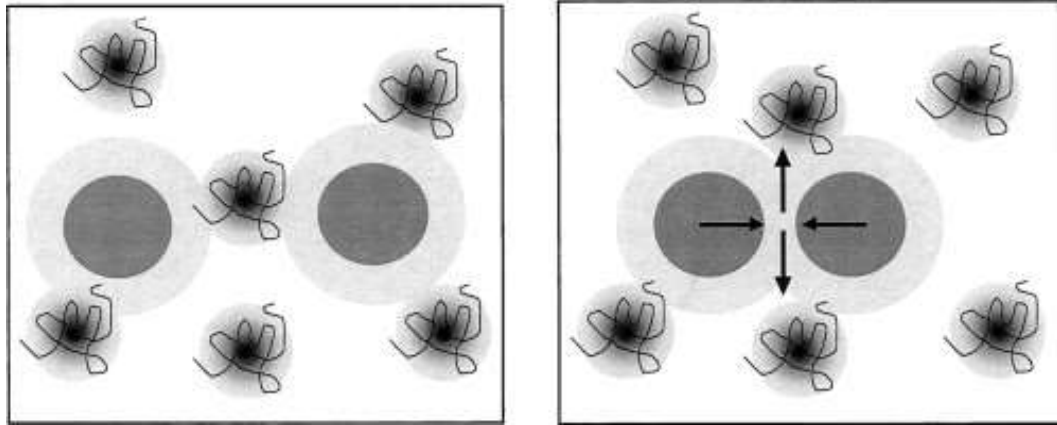
Figure 1.6. Schematic representation of depletion interaction induced by neutral polymers like PEG. Grey spheres are the protein molecules, black coils are the polymer molecules, and the depletion areas are the light grey areas.

This theory was developed by many groups starting from Oosawa and coworkers.

They derived an attractive force between particles and molecules known not to have any

direct interaction. The magnitude of this force is related to the osmotic pressure of the

solution and was hypothesized to be responsible for the macroscopic aggregations of

suspended particles.[38] Ogston et al. used simple thermodynamic expressions; like osmotic

pressures to describe the precipitation that is taking place in uncharged binary and ternary

polymer solutions using aqueous solutions of PEG and dextran as models.[39]

Ingham and Atha studied the solubility of various proteins in the presence of

different sizes and concentrations of PEG and established the linear dependence of log S

(S is the solubility in g/L) with PEG concentration in all studied proteins. Although no

relation between solution density and PEG molar mass was observed,[35] the slope of the solubility curves decreases as the molecular weight of PEG decreases, whereas no changes were observed with temperature and pH. This observation coupled with the failure of concentrated PEG solutions up to 30% (w/v) to have any detectable effect on the melting temperature of ribonuclease A (RNase A) support the theory for no direct interaction between the polymer and the investigated proteins. This agrees with the exclusion model. Ingham and Atha referred to this model as the steric exclusion model.[40]

Lee and Lee investigated the preferential solvent interaction with different proteins as a function of PEG concentration and PEG molecular weight at different pH values by measuring solution density. Their analysis was based on multicomponent thermodynamics.[41-43] They concluded that phase separation of the studied proteins in the presence of PEG is due to an unfavorable thermodynamic interaction between the protein and PEG, partially due to the unfavorable interaction between PEG and the charged residues at the protein surface. These effects result in preferential hydration of the protein and an increase in its chemical potential.[42, 43] In agreement with the steric exclusion model, Timasheff et al. reported an increase in β-lactoglobulin[44] and other investigated proteins[45] preferential hydration with increasing PEG molecular weight and showed that the exclusion is independent of PEG concentrations. Timasheff and co-workers confirmed the theory of Lee and Lee that the exclusion of PEG from proteins surfaces is primarily steric. However, Timasheff et al. opposed the part of the theory that states it is partially due to unfavorable interaction between PEG and the charged residues at the protein surface. Instead, they showed favorable interactions between hydrophobic proteins and PEG that compete with the exclusion.[44, 45] This point is of importance in the present study because

elastin is one of the most hydrophobic proteins found in nature. Also, in PEG-lysozyme mixtures the addition of low molecular weight PEGs were reported to stabilize the mixture, whereas high molecular weight PEGs were destabilizing, and opposing the depletion theory expectations, PEG induces repulsion among the lysozyme molecules.[46]

In summary, the excluded volume, recently called depletion theory, cannot alone quantitatively explain all PEG proteins interactions, and an attractive interaction between PEG and hydrophobic residues at the protein's surfaces should be taken into consideration.[44-48]

1.4 Deuterated Water versus Protonated Water (^2H_2O versus ^1H_2O)

Deuterated water (^2H_2O) and protonated water (^1H_2O) are different in both chemical and physical properties. ^2H_2O has a higher freezing point, boiling point, density, viscosity and ionization constant pK_w.[49, 50] Moreover, ^2H_2O is a more structured liquid[49, 51]; the ^2H – O –bond is shorter by 3% than the ^1H – O bond resulting in hydrogen bond shorter by 4% in ^1H_2O.[51] Thus, the solvent isotope effect plays an important role on the physical and chemical properties of proteins in solutions.

Kresheck et al. predicted that the hydrophobic bonds between the amino acids side chains are stronger in ^2H_2O than in ^1H_2O through studying the energetics of the solubility of propane, butane and several amino acids in ^1H_2O and ^2H_2O.[52] Also, a recent study concluded that more nonpolar amino acid (leucine) is adsorbed onto a polystyrene surface with ^2H_2O rather than ^1H_2O as the solvent.[53] This means less hydrophobic surface area is exposed in ^2H_2O than in ^1H_2O.

Many proteins were found to be more stable in their folded state in ^2H_2O than ^1H_2O. Examples include RNase A (pancreatic enzyme that catalyzes the cleavage of single-stranded ribonucleic acid RNA),[54, 55] ubiquitin,[54] domain 1 of rat CD2 (an immunoglobulin G , IgG protein)[56] and azurin (a bacterial enzyme that plays role in single-electron transfer).[57] RNase A showed a stronger hydration and an increase in compactness in ^2H_2O.[54] Additionally, in the case of domain 1 of rat CD2, Parker and Clarke hypothesized that the observed higher stability of the folded protein in ^2H_2O is due to enhancement in the hydrophobic interactions, which is a result of stronger solvent-solvent interactions (stronger hydrogen-bonding in ^2H_2O).[56] Also, an increase in protein aggregates is observed in ^2H_2O for proteins where hydrophobic forces drive aggregation.[58]

Cremer et al. measured the lower critical solution temperature (LCST) for elastin-like poly peptides (ELPs) to be lower in ^2H_2O in comparison with ^1H_2O in all the studied circumstances.[59] They hypothesized this is due to hydrogen-bonding stabilization between ^2H_2O and what they believed are secondary structures with β-turns present in elastin like peptides (ELPs). Although this hypothesis disagrees with the more recent finding that there is no stable secondary structure in ELPs,[60] it still indicates that ELPs are more compact in ^2H_2O than ^1H_2O.

It is worth noting that the Hofmeister effect was found to vary between ^1H_2O and ^2H_2O. It is believed that this is due to differences on the polymer's accessible area as well as a difference in the ion hydration by ^1H_2O and ^2H_2O.[61]

1.5   Goals and Methods

Elastin is one of the most abundant elastomers in nature. It is essential for many organs and tissues that require elasticity and reversible coil to function. The recoil force is

believed to be entropically driven, and the exact mechanism has not been revealed. This research investigated the physicochemical and mechanical properties of elastin responsible for its elasticity in both microscopic and macroscopic aspects using the following approaches.

1.5.1 Double Quantum Nuclear Magnetic Resonance (2Q NMR)

The change in water ordering as a function of stretching an elastin fiber was measured and this is discussed in detail in Chapter 2. It is hypothesized that stretching elastin fibers decreases the entropy (increase ordering) of the solvent due to an increase in water exposed hydrophobic surface area. This hypothesis was examined using solid state NMR coupled with Multiple Quantum Filtered (MQF) spectroscopy through a novel double quantum (2Q) pulse sequence that has been previously developed and validated by the Wittebort group to study solvent ordering at the surface of elastin.[62] The ordering of the water at the surface of elastin fiber was measured quantitatively as a function of stretch and in the presence and absence of Hofmeister ions and polyethylene glycol (PEG) that are known to modulate the hydrophobic effect systematically.

1.5.2 ^{13}C NMR

The change in backbone ordering of elastin fiber was measured as a function of stretch. If the configurational entropy is responsible for recoil, as in rubber, then changes in backbone ordering with stretch should be observed. This work is discussed in Chapter 3. The time scales and the order parameter, S, for chain motions were determined by measuring ^{13}C NMR relaxation times, T_1 and T_2, and the residual shielding anisotropy of the ^{13}C carbonyl groups in the elastin polypeptide backbone.

1.5.3 Thermomechanical experiments

Elastin recoil is entropy driven. Stretching the fiber decreases the solvent and/or the polymer entropy which, in turn, makes recoil spontaneous. This was measured quantitively as described in Chapter 4. The macroscopic mechanical properties of elastin fibers were studied using thermomechanical methods. Stretch and temperature induced changes in the free energy, entropy, enthalpy and heat capacity were quantitatively measured using a homebuilt apparatus. Experiments were performed in the presence and absence of Hofmeister ions and polyethylene glycol (PEG) that are known to perturb the hydrophobic effect.

CHAPTER 2 2Q NMR STUDY OF SURFACE ^2H_2O ON ELASTIN FIBERS

2.1   Introduction

Multiple quantum filtered nuclear magnetic resonance (MQF NMR) Spectroscopy

is an established approach for characterization and quantification of the anisotropic motion,

the motion that results from nuclear spins ordering. The basic principle of this approach is

to filter out the large isotropic signal that masks the smaller anisotropic signal in most

biological systems, such as elastin. In general, isotropic molecular motion averages out the

dipolar and quadrupolar interactions resulting in a high-resolution spectrum. Alternatively,

anisotropic molecular motion results in non-zero residual dipolar and quadrupolar

interactions that cause the splitting of the lines in the spectrum.

Double quantum filtered (DQF) NMR is the technique used to detect the anisotropic

motion and to resolve the residual couplings in spins with spin number $I = 1$ such as ^2H or

in coupled spins with $I = ½$ such as $^1H - ^1H$ coupled spins. In bulk water, molecules reorient

isotropically and this averages the nuclear quadrupole coupling in ^2H_2O to zero. However,

^2H_2O at a hydrophobic surface is weakly ordered leaving a small, residual coupling. With

techniques from multiple quantum NMR, this can be used to filter (remove) the bulk water

signal and detect only the signal from molecules oriented at the hydrophobic surface. This

technique has been used in many biological systems for different purposes.

It has been used to characterize the different layers of blood vessels and measure their mechanical strain [63], to differentiate between the various layers of sciatic nerve [64], to study the interactions of water with collagen in tendon [65, 66] and the effect of mechanical stress on these interactions.[67] Also, DQF NMR was used to study water ordering at the surface of elastin as a function of temperature and applied external strain.[68, 69] More recently, a novel DQF NMR pulse sequence has been developed by the Wittebort group and used to study the solvent ordering at the surface of elastin.[62]

Elastin is one of the most hydrophobic proteins in nature. It is an elastomer that gains elasticity only when swollen with water and its elasticity is entropy driven. The recoil is spontaneous to regain the entropy of the system (protein:water) that is lost when elastin is stretched. It is hypothesized that stretching, in addition to decreasing the entropy of the polymer, also decreases the solvent entropy due to exposure to an increased hydrophobic surface area. Primary goal of this dissertation is to deduce the role of hydrophobic hydration as a driving force in elastin recoil. In this Chapter, solvent entropy is studied as a function of applied mechanical strain and in different hydrating solutions that are known to modulate the hydrophobic interaction using the previously developed ^2H DQF pulse sequence by the Wittebort group.[62] studying the solvent at the molecular level is in parallel with the thermomechanical studies in Chapter 4.

2.2 Theory

Nuclear spin number, I, is correlated to the number of subatomic particles in the atomic nucleus. If the nucleus contains an even number of both neutrons and protons, then $I = 0$ and there is no angular momentum associated with this nuclear spin. In other words, it cannot be detected by NMR. If the nucleus contains an odd number of neutrons or

protons, then $I = \frac{1}{2}$, 3/2, 5/2 and so on. The simplest example is ^{1}H, $I = \frac{1}{2}$, which has an even distribution of charge over a sphere. In general, the number of possible orientations for a nuclear spin is equal to $2I + 1$, i.e., for ^{1}H it is 2 possible orientations, (Figure 2.1 (a)). Finally, if nucleus contains an odd number of both neutrons and protons, then $I = 1$, 2, 3 and so on.
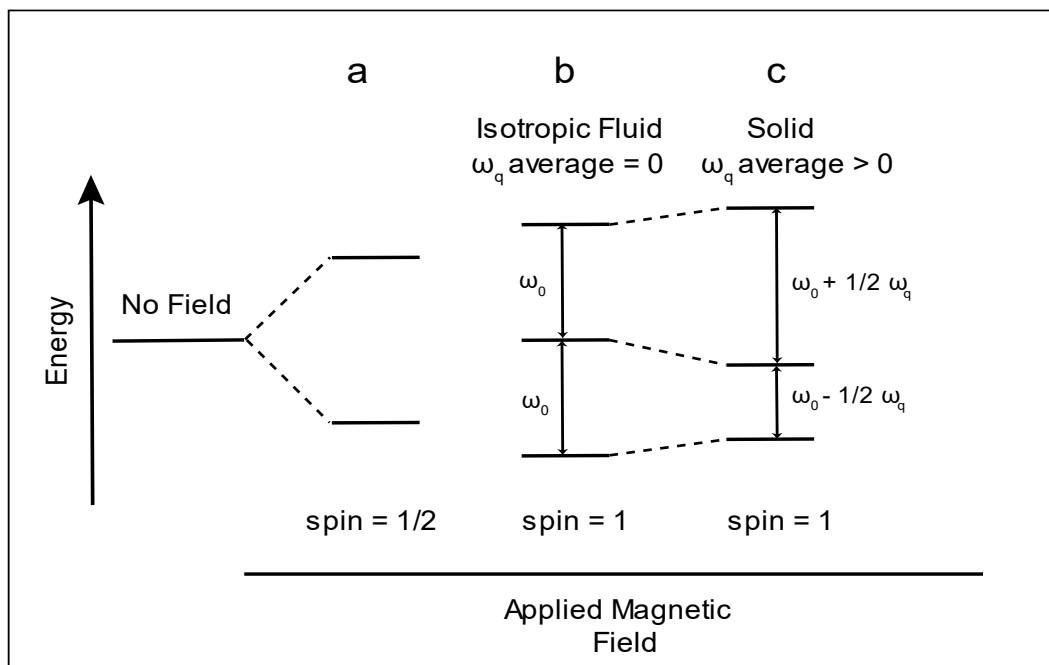
Figure 2.1. Energy levels of (a) spin-1/2, (b) spin-1 in isotropic fluid and (c) spin-1 in solid. ω_0 is the Larmor frequency and ω_q is the quadrupolar coupling.

The nucleus of concern in this Chapter is ^{2}H. It has a spin number $I = 1$, and subsequently, there are 3 possible orientations (spin states) with different energies, (Figure 2.1 (b-c)). The energies are different because the spin possesses an electrical quadrupolar moment (like any spin with $I > \frac{1}{2}$) that interacts with the electric field gradient created by the asymmetric distribution of the electron clouds around the nucleus.[70, 71]

The quadrupolar coupling (ω_q) depends on the nuclear quadrupolar moment (nuclear property), the electric field gradient (molecular property), the phase of matter and

the molecular orientation.[71] In isotropic fluids, ω_q is averaged to zero whereas in anisotropic fluids/solids it is greater than zero.

The elastic fibers of elastin are hydrated; about half of the hydrated fiber weight is water. Some fraction of this water reorients isotropically as in bulk water, and the remaining fraction is in rapid exchange with water ordered on the solvent accessible surface of the fiber. When the elastin is hydrated in ^2H_2O, the quadrupolar coupling, ω_q, of ^2H is averaged to zero in the bulk water and is nonzero ($\omega_q > 0$) for water on the surface of the fiber. To observe only the water at the protein surface, the NMR signal from bulk water is eliminated through double quantum filtration, (Figure 2.2),which was achieved with a novel pulse sequence developed by Wittebort and co-workers.[62] The residual coupling is used to generate double quantum (2Q) coherence and then measured indirectly after filtering (eliminating) the bulk water signal through the designed pulse sequence with a 64 steps of phase cycling incorporated in the pulse sequence.

The new pulse sequence consists of four main steps, (Figure 2.3). The first step is the preparation of the 2Q coherence through two 90° pulses that partially convert I_z magnetization into 1Q and 2Q coherence. The magnitudes of the 1Q and 2Q coherences depend on the coupling, ω_q. The 180° pulse between the two 90° pulses refocuses the offset so it does not contribute to evolution of the spin system during the first indirect time, t_1. The second step is evolution, in which the 2Q coherence evolves at twice the Larmor frequency, $2\omega_0$, while the 1Q coherence evolves at the Larmor frequency. So, at constant evolution time (t_2), the 2Q and 1Q are separated in phase. Since 2Q coherence cannot be detected directly, it is converted back into I_z by the next two 90° pulses in the same way it is generated from I_z in the preparation step.
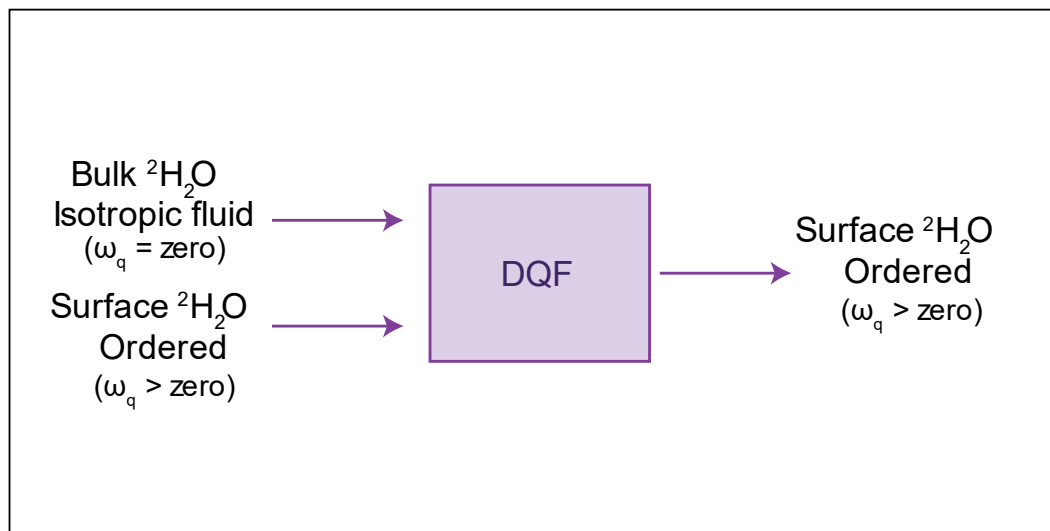
Figure 2.2. Schematic representation of double quantum filtration (DQF) to obtain the 2Q signal.

In the last step, the NMR signal is detected following a 90° pulse which converts I_z into observable magnetization. This is repeated with 64 steps of phase cycling so that only the 1Q signal resulting from 2Q coherence is detected as a function of incrementing the preparation/conversion time, t_1. The underlying principle of the phase cycle is that shifting transmitter pulses by, for example, 180° inverts the 1Q coherence and leaves the 2Q coherence unchanged.

Two types of experiments were employed: the evolution experiment with fixed t_1 and the preparation experiment with fixed t_2. After double Fourier transformation of the evolution data table, $S(t_1,t_2)$, peaks from the 1Q and 2Q signals are separated in the indirect dimension, f_2. Peaks at f_{os} and $2\,f_{os}$ are the 1Q and 2Q signals, respectively, where f_{os} is the offset frequency. Only the 2Q peak is observed if the phase cycle is properly implemented. In the 2Q buildup curve, $S_{2Q}(t_1)$, the intensity of the 2Q peak as a function of t_1, is obtained by Fourier transformation of the preparation experiment and analyzed using Eq. 2.1.
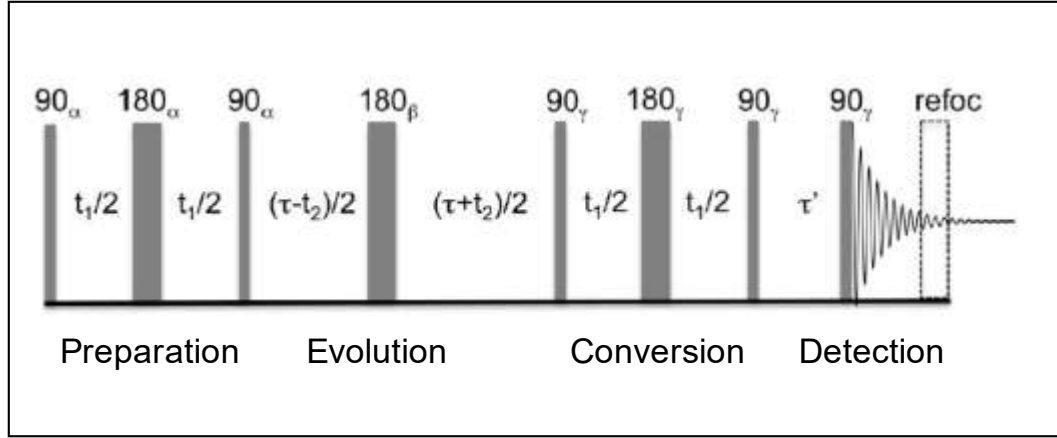
Figure 2.3. The 2Q NMR pulse sequence developed by Wittebort and co-workers.

$$S_{2Q}(t_1) = \frac{1}{2}A_{2Q}\exp\left(-\frac{2t_1}{T_2^{surf}}\right)[1 - u^{-1}[C(u)\cos\omega_q t_1 + S(u)sin\omega_q t_1]] \qquad \text{Eq. 2.1}$$

with $\quad u = (3\omega_q t_1)^{1/2}$, $C(u) = \int_0^u \cos x^2\, dx$ and $S(u) = \int_0^u sin x^2\, dx$

where A_{2Q} is the proportionality constant for the number of spins with $\omega_q > 0$, t_1 is the preparation/conversion time, T_2^{surf} is the transverse relaxation time of spins that contribute to the 2Q signal, ω_q is the quadrupolar coupling and θ represents the possible orientations which are averaged for the unoriented samples used in these experiments. Eq. 2.1 accounts for both coherent evolution of the spin system resulting from the quadrupolar coupling and spin relaxation that occurs in the course of the pulse sequence.

The transverse relaxation time, T_2^{surf} is determined in a separate experiment to reduce the number of the parameters in the fit in $S_{2Q}(t_1)$ to two parameters, A_{2Q} and ω_q. This is achieved by adding a Hahn Echo sequence at the end of the 2Q pulse sequence.[62,72] Also, the Hahn Echo sequence is used directly in a third experiment to determine the transverse relaxation time of the spins in the bulk, T_2^{bulk} and the signal intensity of 1Q

24

coherence (A_{1Q}). Ultimately, an important parameter, the fraction of ordered deuterated water within the time of the experiment ($f = \frac{A_{2Q}}{A_{1Q}}$) is measured, (Figure 2.4).
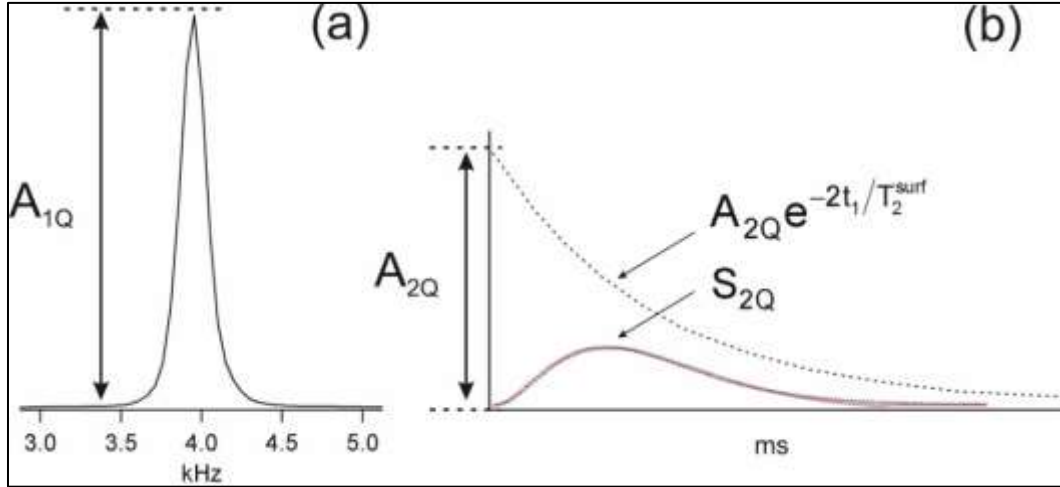
Figure 2.4. (a) A_{1Q}, the peak intensity of the 1Q signal evaluated from the first point of T_2^{bulk} experiment. (b) A_{2Q}, peak intensities are plotted as a function of preparation time t_1 (ms).

2.3   Materials and Methods

2.3.1   Elastin Fibers purification Protocol

The extensive details of the purification protocol adapted from Van Kuppevelt et al[14] that was used to prepare all the samples in this Work is reported here. About 100 g of freshly obtained bovine nuchal ligaments (Animal Technologies, Tyler, TX) were freed carefully from adhering fatty tissue and membranes, and cut using electric food slicer (Model 610, EdgeCraft Corporation, Avondale, PA) to thin uniform strips (~ 3 mm × ~ 5 mm× ~ 10 mm).

The thin strips were placed in 3 L Erlenmeyer flask, and the aqueous extraction was performed by adding1 L of cold 1.0 M NaCl (sodium chloride, Sigma-Aldrich, St. Louis,

MO) that contains 0.02% (w/v) NaN$_3$ (sodium azide 99%, Alfa Aesar, Haverhill, MA) with constant stirring at 4 °C overnight. This extraction procedure was repeated three times to remove aqueous soluble proteins. Afterwards, the thin strips were recovered by paper funnel filtration and the organic extractions were initiated by suspending the strips in 1 L of ethanol (Ethyl Alcohol Denatured 95%, Aldon Corporation, Avon, NY) with constant stirring for 90 min at room temperature. The series of organic extractions were done using the following solvents: (*i*) 1 L of chloroform-methanol (2:1) (both Chloroform and methanol are ACS, Pharmaco, Brookfield, CT) for 90 min at room temperature (*ii*)1 L of acetone (Acetone ACS, VWR International, Radnor, PA) for 30 min, and (*iii*) 1 L of diethyl ether (Deiethy ether ACS, Sigma-Aldrich, St. Louis, MD). The strips were recovered and left to dry in a desiccator overnight. These organic extractions were intended to remove lipid-containing molecules.

The dried strips were incubated in 1.5 L 97% formic acid (Alfa Aesar, Haverhill, MA), and cyanogen bromide (Alfa Aesar, Haverhill, MA) was added to a final concentration of 1%, and left to react for 24 h under non-oxidizing conditions at room temperature. The mixture was then diluted with deionized water twice its volume, filtered, and washed with deionized water 50 times. This step of the purification protocol ensures the hydrolysis of most proteins because cyanogen bromide cleaves proteins at methionine residues present in most proteins, but not in elastin.

After the last washing step, the strips were suspended in 1 L of Tris buffer (8.02 pH) that contains 0.5% (v/v) β-mercaptoethanol (≥ 98% pure 2-mercaptoethanol, Bio-Rad Hercules, CA), 6.0 M urea (Urea 99.5%, Acros Organics, Fair Lawn, NJ) and 0.02% (w/v) NaN$_3$.[73] The suspension was stirred overnight at room temperature. In the next day, the

strips were recovered and washed with deionized water ten times, and then were resuspended in 0.1 M ammonium hydrogen carbonate (99.0%, Alfa Aesar, Ward Hill, MA) solution (pH 8.2) that contains 0.02% (w/v) NaN_3 and 10,000 U of trypsin for 4 h at 37 °C. This short trypsin digestion was optimal to remove the remaining microfibrillar components and leaving the elastin fibers intact as most of the lysyl groups, the target of trypsin hydrolysis, are cross-linked in mature elastin.

In the last step of the purification protocol, elastin strips were washed with deionized water and extracted over three nights in solutions of cold 1.0 M NaCl that contains 0.02% (w/v) NaN_3 at 4 °C. Finally, the purified strips of elastin were washed with deionized water, dried using a vacuum desiccator overnight and stored at –80 °C.

2.3.2 Sample Setup

About 20 mg dried and purified elastin fiber, ~1mm $\times$ 12 mm, was glued with cyanoacrylate gel (Super Glue) to a ~15mm 1/16-inch diameter G10 rod. The fiber was equilibrated overnight against a particular solvent/hydration solution to a known mass and inserted into a 3 mm NMR tube (length ~3 cm). Then, the NMR tube was glued on one side and sealed with parafilm on the other. The fiber was stretched to a measured length by moving the rod and fixed in place with parafilm, (Figure 2.5).
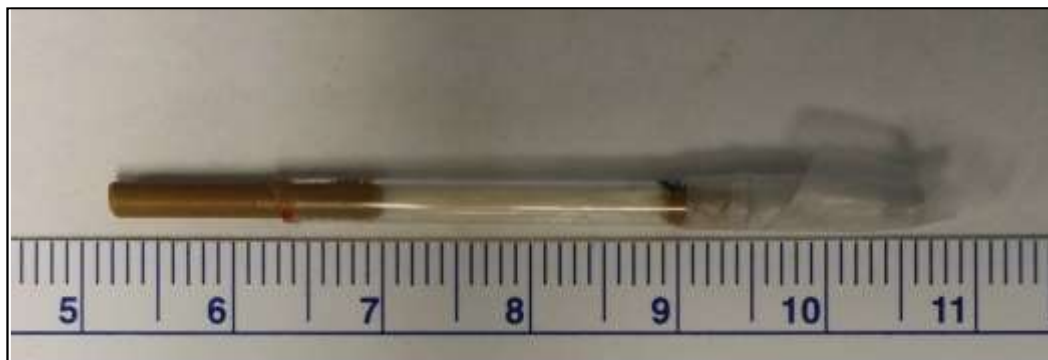
Figure 2.5. The hydrated elastin fiber in the 3mm NMR tube. The parafilm is removed to stretch the sample and replaced to maintain the sample length.

The effect of different solutes: 200 PEG (polyethylene glycol 200, Alfa Aesar, Ward Hill, MA), 20 kDa PEG (Polyethylene glycol 20,000, Alfa Aesar, Ward Hill, MA), sodium sulfate (Na_2SO_4 ACS, Fisher Chemical, Fair Lawn, NJ) and sodium perchlorate ($NaClO_4$ ACS 98.0-102.0%, Beantown Chemical Corporation, Hudson, NH) on the deuterated water (99.9% D, Cambridge Isotope Laboratories, Andover, MA) ordering at the surface of elastin was studied, (Table 2.1),at four different stretch percentages when possible: 0% (relaxed fiber), ~ 15%, ~30% and ~ 40%, Eq. 2.2.

$$\text{Stretching \%} = \frac{Stretched\ length - Relaxed\ length}{Relaxed\ length} \times 100\% \qquad \text{Eq. 2.2}$$

Table 2.1. The masses of all elastin fibers used in this Chapter experiments, and the masses of ^2H_2O once hydrated in the different hydration solutions.

Elastin sample	Hydration solution	Elastin dry mass (mg)	^2H_2O mass in hydrated elastin (mg)
Fiber 1	10% 200 PEG	21.6	20.3
	10% 20 kDa PEG	21.6	24.4
	High purity ^2H_2O	21.6	24.5
	50% ^2H_2O	21.6	10.5
Fiber 2	10% 200 PEG	25.9	28.3
	5% 200 PEG	25.9	31.6
	High purity ^2H_2O	25.9	30.6
Fiber 3	10% 20 kDa PEG	17.7	15.8
	5% 20 kDa PEG	17.7	18.7
	High purity ^2H_2O	17.7	ND (Not Determined)
Fiber 4	1 mol/kg NaClO$_4$	19.8	37.4
	0.5 mol/kg NaClO$_4$	19.8	31.9
	High purity ^2H_2O	19.8	25.2
Fiber 5	0.1 mol/kg Na$_2$SO$_4$	15.8	18.4
	0.5 mol/kg Na$_2$SO$_4$	15.8	18.8

2.3.3 NMR Experiments and Spectrometer Instrumentation

Five experiments were conducted to determine the fraction of ordered water (**f**) and the residual quadrupole coupling (ω_q). The first experiment, a simple Bloch decay, was used to determine the 90° pulse width. The second experiment was an inversion recovery and used to determine the longitudinal or spin- lattice relaxation time (T_1). This was used to set the recycle time, typically set to 5 times T_1. The third experiment, a Hahn Echo[74], was used to measure transverse or spin- spin relaxation time (T_2^{bulk}) and to determine the signal intensity, A_{1Q}, which is proportional to the total ^2H_2O in the sample. The fourth experiment was the 2Q buildup curve with the pulse sequence described in the theory section.[62, 72] Finally, spin- spin relaxation time (T_2^{surf}) was measured by inserting a Hahn Echo sequence at the end of the 2Q pulse sequence with t_1 set to the delay with the highest 2Q signal. [62, 72]

^2H NMR spectra were obtained on an 11.7 T (500 MHz) instrument with a Libra data system (Tecmag, Houston TX,) and homebuilt probes and RF electronics. The probe is based on a design previously described.[75] The 90° pulse width was ~ 4.5 μs with 62 watts RF power at the ^2H frequency (76.05 MHz).

2.4   Results and Discussion

Both the effect of the mechanical strain and the hydration solution on the quadrupolar coupling ($\nu_q = \frac{\omega_q}{2\pi}$) and the fraction of ordered water (**f**) of the elastin fiber were studied.

The "static" water residual coupling in crystals of ^2H_2O ice, 200 kHz,[76] is large compared to the measured residual coupling (ν_q) of ^2H_2O in hydrated elastin, 15 – 95 Hz

and is found here to vary with stretch, the addition of a solute to the solvent (water) and changing the isotope from ^1H_2O to ^2H_2O. The transverse relaxation time (T_2) of ^2H_2O which is 243 ± 14 ms in pure solvent [72] is reduced significantly to $6-22$ ms and $6-17$ ms, when measured with and without 2Q filtration in hydrated elastin fiber, respectively. The shorter relaxation times indicate that the rate of water reorientation in elastin is slow compared to pure water and that this slows with stretch. Without added solute, a nearly tenfold increase in the 2Q signal is observed when the sample length is stretched by $\sim 30\%$. This is due to an increase in the fraction of the water that has access to the predominantly hydrophobic surface of elastin on the timescale of the ^2H NMR experiment. Changes in the residual coupling (ν_q) are observed when changing the hydration solutions. More significant changes take place in the fraction of the water that is weakly ordered (**f**). Stretching this highly hydrophobic protein increases the surface area exposed to the water resulting in an increase in the ordered water which is measured here at the microscopic level.

2.4.1 Hydration of Elastin Fiber in ^1H_2O versus ^2H_2O

Three batches of elastin fibers were purified using the purification procedure described previously. To confirm the reproducibility and the consistency in physical and mechanical properties of these fibers, three 2 Q build up curves of a representative fiber from each batch hydrated in ^2H_2O are reported, (Figure 2.6).
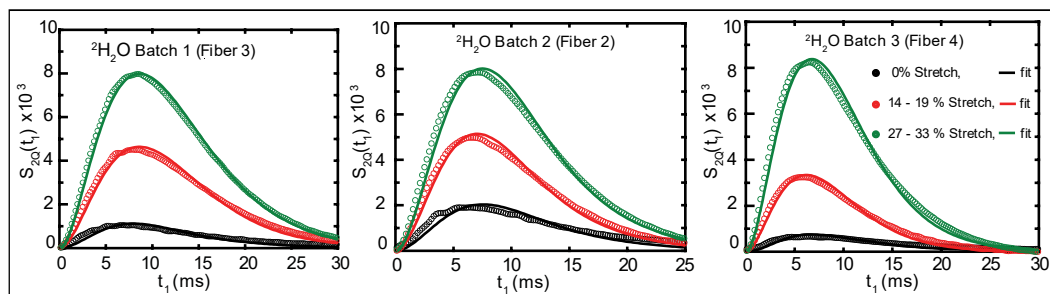
Figure 2.6. 2Q signal intensity as a function of time at different stretches of hydrated elastin fibers in ^2H_2O from the three different purified batches of elastin.

The solutes (PEG, Na_2SO_4 and $NaClO_4$) used in the studies in this Chapter are also used in the thermomechanical experiments described in Chapter 4. To investigate the difference between ^2H_2O and ^1H_2O, NMR experiments were carried out in ^2H_2O and in 50.3% (w/w) $^2H_2O/^1H_2O$ as the hydrating solvents of the elastin fiber. The results of NMR experiments in both relaxed and ~30% stretched fiber are compared in Figure 2.7 and Table 2.2.
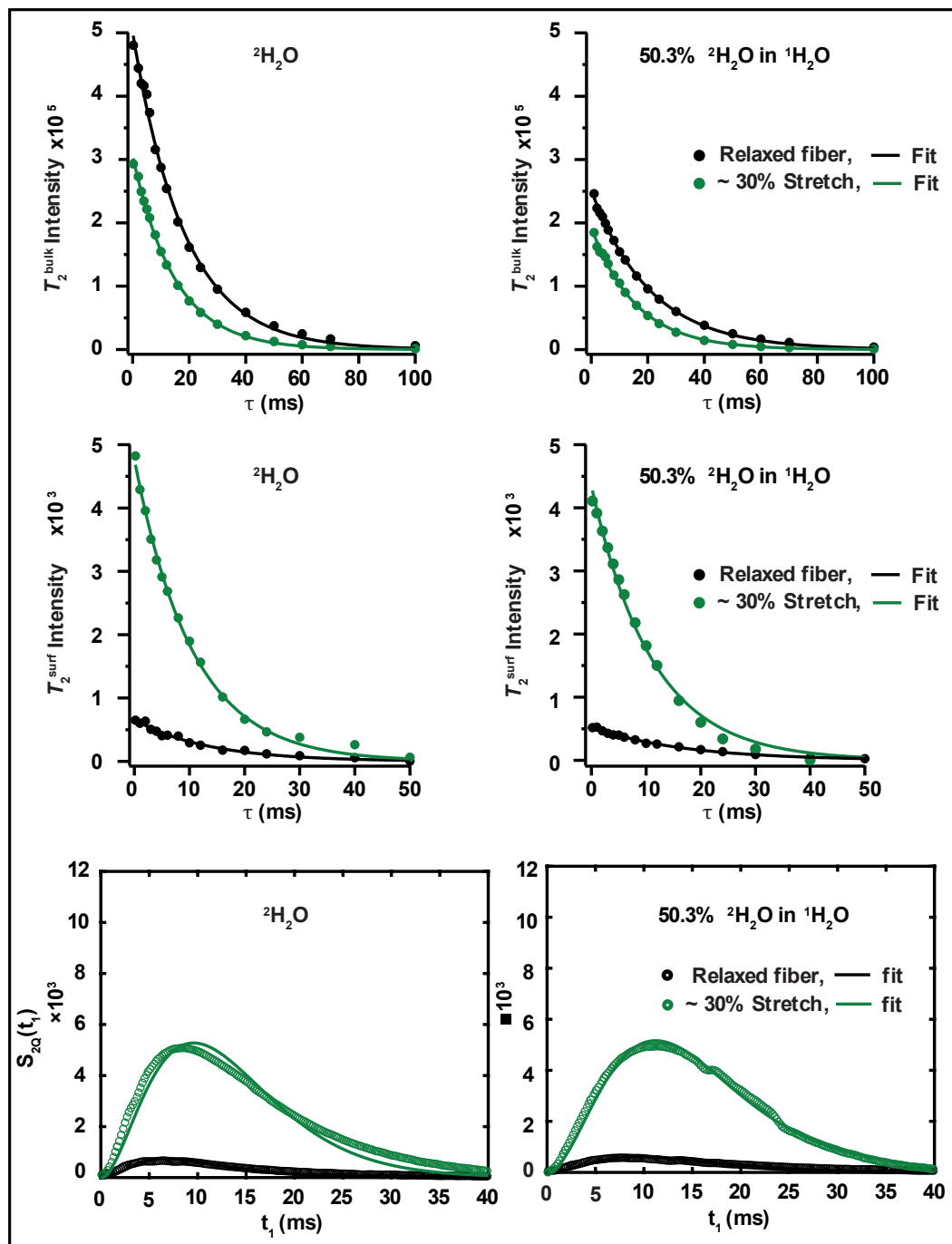
Figure 2.7. T_2^{bulk}, T_2^{surf} and 2Q signal intensities as a function of time in 0% (relaxed) and ~ 30% stretched elastin fiber (Fiber 1) hydrated in ^2H_2O versus in 50% ^2H_2O in ^1H_2O.

Table 2.2. The experimental T_1, T_2^{bulk} and T_2^{Surf} values and the results of the least linear square fit of the 2Q experiments in Figure 2.6 using Eq. 2.1 in both the relaxed (0%) and 30% stretched fiber hydrated in ^2H_2O and in 50% ^2H_2O in ^1H_2O.

Hydration solution	Stretch %	T_1 (ms)	T_2^{bulk} (ms)	T_2^{Surf} (ms)	T_2^{Fit} (ms)	ν_q (Hz)	f
^2H_2O	0%	67.5 ± 0.7	18.3 ± 0.4	13.4 ± 0.8	18.7	55	0.01
	29 %	66.0 ± 0.6	14.8 ± 0.2	10.5 ± 0.2	10.7	15	0.72
50.3% (w/w)^2H_2O/ 49.70 ^1H_2O	0%	79.7 ± 0.8	21.0 ± 0.3	16.8 ± 0.5	21.1	38	0.01
	30 %	77.6 ± 0.6	15.9 ± 0.3	11.1 ± 0.3	15.9	21	0.36

T_2^{Surf} (measured with 2Q filtration) and T_2^{Bulk} (measured without 2Q filtration) directly describe the reorientational rates of water in elastin. Decreases in T_2 values indicate longer solvent reorientation rates. Thus, reducing the solvent deuteration from 100% ^2H_2O to 50% ^1H_2O, (Table 2.2), leads to increased values of both T_2^{Surf} (measured with 2Q filtration) and T_2^{Bulk} (measured without 2Q filtration). This is due to the weaker H-bonding and reduced viscosity in ^1H_2O. The quadrupolar couplings (ν_q) are small and range from 15 – 55 Hz. In both solutions, the fraction of ordered solvent (**f**) increases dramatically with stretch and this is accompanied by a small decrease in T_2 values, both of which indicate increased interaction at the solvent protein interface.

Hydrophobic interactions are observed to be stronger in ^2H_2O compared to ^1H_2O. This results in increased compaction of hydrophobic proteins and, subsequently, a decrease in the exposed hydrophobic surface area to the solvent.[52, 53, 56, 58, 77] Consequently, it is expected for a hydrophobic protein like elastin to have smaller surface area exposed to hydration by ^2H_2O compared to ^1H_2O. In this experiment, 50% (w/w) $^2H_2O/^1H_2O$ was used, this means less available ^2H_2O for NMR detection by half (2Q signal declines), but more hydrophobic surface area is exposed to the available ^2H_2O (2Q signal increases). The two effects counterbalance each other and results in a similar 2Q buildup curve with almost same signal intensity in both relaxed (0% stretch) and 30% stretched fiber, (Figure 2.7). In both solutions, stretching the fiber increases the 2Q intensity by about an order of magnitude. This is an anticipated result due to the increase in the hydrophobic surface exposed to the solvent with stretch which results in more ordered water at the surface.

2.4.2   Hydration of Elastin Fiber in PEG Solutions

Two elastin fibers were hydrated separately in solutions of 200 Da PEG and 20 kDa PEG in ^2H_2O, (Fiber 2 and Fiber 3 respectively), to study the effect of PEG on water ordering at the protein surface. Furthermore, the effect of the mechanical stretch on T_1, T_2^{bulk}, T_2^{Surf} and 2Q buildup was investigated in each solution at three concentrations: 0, 5% and 10% (w/w) and four stretches: 0 %, ~15 %, ~30 % and ~ 40 % when possible. The results from both fibers are shown in Figures 2.8 – 2.10 and Tables 2.3 – 2.4.

The trends observed in the previous section for both T_2^{Surf} and T_2^{bulk} are maintained in both samples, i.e., T_2^{Surf} is smaller than T_2^{bulk} and both decrease with the increase in stretch and the increase in PEG concentration, (Figure 2.7 and Figure 2.8). T_1 on the other hand varies slightly with no obvious trend, (Table 2.3 and Table 2.4). The quadrupolar

coupling (υ_q) is small and increases by a small amount with an increase in the PEG concentrations. The fraction of the ordered solvent (**f**) significantly increases with sample stretch. However, **f**, the fraction of surface accessible solvent, is highly dependent on the PEG size and concentration. The **f** values are much smaller in 200 Da PEG than 20 kDa PEG. Moreover, **f** increases to a lesser extent with stretch as the PEG concentrations increase. Finally, the 2Q signal intensity increases dramatically with the increase in stretch, (Figure 2.9). A roughly ten folds increase in magnitude is observed when the hydrated elastin fiber in ^2H_2O is stretched 40%. Adding PEG slightly decreases the fiber elasticity, and as its concentration rises from 0% (^2H_2O) to 10 %, the 2Q signal intensity is drastically reduced. This is seen clearly when the hydrated fiber in 10% (either 200 PEG or 20 k Da PEG) is stretched by 40% and the 2Q intensity only increases 5 folds.
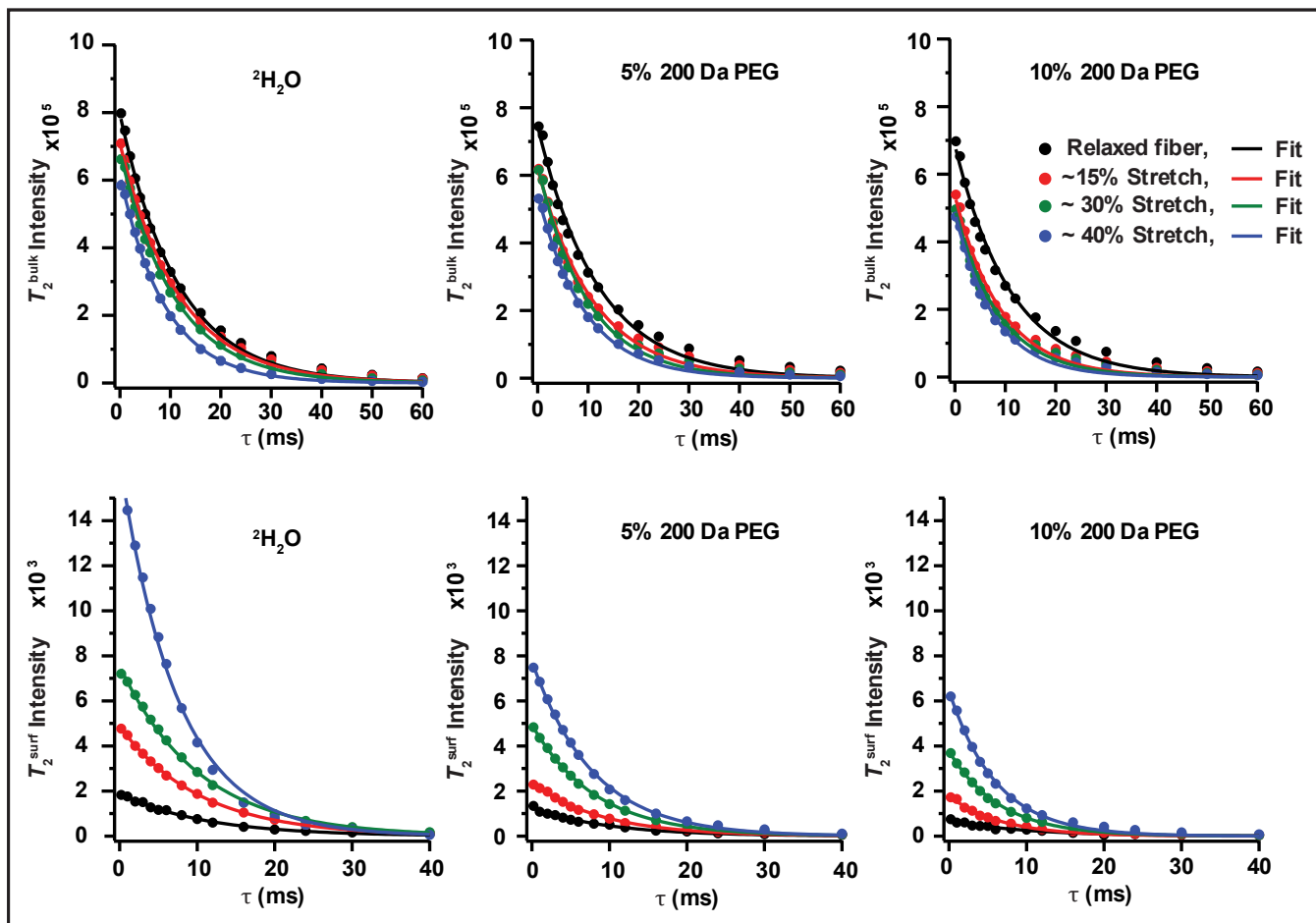
Figure 2.8. T_2^{bulk} and T_2^{surf} intensities as a function of time at different stretch% for hydrated elastin fiber (Fiber 2) in 200 Da PEG solution.
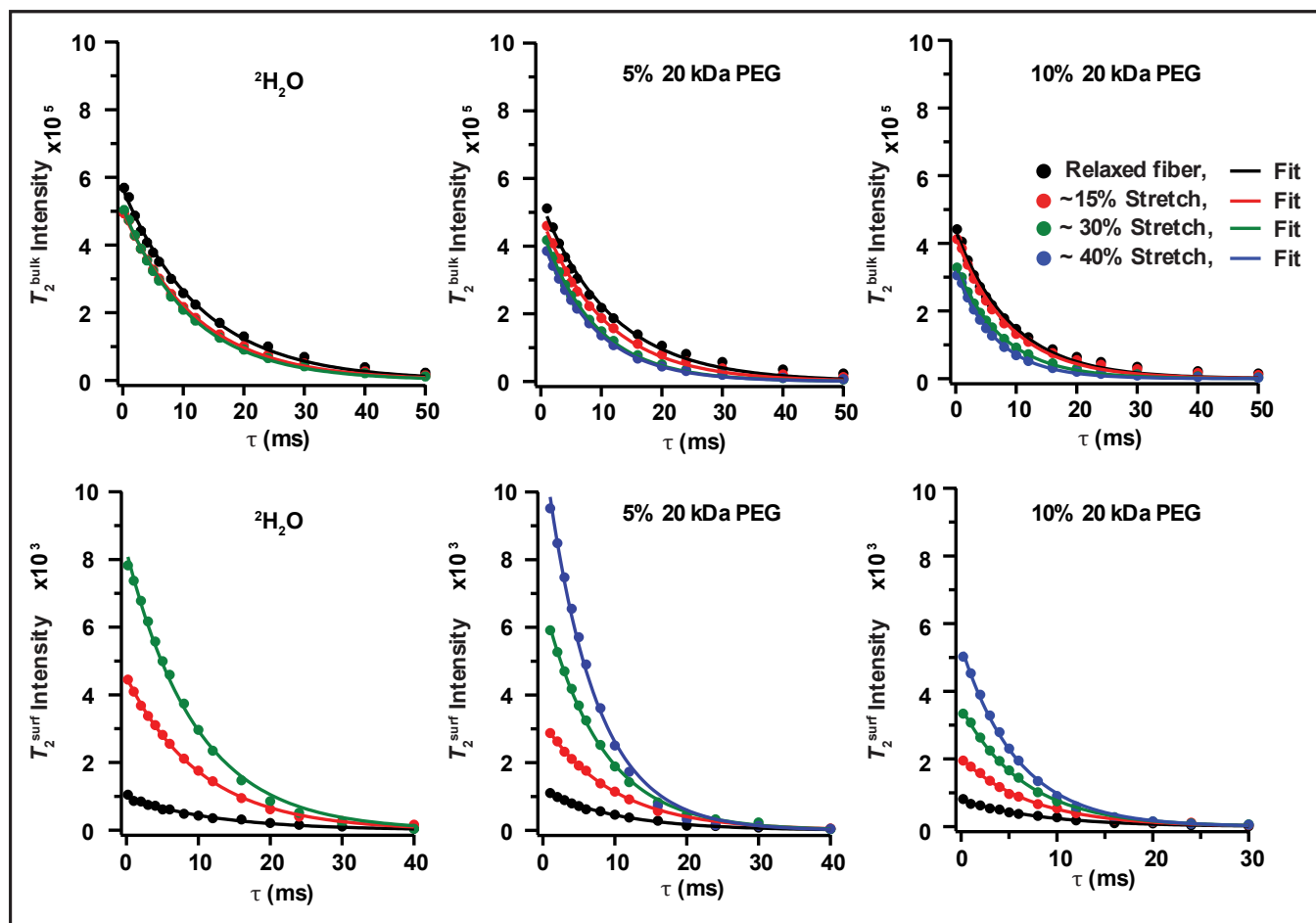
Figure 2.9. T_2^{bulk} and T_2^{surf} intensities as a function of time at different stretch% for hydrated elastin fiber (Fiber 3) in 20 kDa PEG solution.
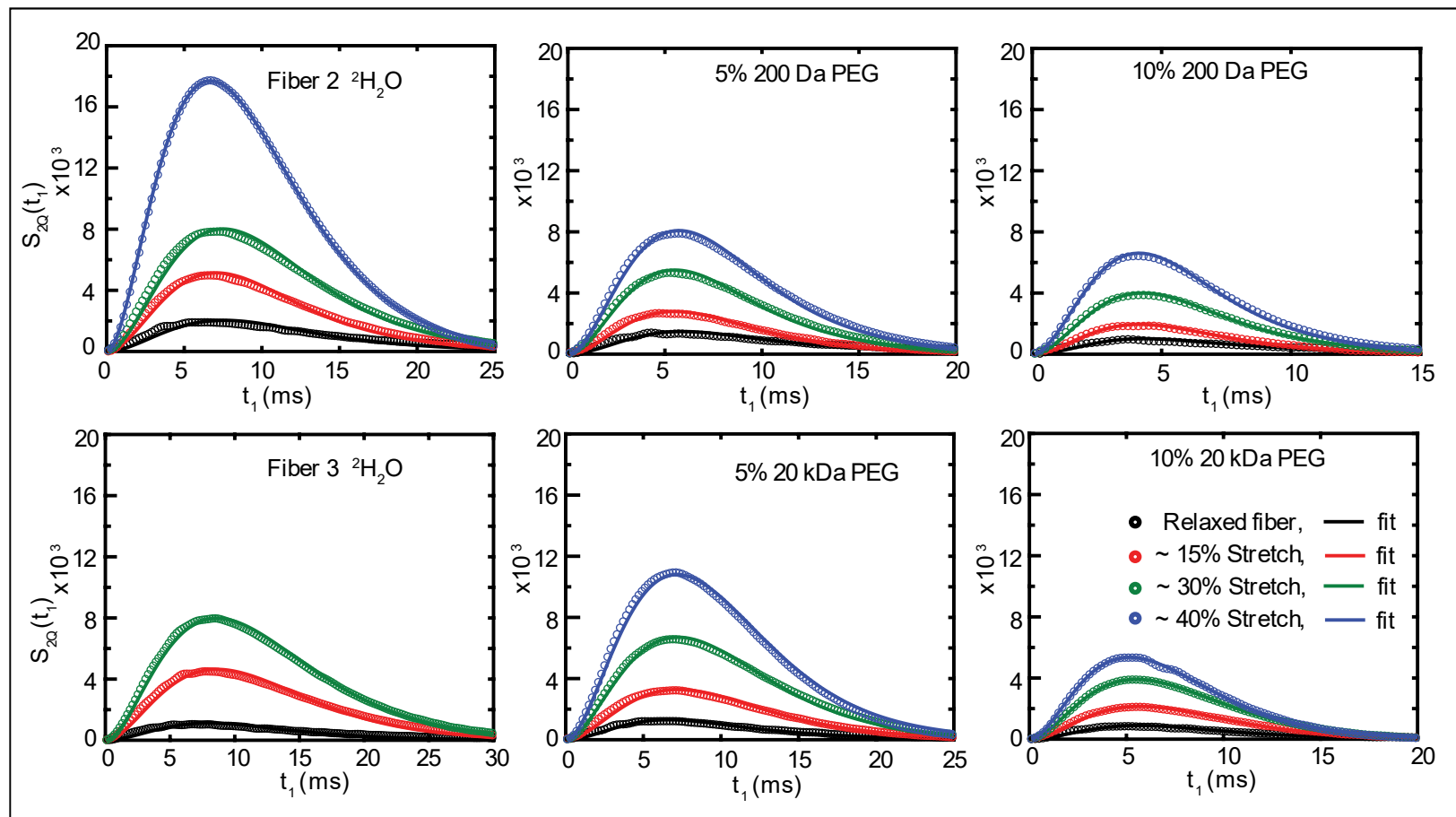
Figure 2.10. 2Q signal intensity as a function of time at different stretch% in 200 Da (Fiber 2, upper panels) and 20 kDa PEG solutions (Fiber 3, lower panels).

Table 2.3. The experimental T_1, T_2^{bulk} and T_2^{Surf} values and the fit results of the 2Q experiments as a function of stretch and concentration of 200 Da PEG in Fiber 1.

Hydration solution	Stretch %	T_1 (ms)	T_2^{bulk} (ms)	T_2^{Surf} (ms)	T_2^{Fit} (ms)	ν_q (Hz)	f
0% 200 Da PEG (^{2}H$_2$O)	0%	54.2 ± 0.4	11.6 ± 0.3	11.0 ± 0.3	11.9	35	0.02
	14 %	58.1 ± 0.4	11.7 ± 0.2	10.4 ± 0.1	10.4	35	0.08
	27%	55.6 ± 0.3	10.9 ± 0.2	10.3 ± 0.1	10.3	30	0.17
	40 %	57.3 ± 0.4	9.0 ± 0.1	7.5 ± 0.2	9	30	0.51
5% (w/w) 200 Da PEG	0%	56.4 ± 0.6	11.9 ± 0.4	9.9 ± 0.4	12.3	55	0.01
	15 %	55.1 ± 0.7	11.0 ± 0.4	9.0 ± 0.2	9	50	0.04
	27%	53.1 ± 0.4	9.8 ± 0.3	8.2 ± 0.1	8.2	45	0.10
	40 %	53.6 ± 0.4	9.2 ± 0.2	7.9 ± 0.1	7.95	40	0.21
10% (w/w) 200 Da PEG	0%	54.9 ± 0.7	11.1 ± 0.5	9.9 ± 0.7	11.6	85	0.01
	15 %	48.9 ± 0.7	9.2 ± 0.4	6.7 ± 0.3	6.7	65	0.03
	27%	49.6 ± 0.6	8.8 ± 0.3	6.5 ± 0.1	6.5	60	0.08
	40 %	48.1 ± 0.4	7.9 ± 0.3	6.1 ± 0.1	6.1	60	0.16

Table 2.4. The experimental T_1, T_2^{bulk} and T_2^{Surf} values and the fit results of the 2Q experiments as a function of stretch and concentration of 20 kDa PEG in Fiber 2.

Hydration solution	Stretch %	T_1 (ms)	T_2^{bulk} (ms)	T_2^{Surf} (ms)	T_2^{Fit} (ms)	ν_q (Hz)	**f**
0% 20 kDa PEG (^2H_2O)	0%	57.8 ± 0.5	13.1 ± 0.3	12.4 ± 0.5	13.4	35	0.02
	15 %	59.0 ± 0.4	12.2 ± 0.2	10.4 ± 0.1	10.3	20	0.25
	27 %	57.4 ± 0.3	11.3 ± 0.1	9.7 ± 0.2	9.5	15	0.81
5% (w/w) 20 kDa PEG	0 %	52.0 ± 1.0	11.7 ± 0.4	10.4 ± 0.3	12.1	45	0.02
	14 %	50.2 ± 0.6	10.6 ± 0.3	9.7 ± 0.1	9.7	30	0.11
	26 %	47.7 ± 0.5	8.8 ± 0.1	7.9 ± 0.1	8.8	25	0.39
	38 %	52.9 ± 0.3	8.7 ± 0.1	6.8 ± 0.2	8.7	25	0.69
10% (w/w) 20 kDa PEG	0 %	44.8 ± 0.9	9.3 ± 0.3	8.4 ± 0.3	9.5	50	0.02
	15 %	45.0 ± 0.6	8.9 ± 0.2	7.3 ± 0.1	7.25	35	0.10
	26 %	45.1 ± 0.7	7.7 ± 0.1	6.6 ± 0.1	6.5	30	0.35
	38 %	41.3 ± 0.3	6.6 ± 0.1	5.9 ± 0.1	5.95	30	0.59

In order to eliminate any variations of the results due to the use of two different elastin fibers, the effect of molecular weight of PEG was investigated on the same elastin fiber (Fiber 1) by comparing 10% 200 Da PEG hydration solution with 10% 20 kDa PEG on both relaxed and 30% stretched, (Figure 2.11 and Table 2.5).

The most noteworthy effects of the PEG of two different molecular weights are on the fraction of the ordered water (**f**) and the 2Q signal intensity. Stretching the fiber 30% results in a 5-fold increase in the 2Q signal intensity and an increase from 1% to 10% in the fraction of ordered water when the fiber hydrated in 10% 200 Da PEG compared to a 10-fold increase in the 2Q signal intensity and an increase from 1% to 30% in the fraction of ordered water when the fiber hydrated in 10% 200 Da PEG. The more profound effect observed in the 200 Da PEG Solutions is believed to be due to the interaction of the small molecular weight PEG with the intrafibrillar water,[78, 79] resulting in a more compact fiber with less exposed surface.

The uncharged crowding agent PEG increases the protein- protein interactions through the excluded volume mechanism[37], thus it is expected to increase the compaction of the elastin fiber. This shall decrease the hydrophobic surface area exposed to the solvent and, in turn, decrease the water ordering at the surface, which is observed and measured quantitatively. The effect increases with the concentration and is more profound in the smaller molecular weight PEG.
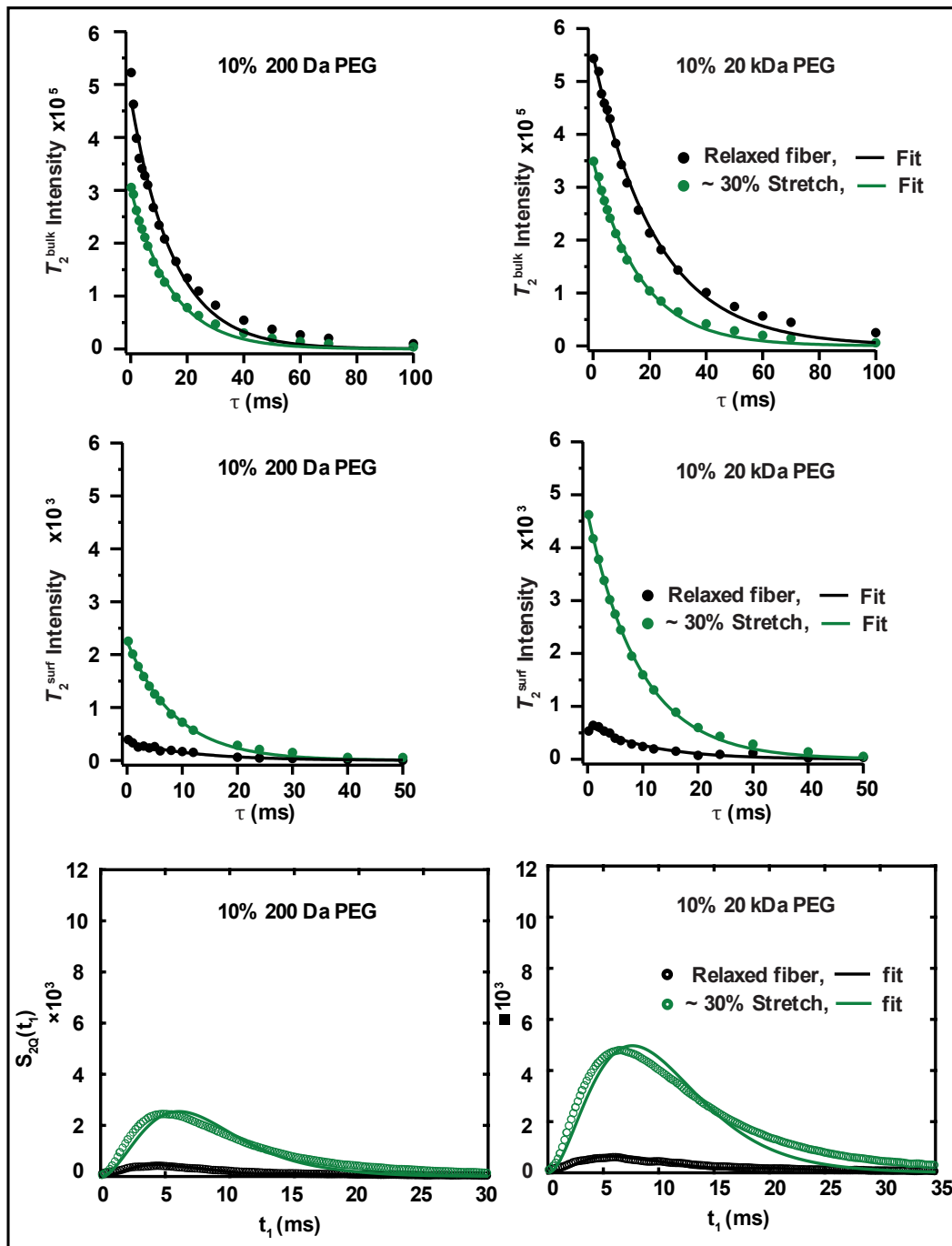
Figure 2.11. T_2^{bulk}, T_2^{surf} and 2Q signal intensities as a function of time at 0% (relaxed) and 30% stretched elastin (Fiber 1) hydrated in 10% (w/w) 200 Da PEG and in 10% (w/w) 20 kDa PEG.

Table 2.5. 10% (w/w) 200 Da PEG versus 10% (w/w) 20 kDa PEG experimental and fit results in the relaxed and 30% stretched fiber, (Fiber 1).

Hydration solution	Stretch %	T_1 (ms)	T_2^{bulk} (ms)	T_2^{Surf} (ms)	T_2^{Fit} (ms)	v_q (Hz)	**f**
10% 200 Da PEG	0%	66.0 ± 1.2	14.9 ± 0.9	12.0 ± 1.2	15.8	95	0.01
	28 %	63.5 ± 1.2	14.4 ± 0.5	8.8 ± 0.2	8.8	40	0.10
10% 20 kDa PEG	0%	74.8 ± 1.4	22.4 ± 0.7	11.1 ± 1.0	23	75	0.01
	31 %	69.3 ± 1.1	16.6 ± 0.4	9.5 ± 0.1	9.5	25	0.31

2.4.3   Hydration of Elastin Fibers in Solutions of $NaClO_4$ versus Na_2SO_4

The effect of Hofmeister ions on the water ordering at the surface of elastin was investigated by hydrating two elastin fibers (Fiber 4 and Fiber 5) separately in different concentrations of $NaClO_4$ and Na_2SO_4 in ^2H_2O. T_1, T_2^{bulk}, T_2^{Surf} and 2Q buildup were measured in 0, 0.5 and 1.0 mol/kg $NaClO_4$ and in 0.1 and 0.5 mol/kg Na_2SO_4 when the fiber was relaxed (0% stretched), ~15 %, ~30 – 35% stretched, (Figures 2.12 – 2.14 and Table 2.6).

The trend observed previously is well-preserved, T_2^{Surf} is smaller than T_2^{bulk}, and both decrease with the increase in stretch, but unlike in PEG, both parameters increase as the salt concentration increases, which is believed due to the increase in the surface tension with higher salt concentrations. T_1, as in the previous studied solutions, varies slightly with no obvious trend, (Table 2.6). As before, the quadrupolar coupling (υ_q) is small in these solutions with not much change with increasing perchlorate concentration, but υ_q does increase with the rise in sodium sulfate concentration. The fraction of the ordered solvent (**f**) significantly increases with the stretch in all solutions, yet it depends on the perchlorate and sulfate concentrations. Very high concentration of perchlorate (1.0 mol/kg) is needed to observe the reduction in **f** compared to only 0.1 mol/kg in sulfate.
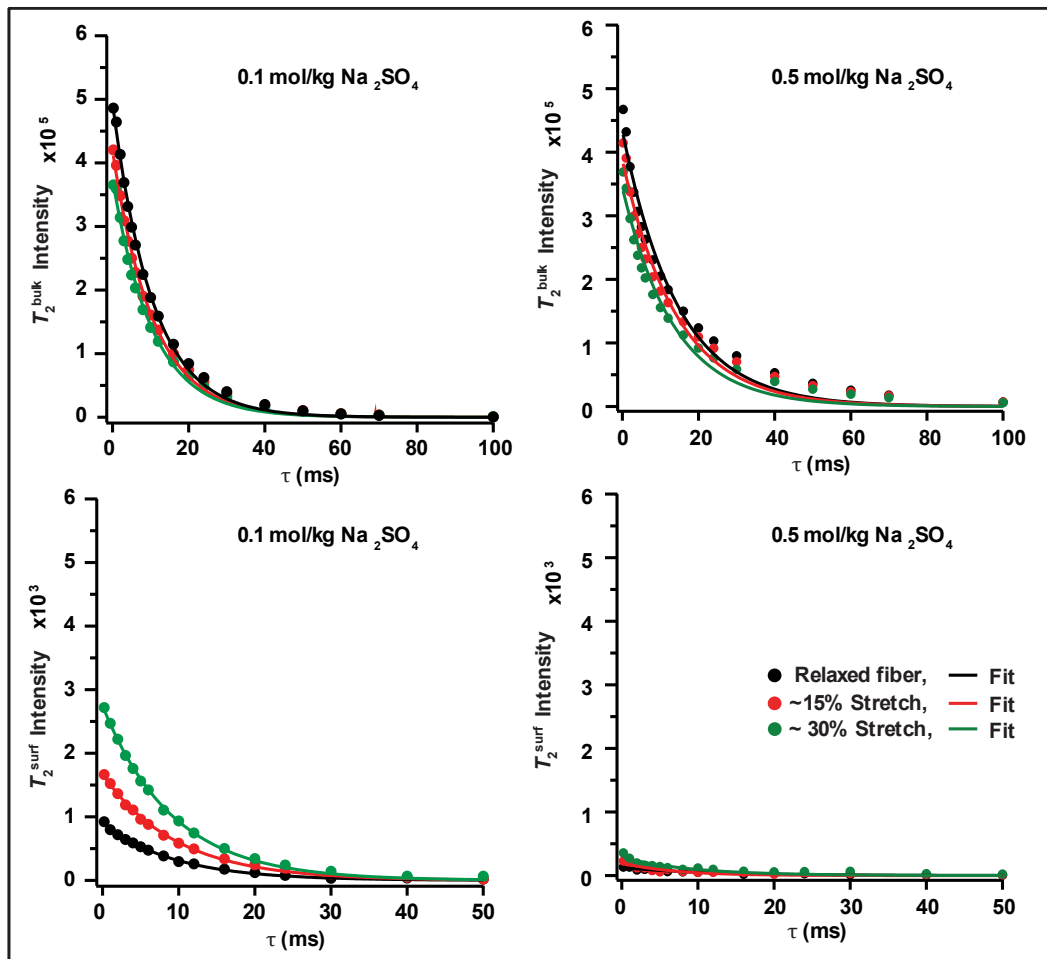
Figure 2.12. T_2^{bulk} and T_2^{surf} intensities as a function of time at different stretch% of hydrated elastin (Fiber 5) in Na_2SO_4 solutions.
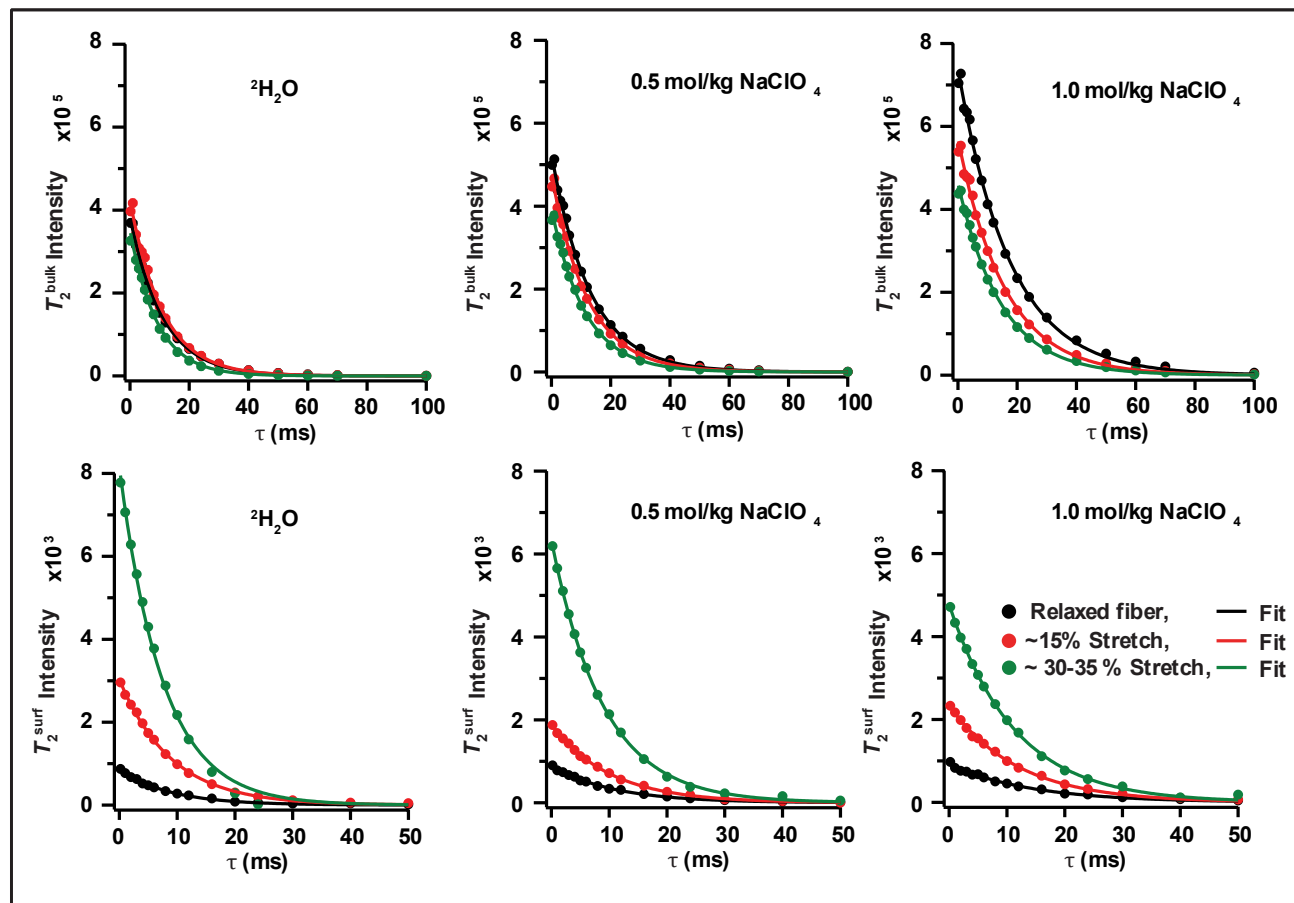
Figure 2.13. T_2^{bulk} and T_2^{surf} intensities as a function of time at different stretch% of elastin fiber (Fiber 4) hydrated in $NaClO_4$ solutions.
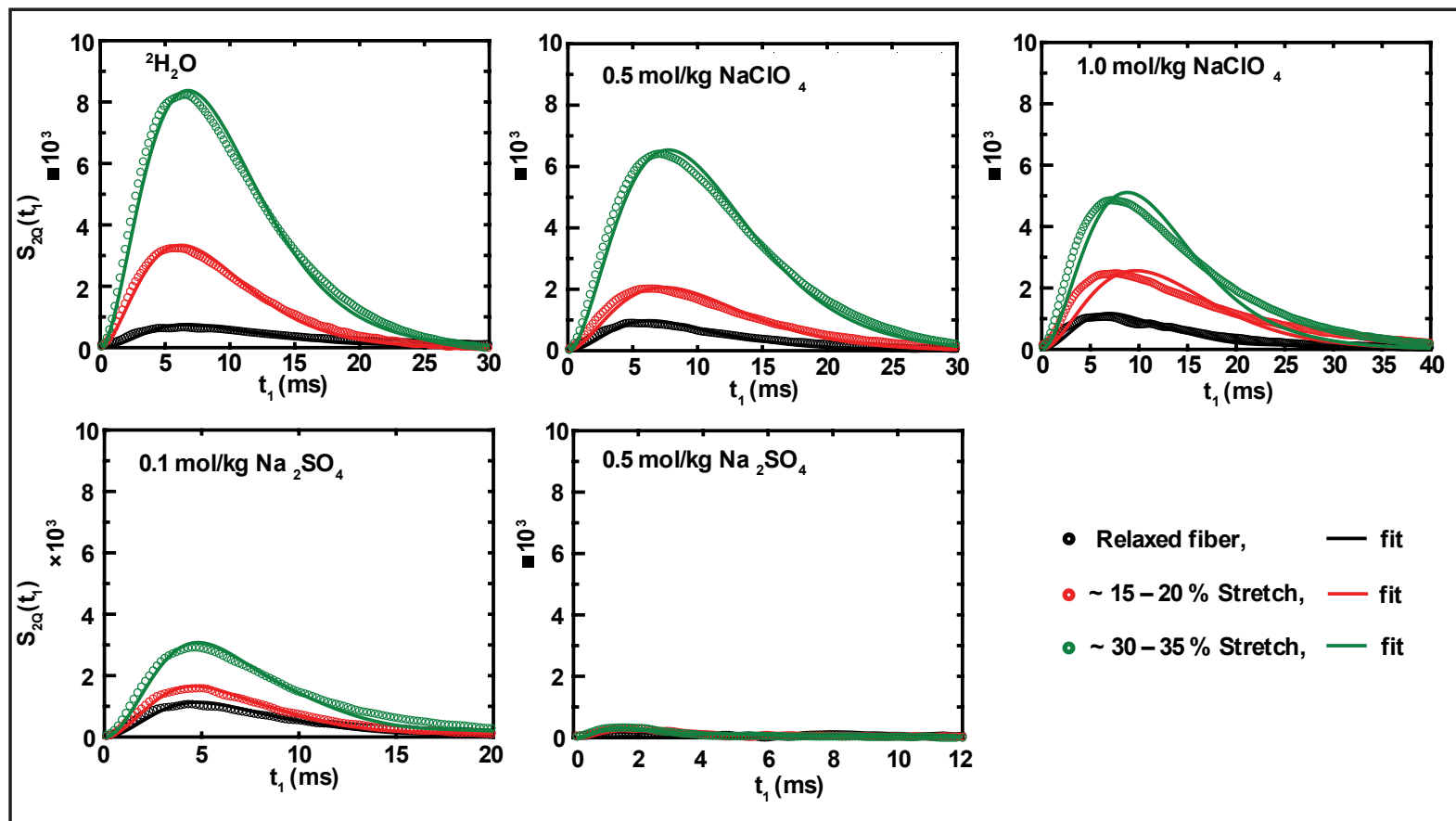
Figure 2.14. 2Q signal intensity as a function of time and stretch of hydrated elastin in solutions of NaClO4 (Fiber 4, upper panels) and Na2SO4 (Fiber 5, lower panels).

Table 2.6. Elastin hydrated in solutions of $NaClO_4$ (Fiber 4) and Na_2SO_4 (Fiber 5) experimental T_2^{bulk} and T_2^{Surf} values and the least square fit results of the 2Q experiments at the studied concentrations and constrains.

Hydration solution	Stretch %	T_1 (ms)	T_2^{bulk} (ms)	T_2^{Surf} (ms)	T_2^{Fit} (ms)	ν_q (Hz)	**f**
	0 %	51.6 ± 0.4	11.1 ± 0.2	8.7 ± 0.2	11.3	56	0.02
^2H_2O	19 %	52.1 ± 0.4	11.0 ± 0.4	9.0 ± 0.1	7	23	0.33
	33 %	51.7 ± 0.2	9.2 ± 0.2	7.5 ± 0.2	7.8	23	0.83
	0%	66.5 ± 0.2	13.1 ± 0.3	10.8 ± 0.3	13.5	52	0.01
0.5 mol/kg $NaClO_4$	20 %	64.1 ± 0.2	12.3 ± 0.3	10.1 ± 0.1	8	16	0.27
	36%	64.0 ± 0.1	11.4 ± 0.3	9.0 ± 0.1	8.8	19	0.65
	0 %	79.3 ± 0.4	17.7 ± 0.4	14.2 ± 0.6	18.2	52	0.01
1.0 mol/kg $NaClO_4$	19 %	74.1 ± 0.3	15.8 ± 0.4	11.9 ± 0.2	11.9	19	0.10
	31 %	75.6 ± 0.3	14.7 ± 0.3	11.3 ± 0.2	11.3	23	0.21
	0 %	50.0 ± 0.4	10.6 ± 0.2	9.4 ± 0.2	10.8	70	0.01
0.1 mol/kg Na_2SO_4	14 %	51.3 ± 0.5	10.6 ± 0.3	9.7 ± 0.2	10.9	75	0.02
	28%	54.0 ± 0.4	10.5 ± 0.3	9.2 ± 0.1	10.8	70	0.04

Kosmotropes like sulfate raise the viscosity and the surface tension when added to water, making it difficult to create the required cavity to accommodate nonpolar solutes (cavity model).[80, 81] Thus, the addition of sulfate reduces the hydrophobic surface exposed to water causing elastin fibers compaction. This is the reason the 2Q signal declined dramatically with the addition of sulfate and was largely eliminated at 0.5 mol/kg, (Figure 2.14).

On the other hand, chaotropes such as perchlorate interact preferentially with the macromolecule and salt in (solubilize) the peptide group, either through specific or nonspecific ion interaction.[80, 82, 83] Thus, the addition of perchlorate increases the hydrophobic surface exposed to water. This explains why not much difference was observed upon addition of perchlorate until the concentration 1.0 mol/kg was reached. At high concentration, chaotropes, in general, start to behave like kosmotropes in what is called a turnover point. Perchlorate is reported to have significant nonlinear behavior compared to other chaotropes, and Molecular dynamics (MD) simulations were used to study its turnover point.[34] The hypothesis is that the polymer collapses and the compaction increases at the turnover point. This effect is similar to that of kosmotropes but due to a different mechanism and assumed to arise from "cross-linking-like bridging effects".[34] This explains the slight decline in the 2Q signal at high concentrations of sodium perchlorate, (Figure 2.14).

CHAPTER 3 ^{13}C NMR DYNAMIC STUDY OF ELASTIN BACKBONE

3.1   Introduction

Elastin is an entropic elastomer that gains elasticity only when hydrated. Stretch decreases the entropy of the system (elastin and water), and recoil is spontaneous to regain entropy.[9, 84, 85] The source of decreased entropy originates from either the increase in ordered water at the expanded hydrophobic surface with stretch (hydrophobic effect)[8, 84] or the increase in backbone ordering (configurational entropy) of elastin backbone similarly to   rubber.[9] The source has not been resolved yet. Here, the main focus is on (*i*) the configurational entropy and its contribution to elastin recoil mechanism and (*ii*) the dynamics of the backbone in the presence and absent of strain.

Solid State NMR with magic angle spinning was previously used to study nuchal bovine elastin when it is dry (rigid) and hydrated (flexible) by Pometun et al.[86] The dry elastin spectrum showed separated peaks including the carbonyl peak at about 175 ppm with side bands typical of a stationary peptide, and these bands completely disappeared upon hydration. This indicates that the backbone in the hydrated elastin is highly disordered with large amplitude motions and the carbonyl group order parameter was estimated to be less than 0.1 ($S < 0.1$). [86] The high degree of mobility of the carbonyl backbone in hydrated elastin was also observed by others measuring only T_1,[87] or T_1 and linewidths which were analyzed using a single correlation time.[88] In another study, T_1 and $T_{1\rho}$ were measured but

analyzed using only the dipolar relaxation mechanism and a spectral density function with a single correlation time.[69]

This Chapter presents quantitative studies into backbone mobility. The amplitudes and time scales of motions in hydrated bovine elastin were investigated in the presence and absence of mechanical strain using solid state ^{13}C NMR without magic angle spinning. The hypothesis is that if configurational entropy contributes to the recoil mechanism, as in rubber, then changes in backbone ordering with stretch should be observed. The backbone order parameter was obtained from the residual shielding anisotropy of the carbonyl NMR signal, and the dynamical timescales of the motions were determined by combining the backbone order parameter with the relaxation rates R_1 and R_2 of the backbone carbonyl (C′) groups measured at two NMR frequencies.

3.2   Materials and Methods

3.2.1   Sample Setup and Experimentation:

The ^{13}C NMR spectra of both stretched and relaxed elastin without magic angle spinning (MAS) were obtained on a 500 MHz spectrometer equipped with a homebuilt probe and a 700 MHz Varian Inova NMR spectrometer.

The elastin fiber sample used in the 500 MHz NMR spectrometer (140 mg dried and purified and ~ 2 mm × 25 mm) was glued with cyanoacrylate gel (Super Glue) to a G10 rod and hydrated overnight in ^{2}H$_2$O to a known mass. After insertion into a 5 mm NMR tube (length ~ 5 cm), the tube was glued on one side and sealed with parafilm on the other. A relaxed elastin fiber inserted in a 5 mm NMR tube is shown in Figure 3.1Figure 3.1. The hydrated relaxed elastin fiber in the NMR tube.. The NMR tube was inserted into

the horizontal coil of the homebuilt ^{1}H/^{13}C probe [75] of the 11.7 T instrument. The probe has a ^{13}C 90° pulse width of 5.6 µs.
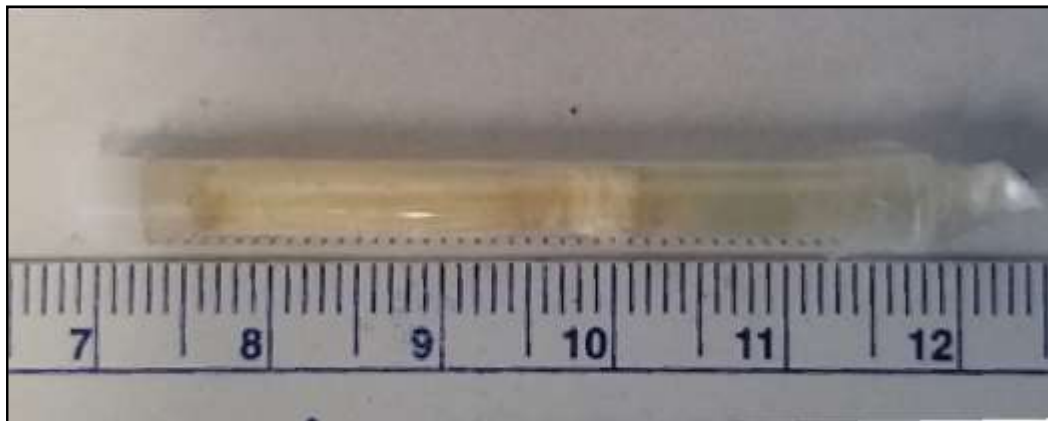
Figure 3.1. The hydrated relaxed elastin fiber in the NMR tube.

To evaluate the residual shielding anisotropy, stationary ^{13}C NMR spectra of the carbonyl backbone were measured with the elastin fiber relaxed and stretched by ~32 % (to 132% of its relaxed length). The spin- lattice relaxation time (the longitudinal relaxation time, T_1) and the spin- spin relaxation time (the transverse relaxation time, T_2) of carbonyl carbon backbone were measured using the standard inversion recovery and Hahn echo experiments with relaxation delays of 4s, respectively.[74, 89]

The inversion recovery experiment starts with a 180° pulse that inverts the equilibrium longitudinal magnetization from z to $-z$. Then, it relaxes due to spin- lattice relaxation during the delay time τ. The equilibrium longitudinal magnetization is fully recovered as τ increases. Finally, the longitudinal magnetization is converted into transverse magnetization by a 90° pulse for detection. This experiment was run at τ values of 0.2, 0.4, 0.8, 1.5, 2, 3, 4.5, 6 and 8 s. T_1 was determined by least squares fit of the signal intensities, S(τ), to the equation $S(\tau) = S_0 + A\,e^{-\tau/T_1}$.

In the Hahn echo experiment (90° – τ/2 – 180° – τ/2 – FID), the 90° pulse rotates the equilibrium longitudinal magnetization into the *x-y* plane, and this is followed by a 180° pulse that refocuses the dephased magnetization and generates an echo signal, $S(\tau)$. The spin coherence, $S(\tau)$, is lost as τ increases, and T_2 was found by a least square fit to the equation $S(\tau) = A\,e^{-\tau/T_2}$.

A sample of ~200 mg dried and purified elastin fiber (~ 2 mm × 29 mm) prepared in a similar manner that described above and analyzed in the 700 MHz spectrometer. The fiber was equilibrated overnight against 10% ^2H_2O/ ^1H_2O solution to a known mass, inserted into a 5 mm NMR tube and then inserted into the unmodified cryoprobe. ^{13}C NMR spectra without magic angle spinning of the relaxed and ~ 122 % stretched elastin fiber were obtained and the relaxation times, T_1 and T_2 were determined using Carr-Purcell-Meiboom-Gill (CPMG) echo and inversion recovery pulse sequences with 4 s recycle delays.[89, 90]

3.2.2 The Order Parameter (*S*) Analysis

Natural elastin is a highly cross-linked proteinaceous material. Because it is highly cross-linked, macromolecular reorientation of the protein does not take place. Thus, the order parameter (*S*) for backbone motion can be estimated directly from the linewidth of the spectra obtained without magic angle spinning (MAS), and motional averaging of the residual shielding tensor is due only to the flexibility of the protein backbone.

The ^{13}C NMR carbonyl peak of hydrated elastin is well separated from other peaks with a large static shielding anisotropy (~116 ppm), and most of the carbonyl groups are from the protein backbone. These factors make the carbonyl peak the optimum ^{13}C signal

to be used to estimate the order parameter (S) for chain motions. The linewidth of the carbonyl peak is a sum of three contributing factors: (*i*) the range of carbonyl isotropic chemical shifts of the different amino acid residues in elastin, (*ii*) the contribution of the spin relaxation time, T_2, to the linewidth ($\frac{1}{\pi T_2}$) and (*iii*) the residual shielding anisotropy ($\Delta\sigma_{Res}$). To account for factor *i*, the carbonyl isotropic chemical shifts were predicted for the amino acid sequence of bovine tropoelastin (the monomer of elastin)[91] using sequence corrected random coil shifts (https://spin.niddk.nih.gov/bax/nmrserver/Poulsen_rc_CS). This routine correctly predicted the experimentally obtained ^{13}C carbonyl shifts in a minielastin studied before.[60, 92] To account for factor *ii*, the experimental spin relaxation time T_2 was convoluted with the chemical shifts using a MATLAB script to generate a simulated carbonyl spectrum that accounts for factors *i* and *ii* described above. The simulated and experimental spectra, (Figure 3.5), are well described by a Lorentzian line shape with signal intensity, I(ppm), given by

$$I(ppm) = \ C\frac{W}{1+\left(\frac{2}{W}(ppm-ppm_0)\right)^2}\ , \qquad\qquad \text{Eq. 3.1}$$

where C is a constant and W is the linewidth.

The residual anisotropy ($\Delta\sigma_{Res}$) is then the difference between the linewidths of the experimental and simulated spectra. In turn, the backbone order parameter was calculated as $S = \ \Delta\sigma_{Res}/\ \Delta\sigma_{Stat}$.[86] The static anisotropy ($\Delta\sigma_{Stat}$) is approximately constant for different polypeptides and was estimated for peptide carbonyls using data compiled by Duncan, $\Delta\sigma = \frac{3}{2}(\delta_{33} - \delta_{iso}) = 116 \text{ ppm}$, where δ_{33} is the largest traceless principal

component of the chemical shift tensor and δ_{iso} is the average of the three principal components of the chemical shift tensor.[93]

3.2.3 Relaxation Rates Analysis

The relaxation rates, $R_1 = T_1^{-1}$ and $R_2 = T_2^{-1}$, of the ^{13}C carbonyl (^{13}C′) were measured at two NMR frequencies, 500 and 700 MHz, with the elastin fiber relaxed and stretched. This data was used to analyze dynamics of the backbone of the natural purified elastin.

The relaxation rates of ^{13}C′ are the result of two relaxation mechanisms that arise from the dipole-dipole (DD) coupling and the chemical shift anisotropy (CSA), Eq. 3.2 – 3.7.[94-96] The DD mechanism arises due to the fluctuations in the magnitude and direction of the magnetic field of the spin as a result of dipole -dipole interaction with a neighboring nuclear spin, and the CSA relaxation mechanism results from the fluctuations in the magnitude and direction of the local magnetic field produced by the electron currents of the molecule due the external magnetic field. The CSA mechanism is dominant in these experiments due to the high magnetic fields used and the large static shielding anisotropy.[71] The standard expressions for the relaxation rates are given below.

$$R_1 = R_1^{DD} + R_1^{CSA} \qquad \text{Eq. 3.2}$$

$$R_2 = R_2^{DD} + R_2^{CSA} \qquad \text{Eq. 3.3}$$

$$R_1^{DD} = \frac{1}{4\,r_{HC}^6}\left[\mu_0\,h\,\gamma_H\gamma_C\right]^2 \times \left[J(\omega_H - \omega_C) + 3\,J(\omega_C) + 6\,J(\omega_H + \omega_C)\right] \qquad \text{Eq. 3.4}$$

$$R_1^{CSA} = \frac{3}{4}\,\delta_{z'}^2\left(1 + \frac{\eta^2}{3}\right)\gamma_C^2\,B_0^2\,\left[J(\omega_C)\right] \qquad \text{Eq. 3.5}$$

$$R_2^{DD} = \frac{1}{8\,r_{HC}^6}\left[\mu_0\,h\,\gamma_H\gamma_C\right]^2$$

$$\times\left[4\,J(0) + J(\omega_H - \omega_C) + 3\,J(\omega_C) + 6\,J(\omega_H) + 6\,J(\omega_H + \omega_C)\right] \qquad \text{Eq. 3.6}$$

$$R_2^{CSA} = \frac{1}{8}\,\delta_{z'}^2\left(1 + \frac{\eta^2}{3}\right)\gamma_C^2\,B_0^2\left[4J(0) + 3\,J(\omega_C)\right] \qquad \text{Eq. 3.7}$$

where r_{HC} is the distance between the ^{1}H and ^{13}C and set to be 1.69 Å, μ_0 is the permeability of vacuum (1.256637×10^{-6} H/m), h is Planck's constant (6.626×10^{-34} Js), γ_H is the gyromagnetic ratio of ^{1}H (2.67522×10^8 rad s^{-1} T^{-1}), γ_C is the gyromagnetic ratio of ^{13}C (6.7283×10^7 rad s^{-1} T^{-1}), ω_H and ω_C are the Larmor frequencies of ^{1}H and ^{13}C (respectively), $\delta_{z'}$ is the largest traceless principal component ($-$ 77 ppm), η is the asymmetric parameter for the ^{13}C carbonyl (0.81), and B_0 is the static magnetic field of the NMR spectrometer.[71, 93, 95, 96]

The spectral density, $J(\omega)$, used here is the extended Lipari- Szabo model free spectral density in the limit that overall reorientation of the protein is quenched due to cross-linking, $\tau_M \rightarrow \infty$,[96-99]

$$J(\omega) = \frac{2}{5}\left(\frac{(1 - S_F^2)\,\tau_F}{1 + (\omega\tau_F)^2} + \frac{(S_F^2 - S^2)\,\tau_S}{1 + (\omega\tau_S)^2}\right) \qquad \text{Eq. 3.8}$$

S^2 is the generalized order parameter for fast and slow chain motions, τ_F and τ_S are the effective correlation times for fast (F) and slow (S) internal motion, and S_F^2 is the generalized order parameter for fast chain motions ($S^2 = S_F^2 S_S^2$). S_F^2 was constrained to the range of $0.4 - 0.6$ that was found in studies of minielastins.[96]

The experimentally determined R_1 and R_2 values at the two magnetic fields (500 MHz and 700 MHz) were fit using Eq. 3.2 – 3.7 with the spectral density function, Eq. 3.8,

to determine the timescales of the backbone motions in natural elastin using MATLAB scripts. Because the relaxation rates for relaxed and stretched were the same within the experimental error, their average rates were used in the data fit. The optimum fit parameters (S_F^2, τ_F and τ_S) were obtained by a grid search for the minimum chi square (χ^2) defined in Eq. 3.9.[95, 96]

$$\chi^2 = \Sigma_{500,\, 700\text{ MHz}} \left[\left(\frac{R_{1,e} - R_{1,c}}{\sigma_{R_{1,e}}} \right)^2 + \left(\frac{R_{2,e} - R_{2,c}}{\sigma_{R_{2,e}}} \right)^2 \right] \qquad \text{Eq. 3.9}$$

The subscripts "e" and "c" indicate the experimentally measured relaxation rates and the calculated rates, respectively, σ is the experimental standard error of the relaxation rates, and the sum is over the two NMR frequencies, 500 MHz and 700 MHz.

A second MATLAB script was used to calculate standard errors of the optimum fit parameters. Five hundred data sets of relaxation rates, R_1 and R_2, were generated randomly with a normal distribution that used the optimum fit rates and the experimental uncertainties as the Gaussian means and standard deviations, respectively. Then, fit parameters were obtained for each data set with the same routine that was used to fit the experimental rates. This created a distribution of values for each fit parameter, and error limits were calculated as the standard deviation of this distribution. The root mean square deviation (RMSD) of the relaxation rates back calculated from the fit parameters was within two standard deviations of the experimental error (σ) of the experimental relaxation rates.[96]

3.3   Results and discussion

Static, natural abundance ^{13}C NMR was used to study backbone ordering and the timescales of dynamics in natural, purified elastin when relaxed and when subjected to

mechanical strain. ^{13}C spectra were acquired at two magnetic fields. the spectra of stretched elastin (red) are essentially superimposable on the relaxed spectra (black) at both magnetic fields, (Figure 3.2). This is particularly apparent in the spectrum obtained on the 700 MHz instrument with higher signal to noise. Also note that the carbonyl signal (170 – 180 ppm) is well separated from other carbon signals.

R_1 and R_2 relaxation data, (Figure 3.3), was used to determine the relaxation rates, (Table 3.1). Within experimental error, both R_1 and R_2 are unaffected by applying mechanical strain. For further analysis, averages of the stretched and relaxed values were used. Intriguingly, R_2 at both magnetic fields is ~ 3 orders of magnitude faster than R_1. Also, R_1 increases at the higher magnetic field but R_2 is the same within experimental error. Previously reported values of R_1 and $R_{1\rho}$ obtained from material prepared by harsh purification techniques were similar to the ones obtained in this work.[69, 72, 100, 101]
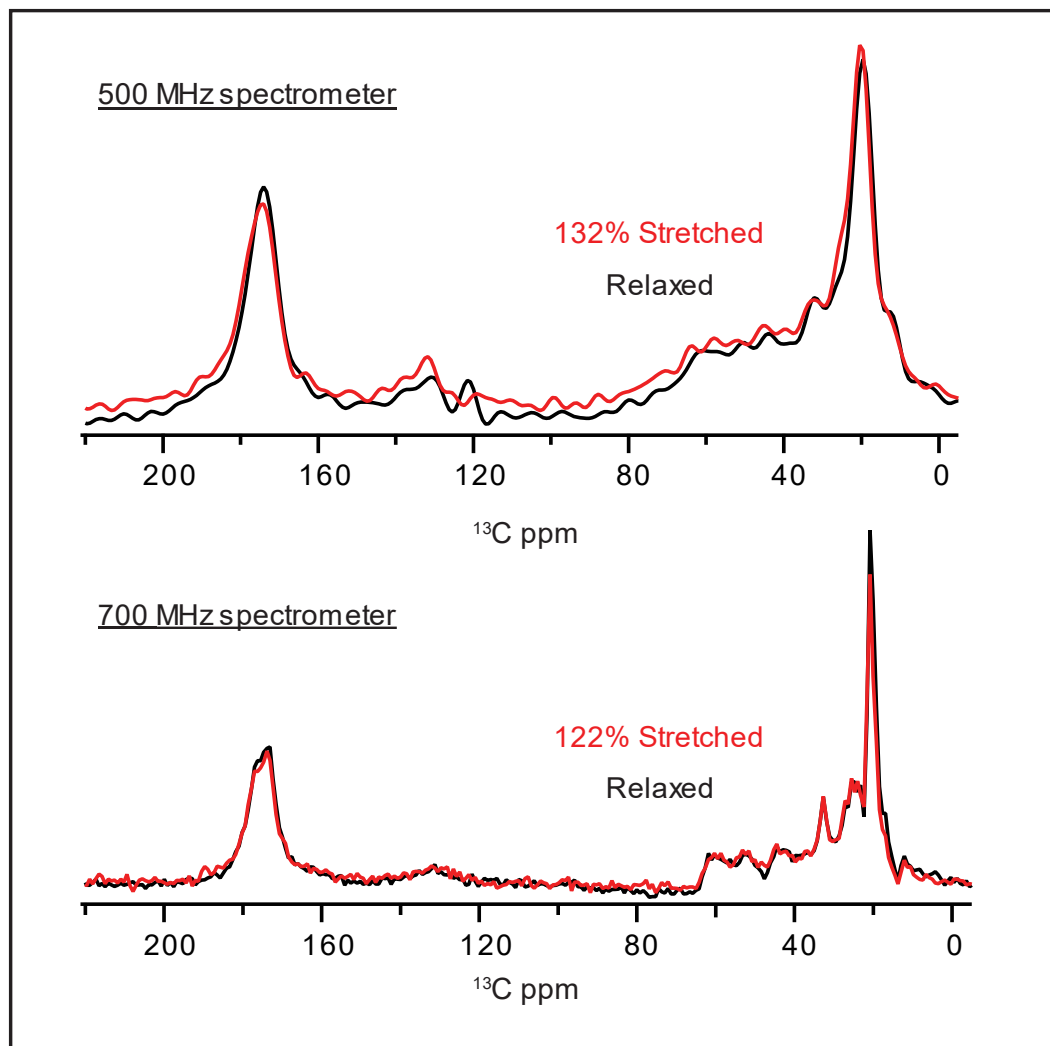
Figure 3.2. Static natural abundance ^{13}C NMR spectra of hydrated elastin both relaxed (black lines) and stretched (red lines) in 500 MHz and 700 MHz spectrometers.
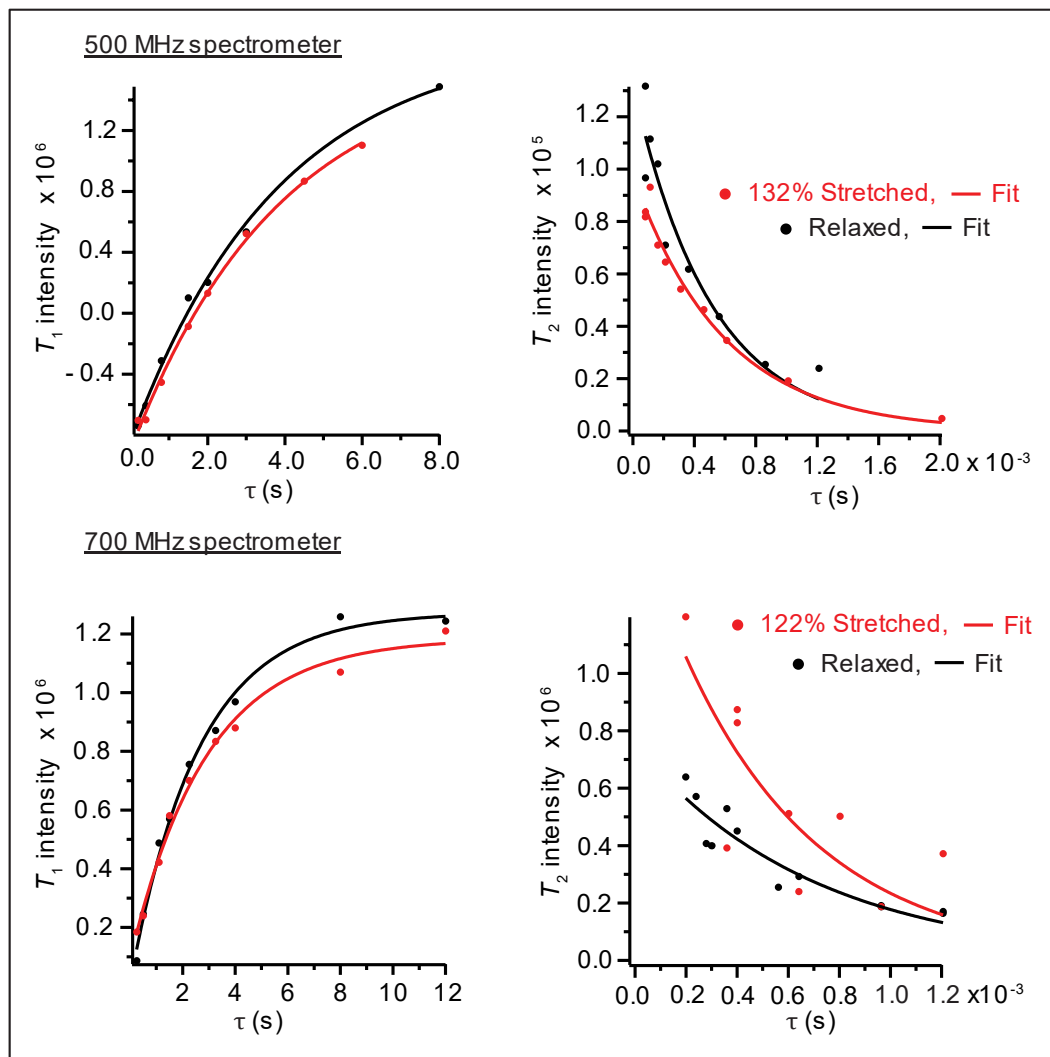
Figure 3.3. T_1 and T_2 of ^{13}C carbonyl of hydrated elastin both relaxed (black lines) and stretched (red lines) in 500 (upper panels) and 700 MHz spectrometers (lower panels).

Table 3.1. Carbonyl ^{13}C R_1 and R_2 of relaxed and stretched hydrated bovine elastin in 500 MHz and 700 MHz spectrometers.

Experiment		R_1 of $^{13}C'$ (s^{-1})	R_2 of $^{13}C'$ (s^{-1})
	Relaxed	0.26 ± 0.03	$(2.0 \pm 0.4) \times 10^3$
500 MHz spectrometer	132% stretched	0.26 ± 0.03	$(1.7 \pm 0.2) \times 10^3$
	Average	0.26 ± 0.02	$(1.8 \pm 0.2) \times 10^3$
	Relaxed	0.38 ± 0.03	$(1.4 \pm 0.3) \times 10^3$
700 MHz spectrometer	122% stretched	0.35 ± 0.03	$(1.9 \pm 0.6) \times 10^3$
	Average	0.37 ± 0.02	$(1.7 \pm 0.3) \times 10^3$

The linewidth of the carbonyl peak was used to estimate the generalized order parameter using the residual shielding anisotropy ($\Delta\sigma_{Res}$) as described in section 3.2.2. The linewidths of the experimental spectra (black lines) were fit to a Lorentzian function, Eq. 3.1, are 9 – 10 ppm when the fiber is relaxed or stretched, (Figure 3.4).
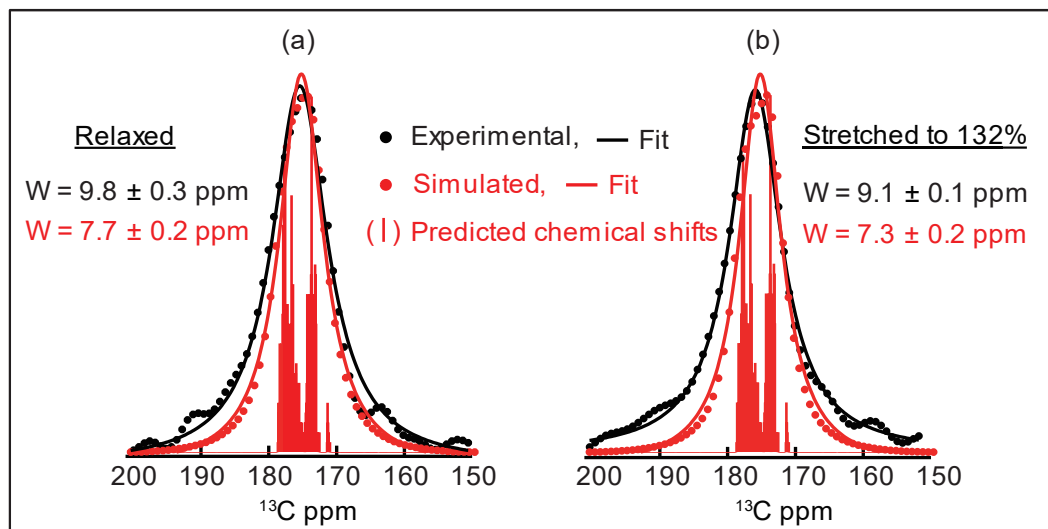
Figure 3.4. Static natural abundance ^{13}C NMR carbonyl spectra, experimental (black) and simulated (red) of hydrated elastin both (a) relaxed and (b) stretched by 132% in 500 MHz spectrometer.

The simulated spectra (red lines in Figure 3.4) account for both the isotropic chemical shifts and the finite line width due to spin- spin relaxation. Narrow lines with the simulated isotropic shifts are the red bars [60, 92, 96] and these were convoluted with the experimentally determined R_2 ($R_2/\pi = 640$ Hz (5 ppm) in relaxed and 540 Hz (4.3 ppm) in stretched spectrum). The linewidths, 7 – 8 ppm, for the simulated peaks were obtained in same manner as the experimental spectra by fitting to Eq.3.1. Then, $\Delta\sigma_{Res}$ is the difference between the linewidths of Lorentzian fits of the experimental and the simulated spectra, and it is in the range of 1 – 3 ppm. Thus, the estimated value of the order parameter ($S = \Delta\sigma_{Res}/ \Delta\sigma_{stat}$) for backbone dynamics in purified elastin is in the range 0.01 – 0.03 and the generalized order parameter (S^2) is ~ 0.001. This is similar to the S^2 values that were determined for the minielastins (24x′ and 20x′) in solution using ^{15}N or ^{13}C NMR relaxation data. Stretch induced ordering of the backbone was not observed within the resolution of these experiments.[96]

The generalized order parameter ($S^2 \approx 0.001$) combined with the average relaxation rates, (Table 3.1), and the constraint ($0.4 < S_F^2 < 0.6$) were used to determine the timescale of elastin's backbone motions using Eq. 3.2 – 3.8. In this way, four experimental parameters (the average R_1 and R_2 values obtained at two NMR frequencies) were used in 3-parameters fit. The χ^2 surfaces show that the correlation times $\tau_S = 2.3 \pm 0.4$ µs and $\tau_F = 210 \pm 50$ ps were well constrained by the data and that $S_F^2 = 0.49$, is less well determined, (Figure 3.5 and Table 3.2).

Compared to soluble minielastins, the elastin backbone is also highly disordered, $S^2 \sim 0$; however, the correlation time for the slow backbone motion (τ_S)is dramatically lengthened, and the correlation time for fast motions(τ_F) is similar to that in soluble minielastins and longer by only a factor of four.[96] I conclude that cross-links, which occur every 20 – 40 residues in elastin, are highly flexible and have little effect on the amplitude of chain mobility. Because only the rate of the slow backbone motion is substantially affected by cross-linking, these dynamical modes likely occur on length scales comparable to the spacing between cross-links, whereas fast backbone dynamics are at the residue level.
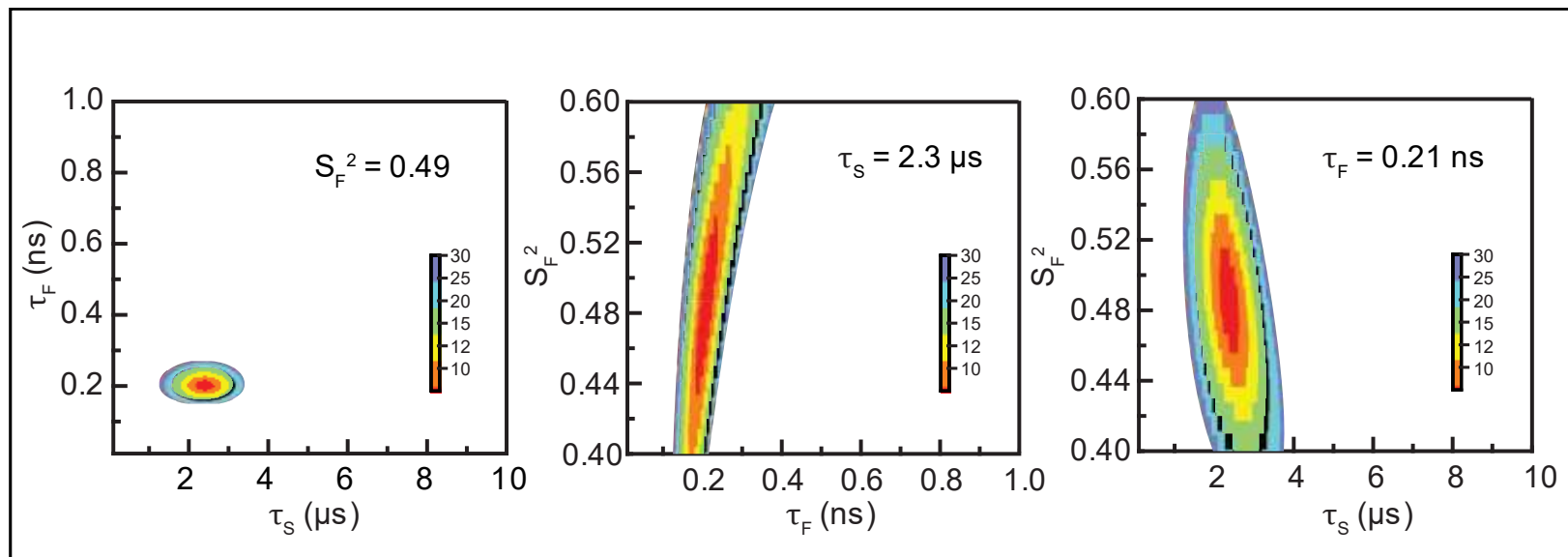
Figure 3.5. χ^2 surfaces of fit parameters to the NMR relaxation rates.

Table 3.2. Fit parameter values obtained by least squares fitting of Eq. 3.2 – 3.8 to the average values of the NMR relaxation data in table 3.1.

Parameter	value
S_F^2	0.49 ± 0.07
τ_F (ps)	210 ± 50
τ_S (μs)	2.3 ± 0.4
rmsd R_1 (s^{-1})	0.0015
rmsd R_2 (s^{-1})	674

CHAPTER 4 THERMOMECHANICAL PROPERTIES OF ELASTIN

4.1   Introduction

The mechanical properties of natural elastin were studied by Weis-Fogh et al. and later, more extensively by Gosline and coworkers using microcalorimetry.[8, 84, 102] They assumed no changes in the fiber volume upon stretch, so they defined the work of stretch of the hydrated elastin as the stored energy (ΔA). They found that the heat released (Δq) upon stretching hydrated elastin is larger than (ΔA) of stretch. Insofar as elastin stretch is reversible, which is confirmed herein, the 2nd law of thermodynamics requires that the entropy change upon stretch, $\Delta S = -\Delta q/T$, is large and negative. Thus, the internal energy and the entropy changes for stretching are both large and negative, so spontaneous recoil is driven by a large increase in entropy and elastin is known as an entropic elastomer. In the ideal spring model, approximately correct for rubber, the heat released upon stretch is much smaller and the change in internal energy is negligible.[103]

Weis-Fogh measured the heat liberated at room temperature upon stretching the fiber by ~ 35% to be five times greater than the applied mechanical work. This corresponds to an internal energy change of ~ – 5 mcal/35mg with an applied mechanical work of ~ 1.3 mcal/35mg.[8]

The more extensive study performed later by Gosline on hydrated bovine elastin found that the ratio of the internal energy change to the applied mechanical work varies inversely with stretch. The ratio of the heat released to work done at 22 °C is 91 for 2% stretch and 3 for 70% stretch. Also, the internal energy change upon stretch varies significantly with temperature over the range of 2 °C – 65 °C. It is large and negative at low temperatures and increases until it reaches ~ zero at 65 °C.[84] This temperature dependence is similar to that associated with hydrophobic interactions. In the hydrophobic effect, water interacting with a hydrophobic surface decreases the entropy of water[84, 102] and this is known to be the dominant force in protein folding.[104, 105] Whereas in the widely accepted Flory model of rubber elasticity, the decrease in entropy upon stretch is due to a decrease in configurational entropy of the polymer.[9] This has not been proven and the alternative, recoil driven by hydrophobic forces, has not been disproven.

An important aspect of Flory's disagreement with Gosline is that Gosline's calculation of the large decrease in energy had neglected any change in volume with temperature and stretch. In thermodynamic terms, Gosline had assumed that the relevant thermodynamic state function was Helmholtz free energy (ΔA) and Flory correctly pointed out that Gosline's measurements were made at constant pressure, in which the correct state function is Gibbs free energy, $\Delta G = \Delta A + P\Delta V$. Flory et al reported no changes in the volume of elastin fiber only when it is hydrated in the presence of a diluents like glycol-water (3:7) mixture or 30% PEG. With these conditions, no change in the internal energy of elastin is reported upon strech.[7, 9] However, Flory and co-workers disregarded that their system is a three-component system and neglected the effect of glycol on both the fiber and water. Later, Flory modified his elastic theory for elastin to include the effects of

solvent interacting with the protein surface, but he did not explicitly consider hydrophobic interactions. It is worthy to note that rubber is fully elastic in the absence of solvent, whereas elastin, the most hydrophobic protein known, is fully inelastic in the absence of water. A full understanding of recoil in elastin should also account for other differences. Unlike rubber, the stretch/recoil cycle for elastin is fully reversible (vide infra), the elastic modulus of elastin is much less, and elastin has a much lower extension without rupture.

Strain-induced changes in free energy (ΔG) and entropy (ΔS) have not previously been reported to my knowledge and the large release of heat upon stretch indicates that the change in length as a function of temperature is a sensitive method for determining a complete force (F) as a function of length (l) and temperature (T) state function for elastin. From the state function, $F(l,T)$, all relevant thermodynamic properties can be determined. Importantly, volume changes with both temperature and force at constant hydration are readily determined and reported using a novel apparatus. Thus, in this Chapter, all relevant thermodynamic properties have been determined as a function of temperature and stretch in (*i*) pure water, (*ii*) with the addition of Hoffmeister ions or polyethylene glycol and (*iii*) when ^1H_2O is replaced with ^2H_2O. By performing all experiments on a single elastin fiber, the exceptional reversibility of the stretch contract cycle of elastin and its unusual physical robustness are confirmed.

Kosmotropes, like sulfate ion perturb the hydrophobic effect and make it difficult to create the cavity needed to accommodate hydrophobic solutes by increasing surface tension.[80, 81] PEG has a similar effect but through preferentially increasing protein hydration.[37, 42, 44] On the other hand, chaotropes, like perchlorate ion perturb protein

structure by interacting with the amide backbone, either through specific or nonspecific ion interactions.[80, 82, 83]

Compared to ^1H_2O, ^2H_2O is a more structured liquid and has stronger solvent-solvent hydrogen-bonds.[49, 51] ^2H_2O stabilizes β-turns structures and destabilizes α-helices.[59] It is believed that ^2H_2O stabilizes folded proteins more than ^1H_2O by affecting the hydrophobic interactions and/or hydrogen-bonding.[54-57] Thus, ^2H_2O is also expected to perturb the hydrophobic effect.

4.2   Theory

Based on the 1st law of thermodynamics, $dU = \delta q + \delta W$, where U is the internal energy of the system (hydrated elastin), δq is the energy added as heat, and δW is the work done on the system. Based on the 2nd law of thermodynamics for reversible processes, $\delta q = TdS$ and $\delta W = -PdV + Fdl$, where T is the absolute temperature, S is the entropy, P is the pressure, V is the volume, F is the applied force and l is the length. Consequently,

$$dU = TdS - PdV + Fdl.$$

Using the definition of enthalpy, $H = U + PV$,

$$dH = dU + PdV + VdP$$

$$dH = TdS + VdP + Fdl$$

Using the definition of Gibbs free energy, $G = H - TS$

$$dG = dH - SdT - TdS$$

$$dG = -SdT + VdP + Fdl$$

70

Using the property of the total differential dG(l,T,P), two useful results are obtained,

$$dG(T, l, P) = -SdT + VdP + Fdl$$

$$\left(\frac{\partial G}{\partial l}\right)_{T,P} = F \text{ and } \left(\frac{\partial G}{\partial T}\right)_{l,P} = -S$$

Integrating the first equation gives

$$\Delta G_{T,P} = \int_{l_0}^{l_1} F \, dl \qquad\qquad \text{Eq. 4.1}$$

Equating cross derivatives of the first and second equation, gives the Maxwell relation,

$$-\left(\frac{\partial S}{\partial l}\right)_{T,P} = \left(\frac{\partial F}{\partial T}\right)_{l,P},$$

and after integration,

$$\Delta S_{T,P} = -\int_{l_0}^{l_1} (\partial F/\partial T)_{l,P} \, dl \qquad\qquad \text{Eq. 4.2}$$

The change in enthalpy ΔH_T and the heat capacity ΔC_P can be calculated from the following equations,

$$\Delta H_T = \Delta G_T + T\Delta S_T \qquad\qquad \text{Eq. 4.3}$$

$$\Delta C_P = \left(\frac{\partial \Delta H}{\partial T}\right)_P \qquad\qquad \text{Eq. 4.4}$$

Eq. 4.1– 4.4 are the fundamental relations used in this study for the analysis of the experimentally obtained $F(l,T)$ data of stretching elastin. The changes in Gibbs free energy (ΔG_T) and entropy (ΔS_T) are obtained by integrating the force and the slope of the force versus temperature with respect to the length, respectively. From these, the change in enthalpy (ΔH_T) and the heat capacity ΔC_P are readily obtained.

71

4.3   Materials and Methods

4.3.1   The Homebuilt Apparatus

The apparatus used for the thermomechanical experiments in this Chapter is a box-shaped (rectangular prism) tank that has 5 faces. The upper face ($8.0 \times 3.0 \times 1.5$ cm) is the lid of the tank and contains two holes designed to insert the heating rod (side) and the thermometer (middle) The right and the left side faces of the tank ($30.0 \times 6.0 \times 1.5$ cm) have an upper groove that matches the dimension of the lid, (Figure 4.1, right panel). The inner right-side face contains a groove to fit a 200 mm ruler. Also, the right side has two holes (0.25 cm in diameter): one is 4 cm down from the lid and the other is 2 cm above the base. Two hollow aluminum rods (0.25 cm outer diameter and 0.2 inner diameter) go through these holes that are connected to pipes, and in turn connected to a pump. The remaining two faces ($30.0 \times 3.0 \times 1.5$ cm) form the front and the back faces of the tank. The whole apparatus is made of Delrin (Online Metal Supply LLC, Houston, MO) except the front and the back faces that are made of Plexiglass (Online Metal Supply LLC, Houston, MO) to give clear vision for the camera. The five faces are fixed together and to a bigger base ($18.0 \times 18.0 \times 1.5$ cm) by screws, (Figure 4.1, left panel). The base has a screw that run through it to the inner compartment of the tank, intended to hold the sample.
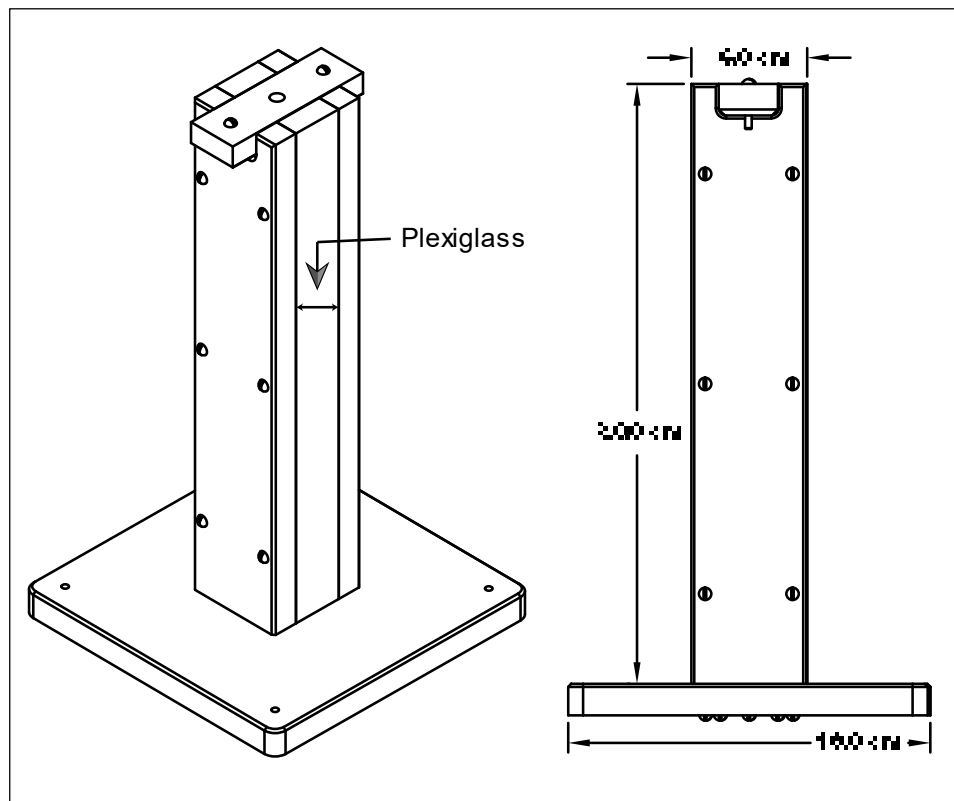
Figure 4.1. Schematic presentation of the assembled homebuilt apparatus.

4.3.2   Sample Setup

A 0.24 g dried and purified nuchal bovine elastin fiber (~ 77 mm × 1.6 mm × 6.4 mm; ~240 mg) was glued to rods at both ends. The upper rod was attached to a thread and the lower rod was fixed to the screw in the base of the homebuilt apparatus, (Figure 4.2).

Outside of the sample compartment, the thread was passed over a light, low friction pulley and attached to calibrated masses to vary the force applied to the fiber. Thus, the applied force equals the attached mass in kg multiply by the gravitational acceleration (9.8 m/s^2). The temperature was regulated through a homebuilt controller with a platinum

resistance thermometer and a rod heater in connection with a proportional-integral-derivative controller (Omron PID e5cc controller with pt100 sensor).

Figure 4.2. The thermomechanical setup. The fiber length, temperature and masses are recorded by the camera.

Temperature variation over each measurement was within 0.1 K and the equilibration times between $l(F)$ and $l(T)$ measurements were 5 min and 3 – 5 min, respectively. Furthermore, the solvent/solution inside the compartment was circulated using a pump that was connected to the pipes in the right side of the apparatus. The fiber length was measured with a 36-megapixel camera (Sony A7R) giving a length accuracy of 0.1 mm which was calibrated using the 200 mm ruler inside the apparatus that was included in every photograph. ImageJ software, was used to convert pixels into mm.

Length versus force, $l(F)$, at fixed temperatures and length versus temperature, $l(T)$, at fixed forces were measured for hydrated purified bovine elastin fiber in the following aqueous solutions: deionized water, 0.1 mol/kg sodium sulfate (Na_2SO_4 ACS, Fisher Chemical, Fair Lawn, NJ), 0.3 mol/kg sodium sulfate, 15% (w/w) 20 kDa PEG (Polyethylene glycol 20,000, Alfa Aesar, Ward Hill, MA), 30% (w/w) 20 kDa PEG, ^2H_2O (99.9% D, Sigma-Aldrich, St. Louis, MO), 0.3 mol/kg sodium perchlorate ($NaClO_4$ ACS 98.0-102.0%, Beantown Chemical Corporation, Hudson, NH) and 1.0 mol/kg $NaClO_4$.

$l(F)$ was measured from 0.09 N to 0.72 N at fixed temperatures from 278 to 318 K in 5 K increments when possible. $l(T)$was measured from 274 to 328 K in 1 K increments at fixed forces of 0.09 N, 0.23 N, 0.40 N and 0.72 N when possible.

4.3.3 Data Processing

Complete state functions, $l(F,T)$, for each of the solutions described above were obtained by combining experiments of $l(F)$ at different temperatures and $l(T)$ at different forces. The linear $l(F)$ data and non-linear $l(T)$ are well-fit by a polynomial that is 1st-order in F and 3rd-order in T over the range of F and T studied here. The two sets of experiments

were combined into a 2-dimensional array and are well-fit to the following polynomial, i.e., virial equation of state using MATLAB scripts:

$$l(F,T) = c_0 + c_1 F + c_2 T + c_{12} FT + c_3 T^2 + c_4 T^3 \qquad \text{Eq. 4.5}$$

Both the goodness of the fit statistics, (Table 4.1), and the virial coefficients of the above equation, (Table 4.2), were obtained from MATLAB Curve Fitting Toolbox™.

Table 4.1. Goodness of the fit statistics.

Solution	SSE (m^2)	R-square	Degree of freedom	adjusted R-square	RMSE (m)
^1H_2O	2.00×10^{-5}	0.998	302	0.998	2.57×10^{-4}
^2H_2O	6.84×10^{-5}	0.994	466	0.994	3.83×10^{-4}
0.1 mol/kg Na$_2$SO$_4$	1.80×10^{-5}	0.998	327	0.998	2.34×10^{-4}
0.3 mol/kg Na$_2$SO$_4$	1.08×10^{-5}	0.998	309	0.998	1.87×10^{-4}
15% 20 kDa PEG	9.76×10^{-5}	0.989	417	0.989	4.84×10^{-4}
30% 20 kDa PEG	3.81×10^{-5}	0.994	436	0.994	2.96×10^{-4}
0.3 mol/kg NaClO$_4$	1.92×10^{-5}	0.999	494	0.999	1.97×10^{-4}
1.0 mol/kg NaClO$_4$	$4.16 \times 10\text{-}5$	0.996	480	0.996	$2.94 \times 10\text{-}4$

Table 4.2. The virial coefficients of equation 4.6 for all the studied solutions.

Solution	c_0	c_1	c_2	c_{12}	c_3	c_4
^1H_2O	2.7	4.4×10^{-2}	-2.3×10^{-2}	-8.6×10^{-5}	7.0×10^{-5}	-6.9×10^{-8}
^2H_2O	5.2	4.3×10^{-2}	-4.9×10^{-2}	-8.0×10^{-5}	1.6×10^{-4}	-1.6×10^{-7}
0.1 mol/kg Na_2SO_4	3.9	4.2×10^{-2}	-3.6×10^{-2}	-8.0×10^{-5}	1.1×10^{-4}	-1.2×10^{-7}
0.3 mol/kg Na_2SO_4	2.2	4.1×10^{-2}	-2.0×10^{-2}	-7.7×10^{-5}	6.1×10^{-5}	-6.3×10^{-8}
15% 20 kDa PEG	2.0	3.7×10^{-2}	-1.7×10^{-2}	-6.5×10^{-5}	5.3×10^{-5}	-5.4×10^{-8}
30% 20 kDa PEG	0.3	2.4×10^{-2}	-2.0×10^{-3}	-2.5×10^{-5}	5.7×10^{-6}	-5.2×10^{-9}
0.3 mol/kg $NaClO_4$	1.9	3.7×10^{-2}	-1.6×10^{-2}	-6.1×10^{-5}	4.9×10^{-5}	-4.8×10^{-8}
1.0 mol/kg $NaClO_4$	1.7	3.7×10^{-2}	-1.5×10^{-2}	-6.3×10^{-5}	4.6×10^{-5}	-4.8×10^{-8}

The sum of squares due to error (SSE) measures the total deviation of the experimental fiber length (l) to the fit obtained using equation 4.5. SSE ~ 0 indicates the fit has a small random error. R-square is the square of the correlation between l and the fit values. This value is close to 1, indicating that a greater proportion of variance is accounted for by the fit. The adjusted R-square considers the residual degree of freedom, the number of data points minus the number of fitted coefficients. The adjusted R-square being close to 1 indicates a good fit. The root mean squared error (RMSE), the fit standard error, estimates the standard deviation of the random component in the data. As SSE, the closer it gets to 0 the better the fit.

The state function $F(l,T)$ in Eq. 4.6 is obtained by solving Eq. 4.5 for F.

$$F(l,T) = \frac{(l - c_0 - c_2 T - c_3 T^2 - c_4 T^3)}{c_1 + c_{12} T} \qquad \text{Eq. 4.6}$$

Finally, the changes in entropy (ΔS_T), Gibbs free energy (stretch work = ΔG_T), enthalpy (ΔH_T) and heat capacity (ΔC_p) with stretch were determined using Maxwell relations as defined in the theory section,[7, 106, 107] numerical integration and differentiation functions in MATLAB and Eq. 4.1 – 4.4, 4.6. Tables of thermodynamic parameters calculated in this way for all solutions at different temperatures and strains are listed in Appendix A (Table A.3 – A.7).

4.4   Results and Discussion

The hydrated elastin fiber length increases linearly with an increase in the applied mechanical force at all temperatures and decreases nonlinearly with the increase in temperature at constant force in all solutions. Solvent deuteration, addition of a Hoffmeister

kosmotrope (sulfate ion) or a protein precipitant (PEG) significantly alter these changes. However, the effect of the Hoffmeister chaotrope is significantly less.

The reversibility and the reproducibility of the results were confirmed in the following section, followed by an extensive description of the results for the hydrated elastin fiber in ^1H_2O and finally ^1H_2O results were compared to the results obtained in the other hydrating solvent/solutions.

4.4.1 Reversibility and Reproducibility

The reversibility of the fiber length with varying force at constant temperature was confirmed by running two cycles of stretch and relax measurements. This test was applied to all $l(F)$ experiments and within the standard errors of the fitted slopes and intercept, repeated stretch and relax cycles are fully reversible, (Figure 4.3). Averages of these two cycles were used for further analysis.
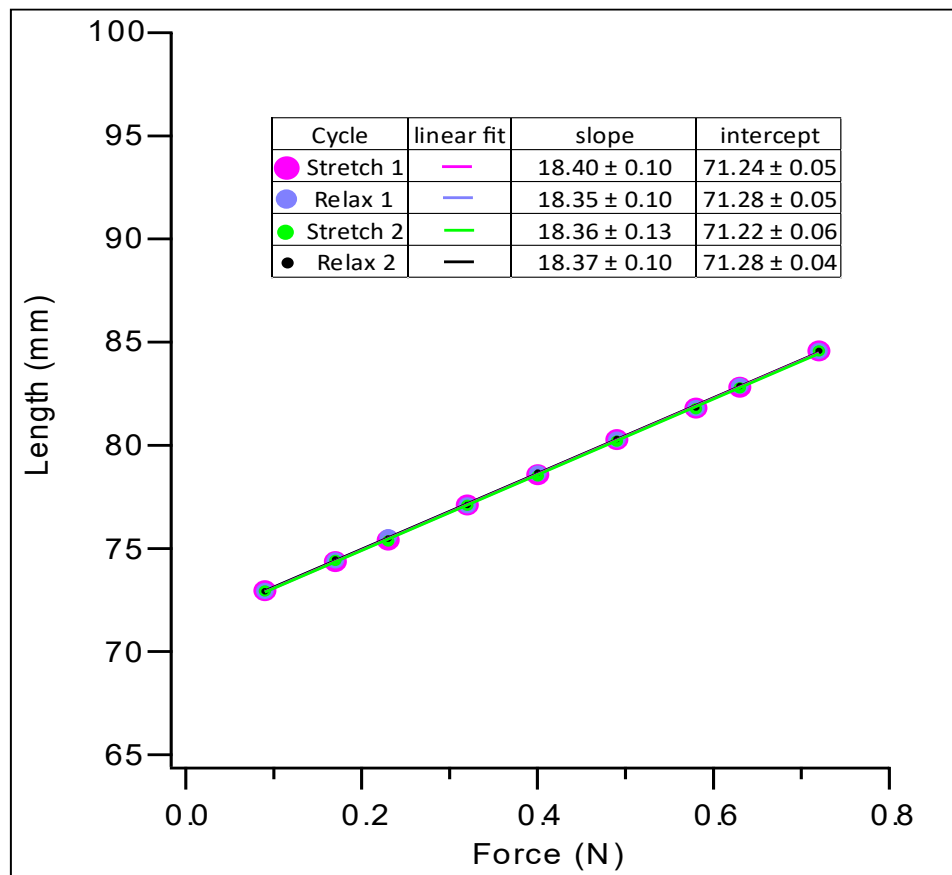
Figure 4.3. Length versus force of two cycles of stretch and relax of the hydrated elastin fiber in ^1H_2O at 298 K and their linear fits.

The reversibility of the fiber length with varying temperature at constant force was confirmed by measuring the length of the fiber while the fiber was cooled back to room temperature in representative $l(T)$ experiments, (Figure 4.4). Within the error limits of the measurement, temperature reversibility is also seen.
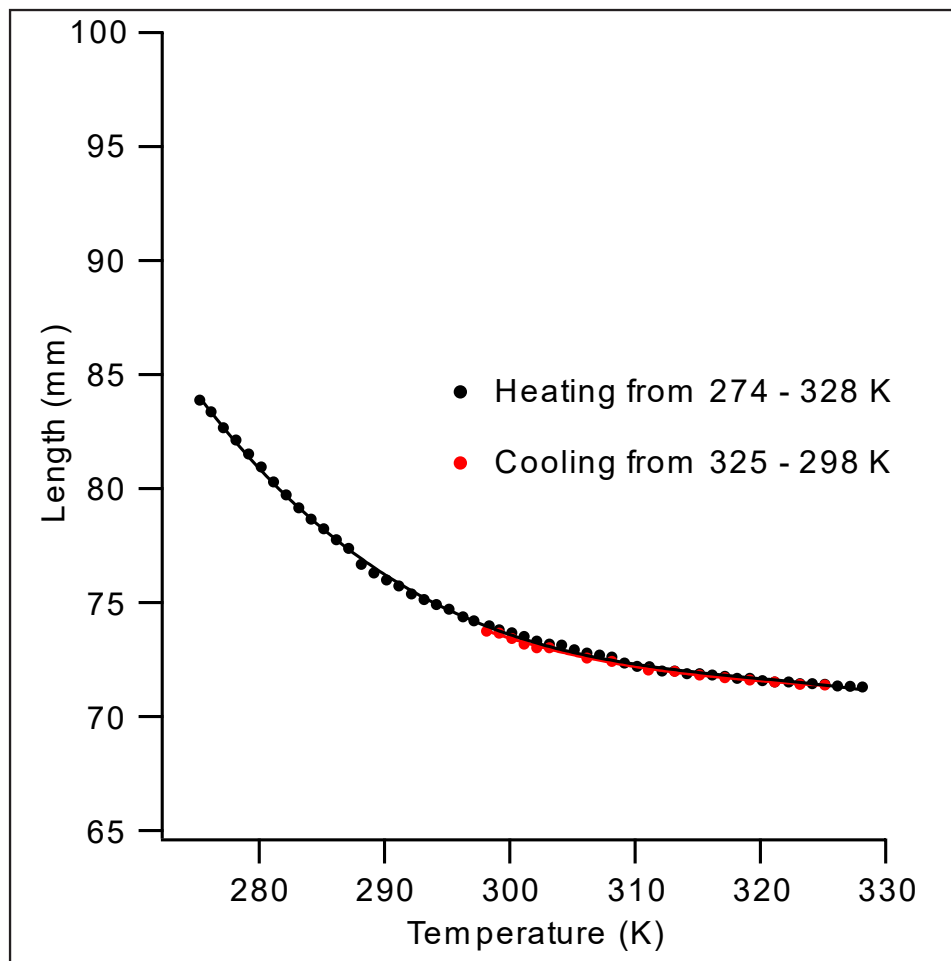
Figure 4.4. Length versus temperature at 0.23 N of the hydrated elastin fiber in 0.1 mol/kg Na_2SO_4 of heat and cool cycle.

All experiments at different solutions were performed on the same fiber to minimize experimental variations. In order to confirm no changes took place in the fiber as a result of the stretching and thermal cycles, the $l(T)$ curve at 0.40 N in ^1H_2O was accurately reproduced after finishing each of the investigated solutions, (Figure 4.5).
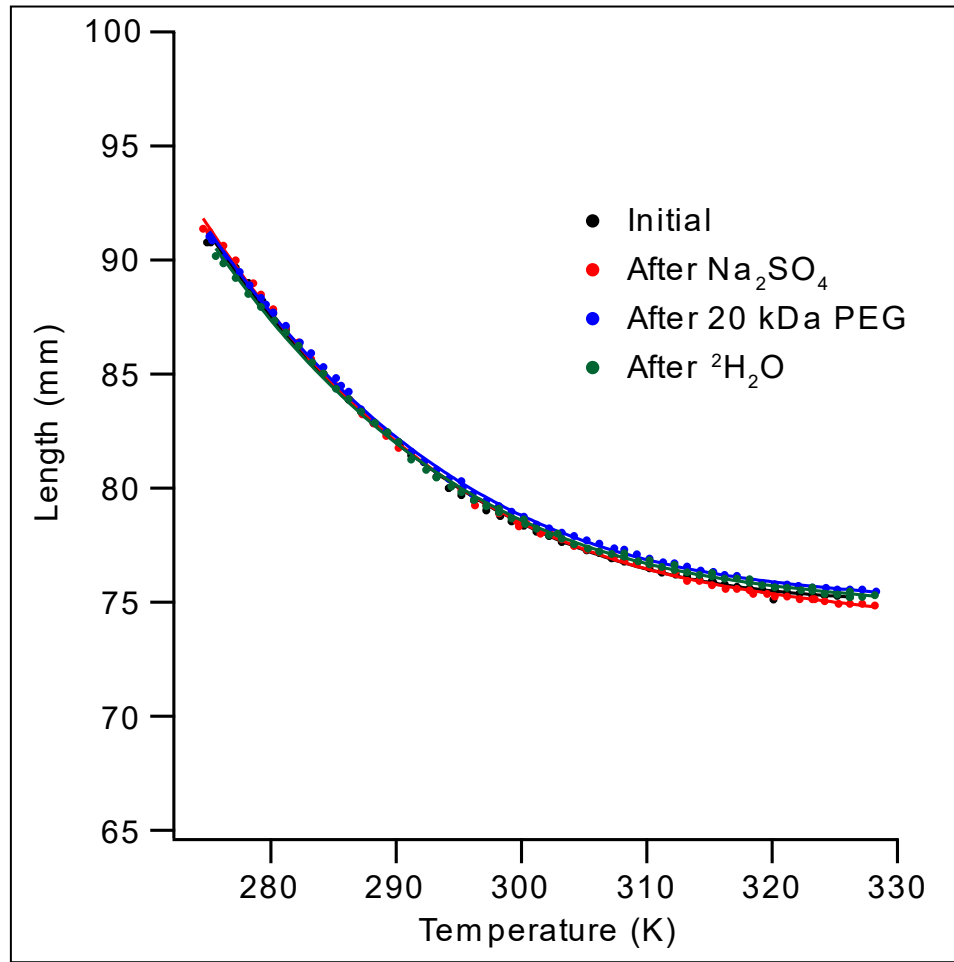
Figure 4.5. Length versus temperature at 0.40 N of the hydrated elastin fiber in ^{1}H$_2$O initially and after finishing each of the studied solutions.

4.4.2   Hydration of Elastin fiber in ^{1}H$_2$O

4.4.2.1 $l(F)$ Experiments in ^{1}H$_2$O

The first set of experiments were performed on the hydrated elastin fiber in deionized water (^{1}H$_2$O). $l(F)$ shows that the length increases linearly with increasing applied mechanical force at all studied temperatures, (Figure 4.6). $l(F)$ data was fit to Eq. 4.7, (Table 4.3).

$$l(F)_T = a + bF \hspace{4cm} \text{Eq. 4.7}$$

The relaxed length (the fit intercept (a) in Eq. 4.7) decreases as temperature increases, i.e., the fiber shrinks with the increase in temperature. Also, the slope of the fit (b) decreases as the temperature increases. It is important to note that the slope is an indirect measure of the elasticity of the fiber. As the slope decreases, the fiber becomes stiffer.
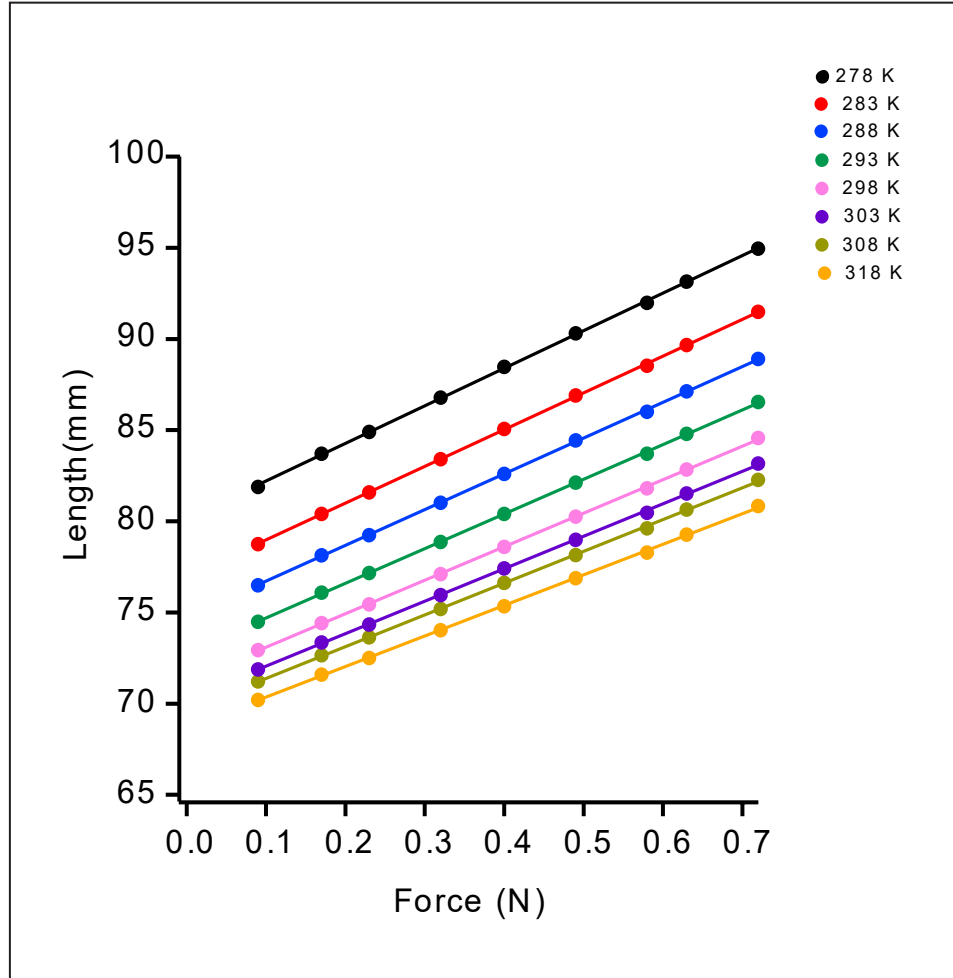
Figure 4.6. The length of the hydrated elastin fiber in $^{1}H_2O$ as a function of the mechanical force of stretching at all studied temperatures.

Table 4.3. The linear fit parameters of $l(F)$ of hydrated elastin in ^1H_2O at all investigated temperatures.

Temperature (K)	$l(F)$ slope (b)	$l(F)$ intercept (a)
278	20.6 ± 0.1	80.16 ± 0.06
283	20.2 ± 0.1	76.96 ± 0.04
288	19.6 ± 0.1	74.75 ± 0.04
293	19.0 ± 0.1	72.80 ± 0.04
298	18.4 ± 0.1	71.26 ± 0.04
303	17.8 ± 0.1	70.27 ± 0.05
308	17.4 ± 0.1	69.64 ± 0.05
318	16.8 ± 0.1	68.68 ± 0.05

4.4.2.2 Young's Modulus in $^{1}H_2O$

Young's modulus(E) is a mechanical property used to measure the stiffness of polymers. It correlates the stress to the strain according to Eq. 4.8.

$$E = \frac{\sigma}{\varepsilon} \qquad\qquad \text{Eq. 4.8}$$

The stress (σ) is defined as the applied force (F) per cross sectional unit area of the polymer (A_{cross}), $\sigma = \frac{F}{A_{cross}}$ and the strain (ε) is the proportional deformation of the polymer ($\varepsilon = \frac{\Delta l}{l_0}$), where Δl is the change in the polymer length and l_0 is the relaxed or unstretched length. Young's modulus increases as the material gets stiffer.

Young's modulus of the hydrated elastin fiber in deionized water was calculated at different temperatures using the dry fiber cross sectional area (6.38×10^{-6} m^2), the initial relaxed lengths (l_0) obtained from $l(F)$ linear fits, and the change of length, Δl, with the applied force from $l(F)$ experimental data. E is well fit to a 3rd-order polynomial, $E(T) = a_0 + a_1 T + a_2 T^2 + a_3 T^3$, with chi square ($\chi^2$) equal 2.94×10^{-6}, (Figure 4.7). E is 0.61 MPa at 278 K, decreases to reach a minimum at 288 K and then increases to ~ 0.64 when the temperature is raised to 310 K, which implies that elastin fiber stiffens with the increase in temperature above 288 K (15 °C).
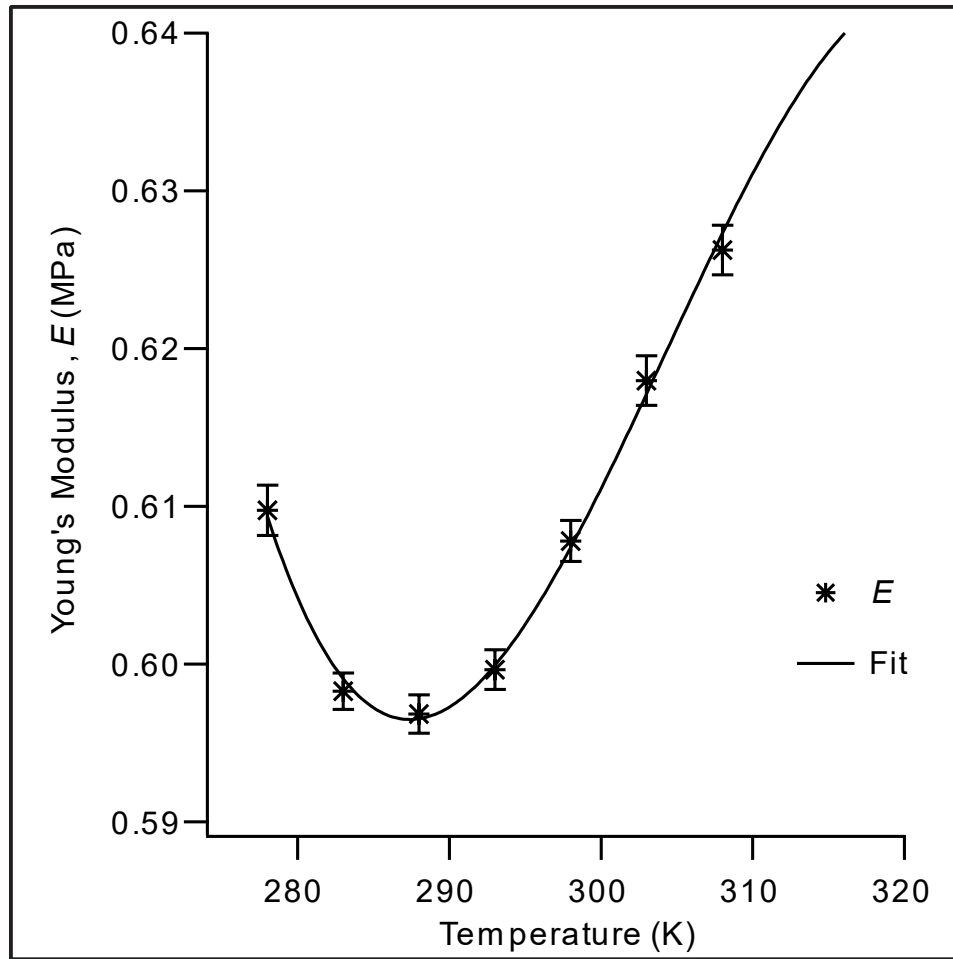
Figure 4.7. Young's modulus (E) of the hydrated elastin in [1]H_2O as a function of temperature and its fit.

4.4.2.3 l (T) Experiments in [1]H_2O

The fiber length as a function of temperature, $l(T)$, at several fixed forces, (Figure 4.8), was investigated and found to decrease substantially with the rise in the temperature. The decrease is nonlinear at all studied forces and $l(T)$ is well fit to a 3rd-order polynomial,

$$l(T) = b_0 + b_1 T + b_2 T^2 + b_3 T^3.$$
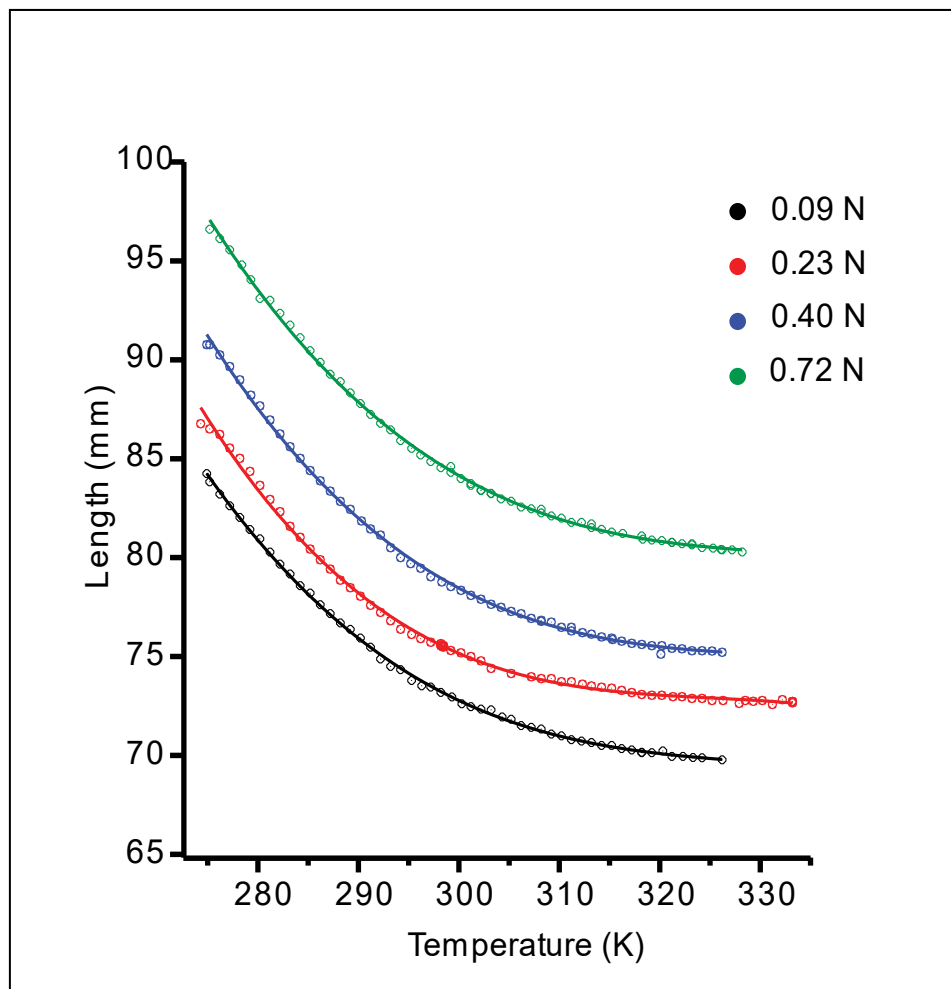
Figure 4.8. The length of the hydrated elastin fiber in ^1H_2O as a function of temperature at all studied forces.

4.4.2.4 Surface Fit of $l(F,T)$ Data in ^1H_2O

The two experiments, $l(F)$ and $l(T)$, were combined to yield the state function $l(F,T)$ (Eq. 4.5), from which the resulting state function $F(l,T)$ (Eq. 4.6) was used to calculate the changes in entropy (ΔS_T), Gibbs free energy (ΔG_T), enthalpy (ΔH_T), and heat capacity (ΔC_p) as a function of temperature at constant strain and as a function of strain at constant temperature.

The large number of highly reproducible data points (>300), and the root mean square error (RMSE) of the fit, 2.2176×10^{-4} m, indicate the high-quality thermodynamic parameters that are obtained from these thermomechanical experiments, (Figure 4.9).
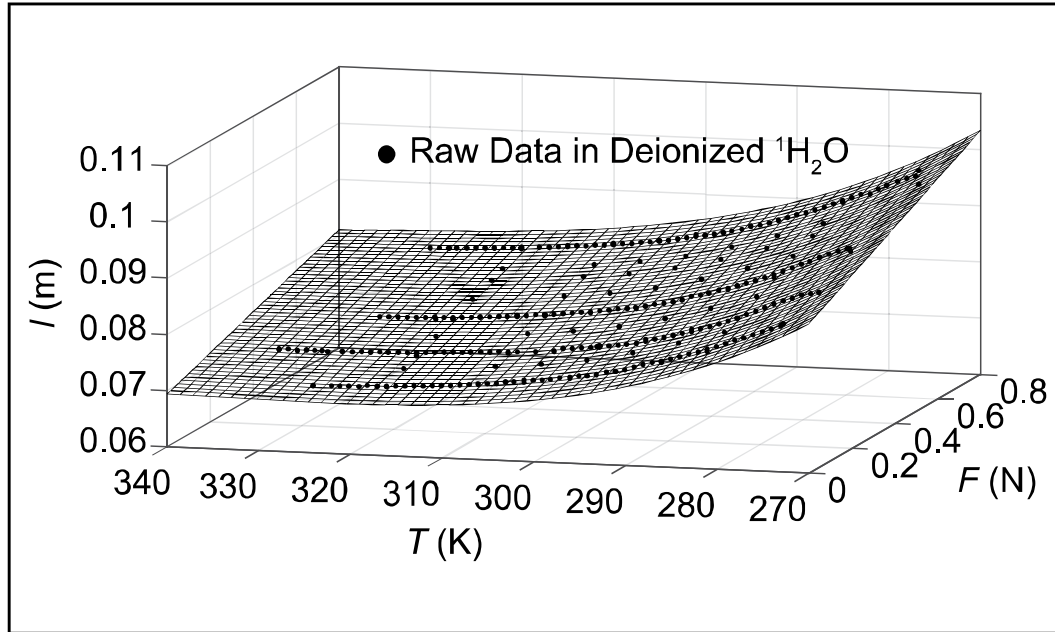
Figure 4.9. Experimental $l(F,T)$ of the hydrated elastin fiber in deionized ^1H_2O stretched from 70 mm to 97 mm at 278 K (5 °C) to 340 K (67 °C) (filled black circles) and the surface fit (mesh surface).

4.4.2.5 Elastin Compared to an Ideal Entropic Elastomer

The temperature dependence of the thermodynamic parameters of recoil are compared between elastin and an ideal entropic elastomer, (Figure 4.10). The comparison is made for equal changes in Gibbs free energy (ΔG_T). Rubber is approximately ideal; however, elastin is quite different.
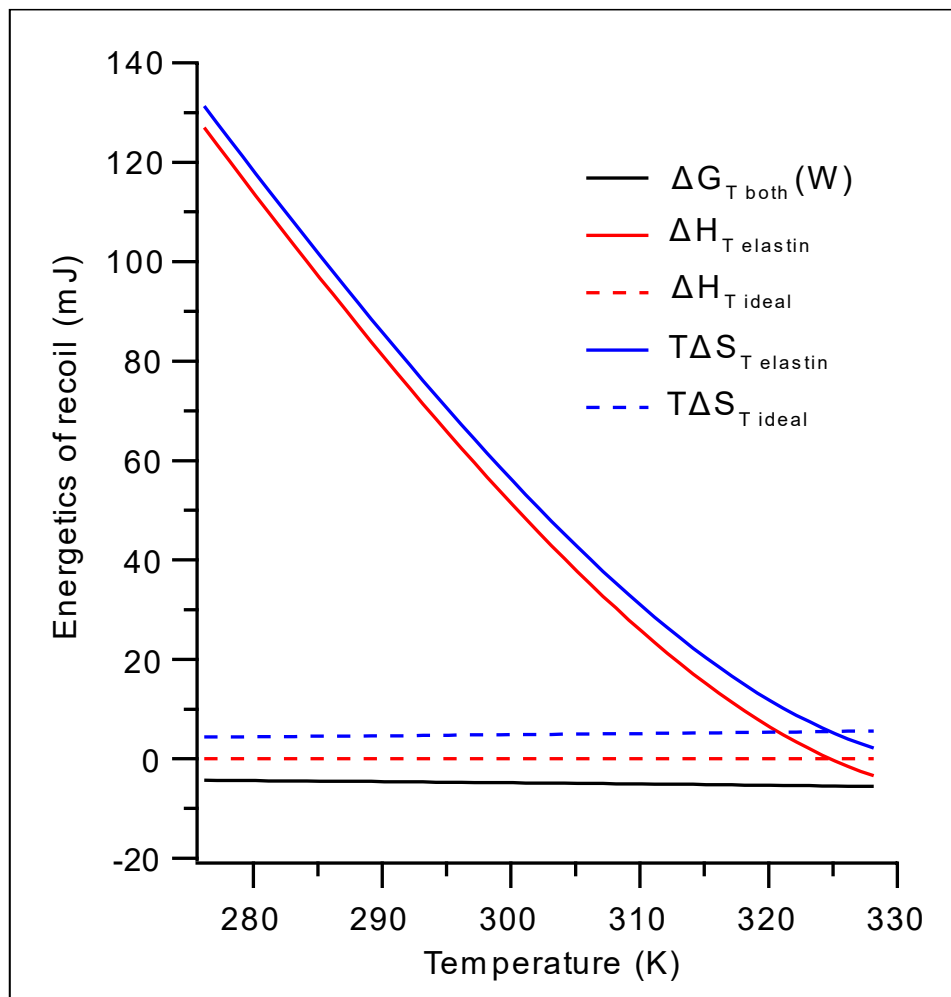
Figure 4.10. The energetics of recoil of 20% stretched elastin fiber hydrated in ^{1}H$_2$O (solid lines) in comparison to the expected energetics of recoil of an ideal entropic elastomer (dash lines) for the same change in the free energy.

Stretching elastin fiber is confirmed to be reversible, thus the energetics of recoil are equal in magnitude to those calculated for stretch with an opposite sign, ($\Delta X_{recoil} = -\Delta X_{stretch}$, X= *G*, *H* and *S*). As expected, the free energy of recoil (ΔG_{recoil}) is negative, and the recoil is spontaneous. For both elastin and the ideal elastomer (rubber), the driving force of recoil is entropic, $T\Delta S < \Delta H$. Otherwise, elastin's energetics of recoil, (solid lines in Figure 4.10) differ completely from that of the ideal entropic elastomer, (dashed lines in Figure 4.10). The ideal entropic elastomer has an enthalpic component ΔH_{ideal} close to zero

at all temperatures and thus ΔG_{recoil} is about the same as $-T\Delta S_{recoil}$.[84, 103] In elastin, ΔH_{recoil} and $T\Delta S_{recoil}$ are large and positive and approach the ideal elastomer only at high temperature, ~ 45°C. This is a direct consequence of the large experimentally observed temperature dependence of the fiber's length.

This dependence of the energetics of recoil on temperature is in agreement with hydrophobic interactions as suggested by the limited data of Gosline.[84, 102] In general, processes driven by hydrophobic interactions are entropic at low temperatures and this decreases with increasing temperature.[108]

4.4.2.6 Thermodynamic Energetics of Stretch in ^1H_2O

The effect of temperature at constant strain (20%) on ΔG, ΔH, $T\Delta S$ and the heat capacity change (ΔC_p) of hydrated elastin in deionized ^1H_2O is investigated, (Figure 4.11 (a, c)). The work of stretch (ΔG_T) is small (~ 6 mJ) and almost constant through the studied temperatures, while both the entropic component ($T\Delta S_T$) and the enthalpic component (ΔH_T) are large and negative and their magnitudes decrease substantially with the increase in temperature, i.e., temperature decreases the contribution of both components to the free energy of the stretch. However, the magnitude of $T\Delta S_T$ is always higher than the magnitude of ΔH_T, confirming that elastin is an entropic elastomer. The change in the heat capacity (ΔC_{pT}) decreases linearly with the increase in temperature. The effect of temperature on both ΔH_T and $T\Delta S_T$ of stretch parallels that of the coacervation process, which takes place in the water-soluble monomer of elastin; tropelastin. Coacervation is the inverse phase transition process, in which tropelastin aggregates with the increase in temperature and facilitates the assembly and the crosslinking to form mature fibers. This process is coupled with an increase in both entropy and enthalpy with the increase in temperature.[109] The

results in this work show that both the entropy and the enthalpy become less negative with temperature at constant strain, coupled with a decrease in both the fiber length and volume.
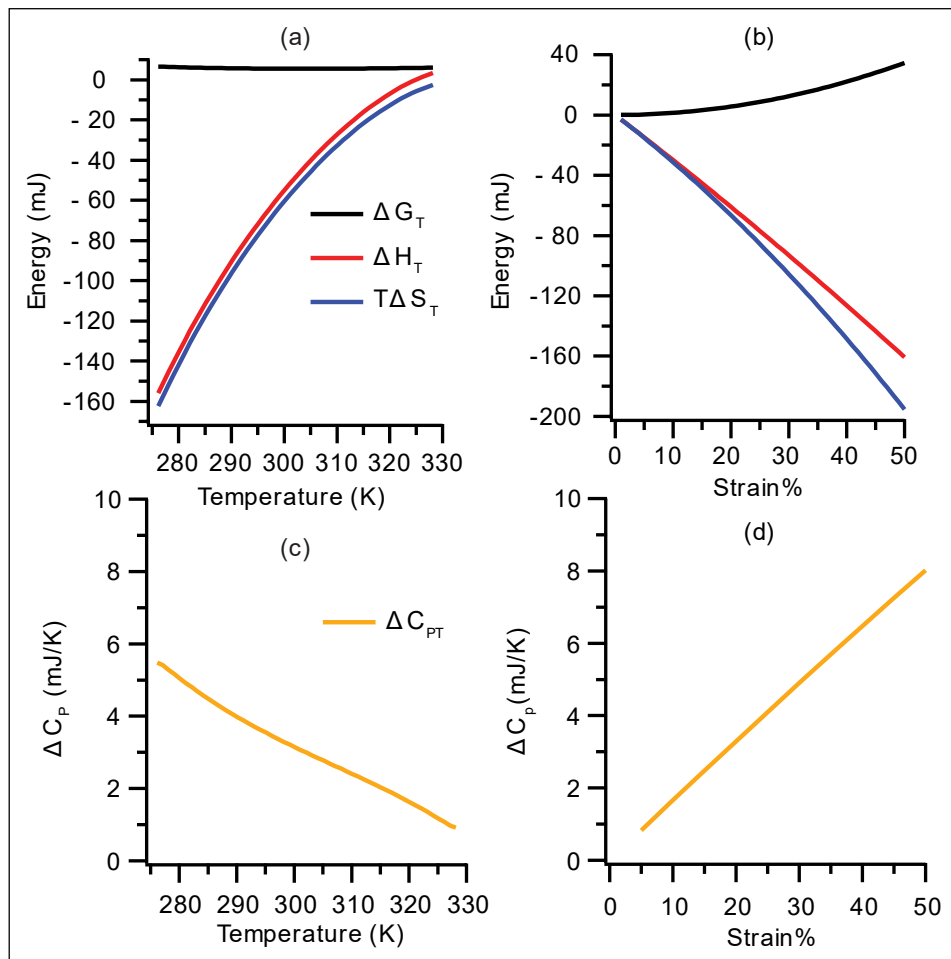
Figure 4.11. Stretch energetics of the hydrated elastin fiber (0.24 g dry mass) in ^1H_2O as a function of (a, c) temperature at constant strain 20% and (b, d) strain at constant temperature 298 K.

The effect of strain at constant temperature (298 K) on ΔG, ΔH, $T\Delta S$ and ΔC_p of hydrated elastin in deionized ^1H_2O is studied, (Figure 4.11 (b, d)). As expected, the work of stretch (ΔG_T) increases with the increase in strain. The magnitude of both the enthalpic component (ΔH_T) and the entropic component ($T\Delta S_T$) increases with strain, i.e., become more negative, with the entropic component magnitude always higher confirming elastin

is entropic. The large release of heat (ΔH_T) with stretching elastin was first observed by Weis-Fogh in calorimetry studies.[8] The ratio of the work to the heat released with stretch determined in this study from the $l(F,T)$ state function is in good agreement with his calorimetric results, as well as with the later more extensive study performed by Gosline.[8,84]

Early on, Tanford identified that an increased heat capacity is a thermodynamic signature of hydrophobic hydration.[110] In this work, the heat capacity (ΔC_{pT}) increases linearly with the increase in strain. This indicates that stretch increases hydrophobic hydration and which is verified experimentally using double quantum filtered NMR (Chapter 2). Qualitatively, the effects of increasing temperature and stretch are in opposite directions. This is, of course, different from most materials in which increasing temperature results in expansion.

4.4.2.7 Volume Changes as a Function of Temperature and Stretch in ^1H_2O

Finally, the changes in volume as a function of force and temperature were determined. Then, Gibbs and Helmholtz free energies were related ($\Delta G = \Delta A + P\Delta V$) and the change in the internal energy ($\Delta U = \Delta G + T\Delta S - P\Delta V$) was calculated.

The fiber shape is approximately rectangular prism and volume = length $\times$ width $\times$ thickness. The fiber length and width were measured directly from photos, and the thickness was calculated assuming the change in thickness is proportional to that in width using the dry dimensions as a reference.

Gosline et al found no change in volume with stretch; however, their experiments were not adequately described.[84] Elastin fiber investigated in this work shows about 5% linear

increase in volume within the maximum experimentally achieved stretched, (Figure 4.12 (a)). In agreement with Gosline's observations,[106] about 40% volume decrease is observed when the temperature is increased from 0 to 55°C, (Figure 4.12 (b)).
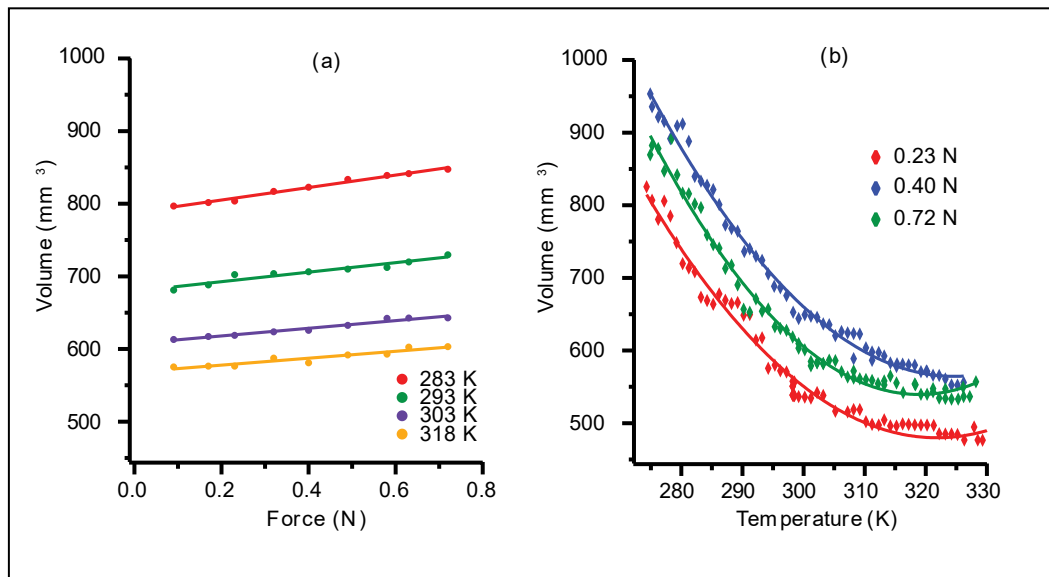
Figure 4.12. The volume of the hydrated elastin fiber in $^{1}H_2O$ as a function of (a) force at constant temperature and (b) temperature at constant force.

4.4.3 Hydration of Elastin fiber in $^{2}H_2O$, Solutions of Hoffmeister ions and PEG

To further investigate the hydrophobic effect, the elastin fiber was hydrated in $^{2}H_2O$, and in aqueous ($^{1}H_2O$) solutions containing 20 kDa PEG, sodium sulfate (Na_2SO_4) or sodium perchlorate ($NaClO_4$), all of which are known to modulate the hydrophobic interactions. The same approach that was used to study elastin in deionized water ($^{1}H_2O$) in the previous section is applied here.

93

4.4.3.1 Young's Modulus (E) and the Spring Constant (k) in the Investigated Solutions

Young's modulus is defined as, $E = \dfrac{F/A}{\Delta l/l_0}$, where F is the applied force, A is the cross-sectional area of the dry fiber, Δl is the extension and l_0 is the relaxed length, i.e., the constant term in the linear fit of the $l(F)$ data (Appendix A, Table A.1 and Table A.2). E for all studied solutions was calculated, (Appendix A, Table A.3).

The work of stretch (ΔG) of the fiber from l_0 to $l_0 + \Delta l$ is related to Young's modulus by $W = \dfrac{EA(\Delta l)^2}{2l_0}$. Thus, the work of stretch is inversely related to l_0. One of the unusual properties of elastin are the changes of the relaxed length (l_0) with temperature and the hydration solvent/solution, (Figure 4.13). Consequently, the work of stretch is significantly affected by this property. To compare the stiffness in different hydration solvent/solutions, the spring constant(k) from Hooke's law ($F = k \times \Delta l$) is used. Spring constant(k) is related to Young's modulus by $k = \dfrac{EA}{l_0}$.

The values of the spring constant (k) are 48.5 – 63.1 N/m and, in general, increase with temperature, i.e., the fiber is stiffer with the increase in temperature, (Table 4.4).

The spring constant (k) is directly proportional to the mechanical force, as k increases, the mechanical force and the work required to stretch the fiber also increase. A slight increase in k is observed in ^2H_2O and 0.1 mol/kg Na_2SO_4 solution compared to ^1H_2O. The values of k are comparable in 0.3 mol/kg Na_2SO_4, 1.0 mol/kg $NaClO_4$ and 15 % (w/w) PEG solutions, and higher than in ^1H_2O. The highest values are in 30% (w/w) PEG. The precipitating agent, PEG, is known to increase protein-protein interactions and decreases the solvent exposed hydrophobic surface. This is accompanied by an increase in the fiber

rigidity or stiffness as the spring constant results show. The chaotrope, NaClO$_4$, known to salt in proteins, shows only a slight increase in fiber rigidity at low concentration and a considerable increase in stiffness at higher concentrations in which it turns over to kosmotropic behavior.[22, 111]

Table 4.4. Spring constant (k) (N/m) for all investigated solutions at different temperatures.

Temperature (K)	^1H_2O	^2H_2O	0.1 mol/kg Na_2SO_4	0.3 mol/kg Na_2SO_4	0.3 mol/kg $NaClO_4$	1.0 mol/kg $NaClO_4$	15% (w/w) PEG	30% (w/w) PEG
283	48.5 ± 0.2	ND	ND	ND	ND	ND	ND	ND
288	49.4 ± 0.2	50.5 ± 0.3	50.6 ± 0.2	53.4 ± 0.2	51.1 ± 0.3	53.4 ± 0.7	53.8 ± 0.4	59.9 ± 0.4
293	50.9 ± 0.2	52.9 ± 0.3	52.5 ± 0.2	55.0 ± 0.2	51.9 ± 0.3	54.7 ± 0.6	55.0 ± 0.4	60.1 ± 0.3
298	52.5 ± 0.2	54.6 ± 0.3	54.2 ± 0.2	56.3 ± 0.2	53.4 ± 0.3	56.6 ± 0.3	56.5 ± 0.4	60.3 ± 0.3
303	54.3 ± 0.2	56.1 ± 0.3	55.7 ± 0.2	57.4 ± 0.2	54.0 ± 0.3	58.4 ± 0.4	ND	ND
308	56.0 ± 0.2	ND	ND	ND	ND	ND	59.2 ± 0.5	61.5 ± 0.4
313	57.4 ± 0.3	58.3 ± 0.4	58.0 ± 0.2	59.6 ± 0.2	55.8 ± 0.3	58.7 ± 0.3	ND	ND
318	ND	ND	ND	ND	ND	ND	61.6 ± 0.5	63.1 ± 0.4

ND: Not Determined

4.4.3.2 Fit Surfaces of $l(F,T)$ in the Investigated Solutions

$l(F,T)$ state functions obtained under different solvent conditions are compared to the ^1H_2O state function, (Figure 4.13). Compared to ^1H_2O, the ^2H_2O and 0.1 mol/kg Na_2SO_4 surfaces are similar with small decreases in height (l_0) and the temperature dependent slope. More significant decreases in both features are observed in 0.3 mol/kg Na_2SO_4 and 15% 20 kDa PEG. The most significant decrease is in 30% 20 kDa PEG where the relaxed length is substantially decreased at low temperature, the change with temperature is nearly eliminated, and the surface essentially converges to the deionized water surface at high temperatures. $NaClO_4$ has a distinct effect. At 0.3 mol/kg concentration, the surface approximately overlaps with the ^1H_2O surface, and at 1.0 mol/kg concentration, it is similar to the 0.1 mol/kg Na_2SO_4 surface.

The relaxed lengths of all studied solutions as a function of temperature from 276 – 328 K (3 – 55 °C) were calculated using Eq. 4.5 by setting F to be equal to zero, (Figure 4.14).

Replacing ^2H_2O with ^1H_2O increases the strength of solvent-solvent hydrogen-bonding making the hydrophobic hydration of the protein more difficult and, in turn, making the protein more compact with less surface area.[49, 53, 54, 77] A decrease in fiber length upon a deuteration is verified, (Figure 4.14 (a)).
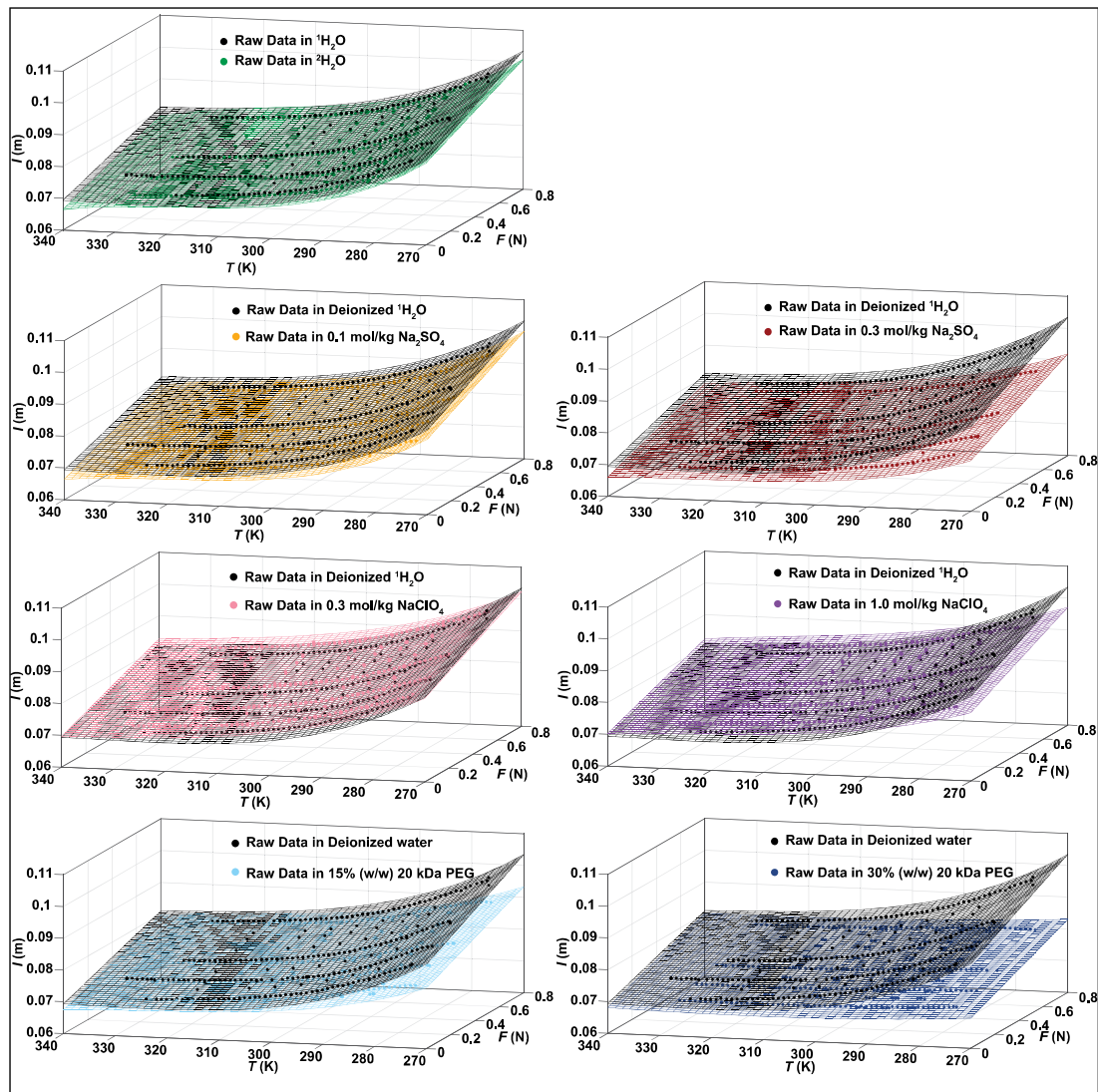
Figure 4.13. The state function $l(F,T)$ (filled circles) of the stretch of the hydrated elastin fiber in all investigated solutions in compare to ^1H_2O and their surface fit.
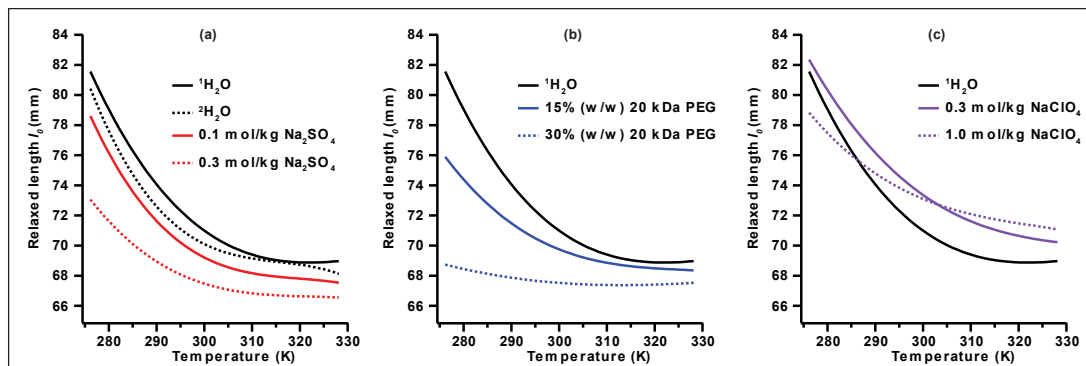
Figure 4.14. The computed relaxed lengths of elastin fiber in all studied solutions as a function of temperature.

The Hoffmeister kosmotrope, SO_4^{2-}, does not bind to protein, is repelled from its surface, and increases solvent surface tension making the cavity formation that is required for hydrophobic hydration at the protein surface more difficult.[23, 24, 27, 112] Thus, sulfate ion is expected to increase elastin compaction, which is confirmed by the substantial decrease in relaxed fiber length, (Figure 4.14 (a)). Consequently, higher concentrations lead to more substantial decreases in the relaxed length.

The crowding agent, PEG, increases protein-protein interactions through preferential hydration [37, 42, 43] and this is confirmed by the very large decrease in relaxed length, (Figure 4.14 (b)).

The Hoffmeister chaotrope, ClO_4^-, directly interacts with the amide groups in the protein backbone leading to disruption of both secondary structure and protein folding.[24, 27, 82, 112] This explains the observed increase in relaxed length that is opposite to the effects of sulfate, PEG and solvent deuteration, (Figure 4.13 (c)).

4.4.3.3 Stretch Thermodynamic energetics in All Studied Solutions

The energetics of stretch (ΔG_T, ΔH_T $T\Delta S_T$ and ΔC_p were determined as functions of strain at constant temperature (298 K), (Figure 4.15 and Figure 4.16), and temperature at a constant strain of 20%, (Appendix A, Figure A.3 and Figure A.4), in all investigated solutions.

ΔG_T is small and increases nonlinearly with strain from 0 – 38 mJ in all solutions, (Figure 4.15 (a_1 – a_3)). The overall effect of isotopic substitution (^2H_2O), or adding Hoffmeister ions (SO_4^{2-}, ClO_4^-) or PEG on ΔG_T is small, i.e., the values are comparable to ^1H_2O and ΔG_T as a function of strain is, to a good approximation, unaffected by varying the solvent conditions. Since strain is displacement, Δl, normalized by the relaxed length, l_0, which decreases in the order of ^1H_2O > ^2H_2O > 0.1 mol/kg SO_4^{2-} > 15% PEG > 0.3 mol/kg SO_4^{2-} >30% PEG, ΔG_T increases in the reverse order for constant displacements, ^1H_2O < ^2H_2O < 0.1 mol/kg SO_4^{2-} < 15% PEG < 0.3 mol/kg SO_4^{2-} < 30% PEG.

Both the entropic ($T\Delta S_T$) component and the enthalpic (ΔH_T) component are negative. Nonetheless, the magnitude of $T\Delta S_T$ is always greater than ΔH_T confirming that the entropic gain is the driving force for elastin recoil in all solutions. The magnitude of both ΔH_T and $T\Delta S_T$ increases with the increase in strain, (Figure 4.15 (b_1 – b_3) and (c_1 – c_3)).
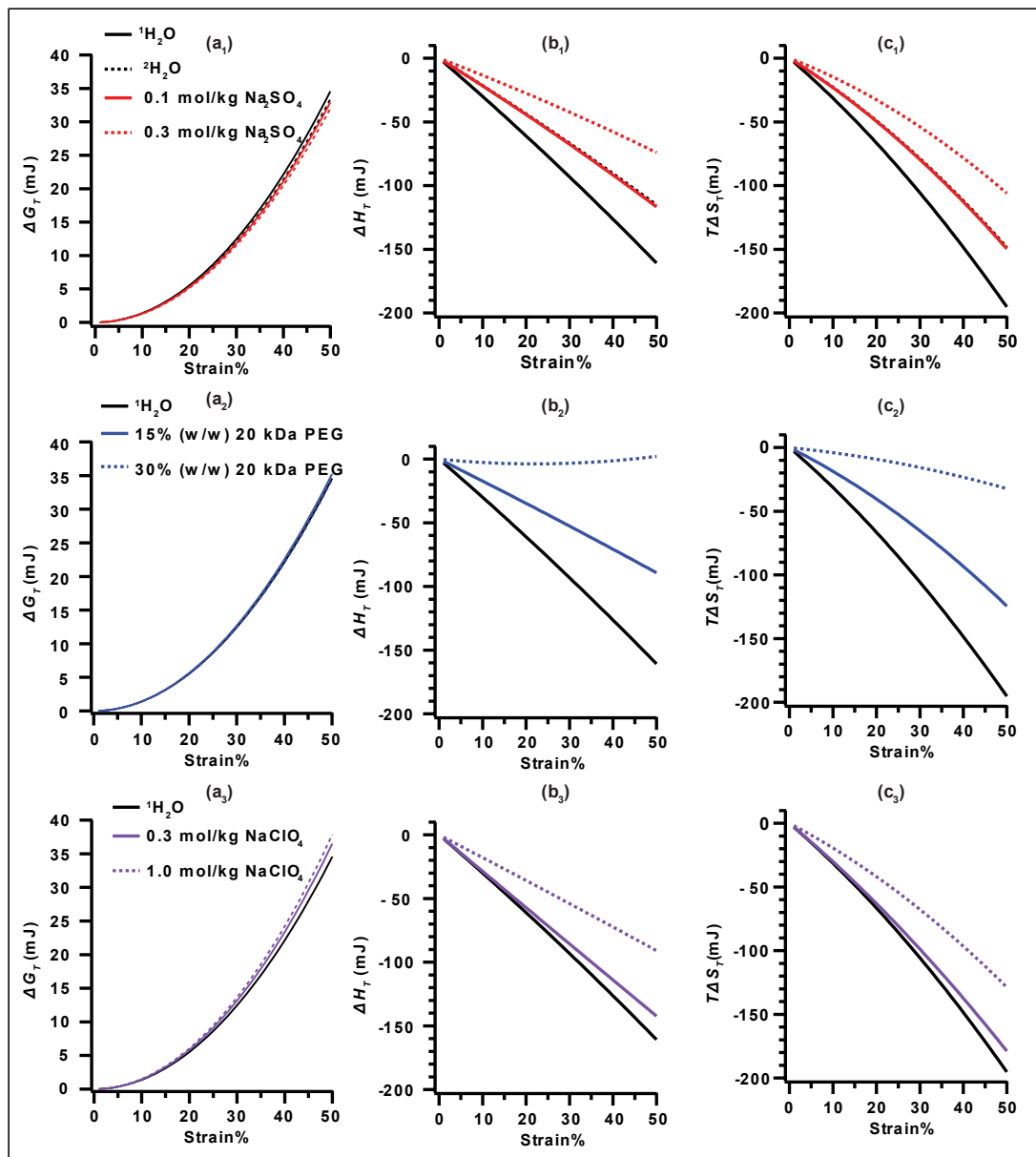
Figure 4.15. Energetics of stretching hydrated elastin (0.24 g dry mass) at 298 K (ΔG_T, ΔH_T and $T\Delta S_T$) versus strain in all studied solutions.

Changing the solvent conditions substantially changes the enthalpic and the entropic driving forces. Solvent deuteration has essentially equivalent changes on ΔH and $T\Delta S$ as 0.1 mol/kg sulfate, whereas larger changes are observed at 0.3 mol/kg. A small decrease in magnitude of both ΔH and $T\Delta S$ is observed in agreement with the increase in the hydrophobic interactions caused by both the kosmotrope ion and the deuterated solvent.

101

The effect of perchlorate on ΔH and $T\Delta S$ is small compared to the effects of deuteration and sulfate ion (at the same concentration). These small effects are completely consistent with the observations that elastin is highly disordered in Chapter 3, i.e., adding a protein denaturant has little effect on its properties. The increased changes in thermodynamic parameters at high perchlorate concentration (1.0 mol/kg) is attributed to the turnover behavior observed in chaotropes at high concentration wherein they behave like kosmotropes.

PEG causes very large decreases in the magnitudes of both the heat released (ΔH) and the loss in strain entropy ($T\Delta S$). In fact, the magnitude of ΔH approaches zero at the high PEG concentration (30%). To control the volume changes in elastin, Flory used 30% glycol solutions and these conditions enabled him to calculate ΔA, which was equal to the entropic component – $T\Delta S$. Subsequently, Flory theorized that elastin behaves as an ideal elastomer.[7, 9] However, he ignored the effect of the third component in his system, PEG, on the elasticity of elastin.

The change in heat capacity (ΔC_p), as in [1]H$_2$O, increases with strain at constant temperature, i.e., the hydrophobic hydration is increased with strain, (Figure 4.16), and decreases with temperature, (Figure A.3).[110]

Solvent deuteration and addition of 0.1 mol/kg sulfate has a minor effect on ΔC_p, whereas a substantial decrease is observed with the higher concentration 0.3 mol/kg sulfate, (Figure 4.16 (a)). This is an anticipated effect, since an increase in ΔC_p is associated with hydrophobic hydration,[105, 110] and with higher concentration of sulfate the fiber is more compact as the length measurement show, i.e., less hydrophobic surface is exposed to hydration.
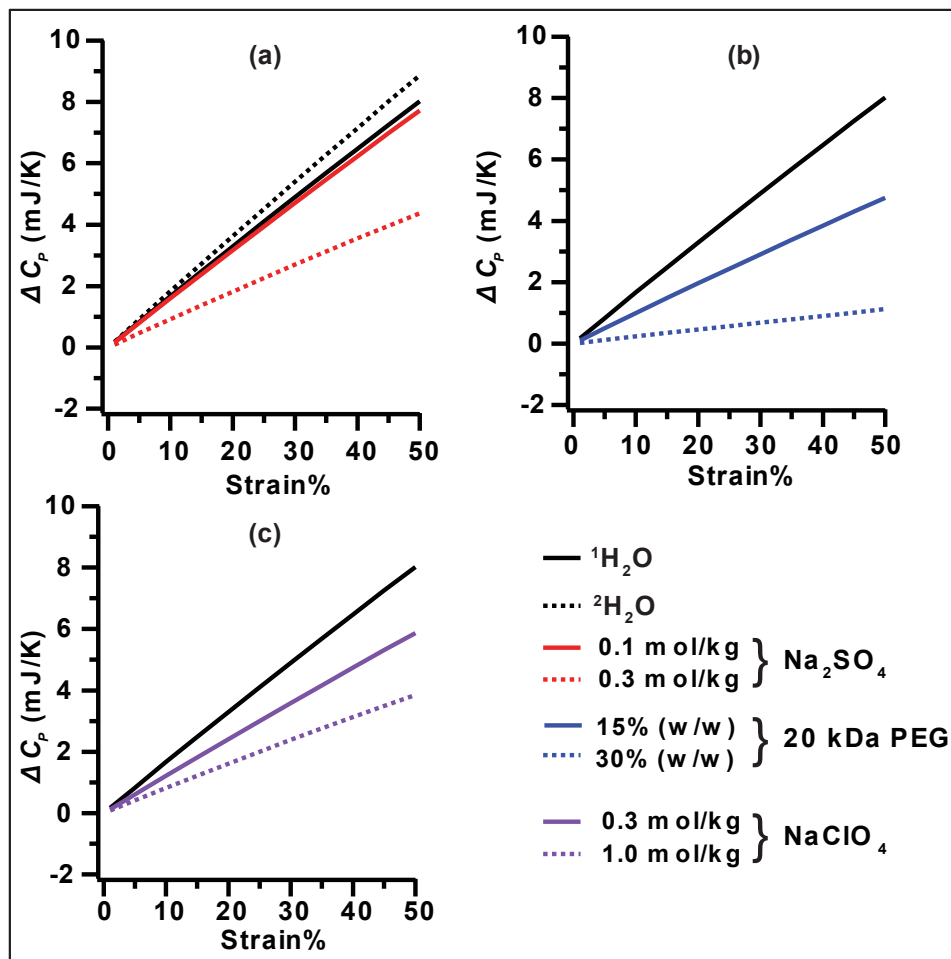
Figure 4.16. The heat capacity change of stretching the hydrated elastin fiber (0.24 g dry mass) as a function of strain in all studied solutions in comparison to ^1H_2O.

PEG causes the largest decrease in ΔC_p which approaches zero at the higher concentration (30%), (Figure 4.16 (b)). This dramatic effect is in agreement with the effect of PEG on the fiber length and volume. The most compact fiber with the least solvent exposed surface area has the smallest heat liberation with strain.

Perchlorate at 0.3 mol/kg concentration has a minor effect on ΔC_p, whereas the higher concentration, 1.0 mol/kg, has a similar effect as the 0.3 mol/kg sulfate due to the turnover behavior, (Figure 4.16 (c)).

103

4.4.3.4 Volume Changes in All Investigated Solutions

The volume of the hydrated elastin fiber as a function of both force, (Figure A.5), and temperature, (Figure A.6), was measured in the different hydration solvent/solutions in the same mannar as in deionized water ^1H_2O, with qualitatively similar results. The volume increase is linearly with the applied force and the decrease with temperature is larger and non-linear. Deuteration (^2H_2O) has no significant effect on the changes in volume in comparison to the deionized solvent (^1H_2O). Sulfate eliminates the increase in volume with force and retains the decrease in volume with temperature. A more significant effect is observed with PEG. The changes in volume with both force and temperature are eliminated. Perchlorate has the opposite effect. It binds to backbone peptide groups and expands the protein giving more surface to the hydration solvent. A significant increase in volume is observed with respect to force and a minor effect with temperature.

The $P\Delta V$ work at constant temperature in the investigated solutions was calculated using the experimentally measured volume versus length, $V(l)$. The slope of $V(l)$ from a linear least square fit was multiplied by the extension (Δl) and one atmospheric pressure (101325 Pa) to evaluate $P\Delta V$ at different strains. This was performed in the studied solutions at 293 K and compared to the work of stretch (ΔG_T) to determine the change in internal energy (ΔU_T), (Table 4.5).

Table 4.5. The $P\Delta V$ work computed from $V(l)$ data and compared with the work of stretch ΔG to stretch elastin fiber by 20% at 293K hydrated in the investigated solutions.

Solution	$V(l)$ slope (m^2)	Relaxed length (l_0 in m)	Δl (m)	$P\Delta V$ (mJ)	ΔG (mJ)
^{1}H$_2$O	$3.8 \pm 0.3 \times 10^{-6}$	7.29×10^{-2}	1.46×10^{-2}	5.65 ± 1.52	5.63
^{2}H$_2$O	$7.6 \pm 0.8 \times 10^{-6}$	7.16×10^{-2}	1.43×10^{-2}	11.05 ± 1.25	5.41
0.1 mol/kg Na$_2$SO$_4$	$6.4 \pm 0.7 \times 10^{-6}$	7.07×10^{-2}	1.41×10^{-2}	9.11 ± 1.03	5.33
0.3 mol/kg Na$_2$SO$_4$	$2.3 \pm 0.9 \times 10^{-6}$	6.84×10^{-2}	1.37×10^{-2}	3.20 ± 1.29	5.11
0.3 mol/kg NaClO$_4$	$1.4 \pm 0.2 \times 10^{-5}$	7.51×10^{-2}	1.50×10^{-2}	20.98 ± 2.35	5.96
1.0 mol/kg NaClO$_4$	$4.8 \pm 0.9 \times 10^{-6}$	7.42×10^{-2}	1.48×10^{-2}	7.20 ± 1.37	6.08
15% 20 kDa PEG	$2.2 \pm 0.3 \times 10^{-6}$	7.08×10^{-2}	1.42×10^{-2}	3.15 ± 0.43	5.67
30% 20 kDa PEG	$3.4 \pm 0.4 \times 10^{-6}$	6.77×10^{-2}	1.35×10^{-2}	4.69 ± 0.51	5.48

The state functions, $H \equiv U + PV$, $A \equiv U - TS$ and $G \equiv H - TS$, with the combined 1st and 2nd laws of thermodynamics can be used to relate the work of stretch (ΔG) with the work of expansion ($P\Delta V$), the change in internal energy (ΔU) and Helmholtz Free energy (ΔA). Stretching the fiber from l_0 to $l_0 + \Delta l$ at constant temperature and pressure, the followings relations are obtained.

$$\Delta G = \Delta A + P\Delta V \qquad \text{Eq. 4.9}$$

And

$$\Delta U = \Delta G + T\Delta S - P\Delta V \qquad \text{Eq. 4.10}$$

The changes in the internal energy (ΔU) calculated using Eq. 4.10 as a function of strain, (Figure 4.17). In general, the magnitude of ΔU increases as the strain increases (become more negative). But this is highly dependent on the solution conditions. The 0.3 mol/kg perchlorate solution, which increases solvent exposed hydrophobic surface has the highest magnitude of ΔU, whereas the solutions/solvent that decrease the hydrophobic surface and volume exposed to hydration (^2H_2O, sulfate and PEG) decrease the magnitude of ΔU to almost zero in 30% PEG.
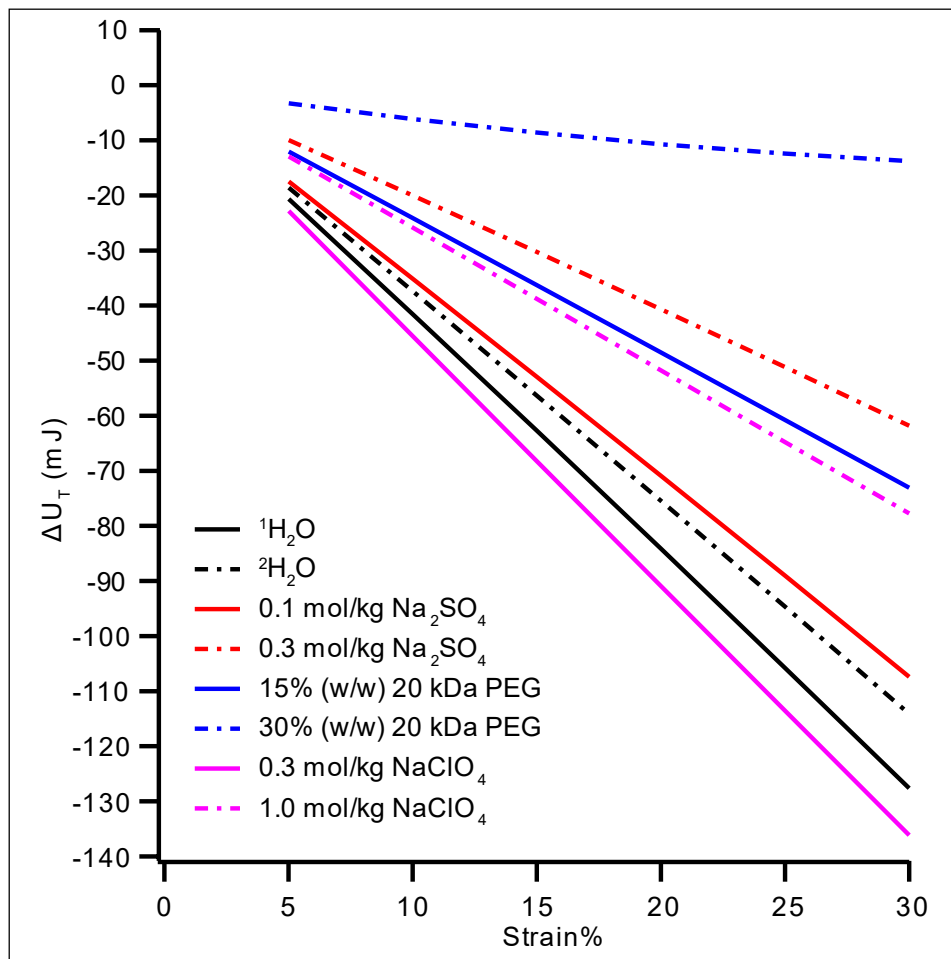
Figure 4.17. The change of internal energy (ΔU) for the hydrated elastin fiber (0.24 g dry mass) in all studied solutions as a function of strain at 293 K.

Although Gosline incorrectly neglected the volume changes upon stretch and used Helmholtz free energy to calculate the change in internal energy, the internal energy does decreases substantially even when the volume changes are taken into account, which is confirmed here. Flory, on the other hand, incorrectly assumed that volume changes could be neglected when the solvent contains glycol or PEG. Additionally, the thermodynamic parameters and the mechanical properties are correlated to the hydrophobic interactions by changing the solvent conditions. (^2H_2O, sulfate and PEG) increase the hydrophobic effect and make the fiber shorter with smaller volume and increases the fiber stiffness. In other

words, simply changing the solvent in this way drives recoil. Moreover, changing the solvent conditions in such manner, decreases the magnitude of the heat liberated, the entropy, and the internal energy with stretch. However, 0.3 mol/kg ClO_4, does not increase the hydrophobic interaction. Instead, it interacts directly with the protein backbone and increases solvent exposed hydrophobic surface area. This has little effect on the fiber stiffness or entropy because elastin is already highly disordered. Nevertheless, it does increase the internal energy change because of its effect on the fiber volume.

CHAPTER 5   CONCLUSIONS

The principal goal of this dissertation is to understand the mechanism of recoil in natural elastin, nature's most abundant elastomeric material. This understanding of recoil mechanism is fundamental to the systematic approach of developing and designing new protein-based elastomers. Elastin has inspired the design of wide variety of proteins with different functions, including protein purification, matrices for tissue engineering and drug delivery. Unlike rubber, elastin is only elastic when fully hydrated wherein water accounts for approximately half of the mass of the elastic material. Thus, a molecular understanding of elastin function necessarily required study of the protein and the hydrate.

NMR spectroscopy is used to study the interaction of the hydrate with this unusually hydrophobic protein using 2Q filtered ^2H_2O NMR. In this experiment, the degree to which the water is ordered and the amount of water interacting with the hydrophobic surface were determined. Likewise, NMR spectroscopy is used to study the timescales of motions in elastin via ^{13}C NMR relaxation of backbone carbonyl atoms, and the amplitude of these motions was determined by measuring the residual chemical shielding anisotropy of backbone carbonyl atoms. Both timescales and the amplitude of motions were studied in stretched and relaxed elastin. Elastin's biological function is to impart elasticity to a variety of tissues in vertebrates. This is a macroscopic function, and a novel thermomechanical instrument was designed, built and used to fully quantitate the

thermomechanical properties of purified elastin. The thermomechanical experiments as well as the NMR experiments were used to probe elastin at the molecular and macroscopic levels using purified elastin material prepared by a recently reported protocol that retains fiber structure while removing other proteins such as fibrin and collagen from the elastic matrix. The old protocols used to purify elastin rely, in general, on harsh conditions such as hot alkali extractions and autoclaving methods. These protocols result in substantially damaged elastin fibers that are highly fragmented and lack important amino acid sequences present in intact fibers, and so hamper any effective study of elastin recoil.[113] In this work, elastin fibers were purified using a novel more recent protocol that optimizes the conditions to yield pure, intact and smooth fibers.

Using 2Q NMR, ordering of deuterated water (^2H_2O) at the surface of the most hydrophobic protein known, elastin, was observed and measured quantitatively. Stretching the fiber up to 30% increases the ordered water by one order of magnitude showing for the first time that the hydrophobic effect, i.e., ordering of water at a hydrophobic surface, contributes to the spontaneous, entropy driven recoil in elastin. Moreover, the ordered water magnitude is highly dependent on the solvent conditions. Addition of PEG, sulfate or high concentrations of perchlorate (1.0 m), all of which increase the hydrophobic interactions thereby reducing solvent exposed surface area, result in less ordered solvent at the surface in a concentration dependent behavior. At lower concentrations, perchlorate is chaotropic and interacts weakly with peptide groups. This "salts in" the protein's peptide bonds and has a much small effect on the ordered water magnitude with stretch, whereas at high concentration (1.0 m) starts to behave like a kosmotrope and decreases the ordered water magnitude.

110

Structure and dynamics in mature elastin were studied using solid state ^{13}C NMR without magic angle spinning. The residual shielding anisotropy of backbone carbonyls in the highly cross-linked protein was found to be $1 - 3$ ppm and thus small compared to the static shielding anisotropy, 116 ppm, for peptide carbonyl atoms. Since the protein is highly crosslinked, rotational diffusion cannot occur, and the residual anisotropy corresponds to an overall order parameter ~ 0.01 for motions of the protein backbone. A backbone order parameter approaching zero was also recently determined in Wittebort laboratory for several minielastins in solution.[60, 96] Thus, structural ordering of the protein as a result of coacervation and/or crosslinking does not occur. The vanishing order parameter also indicates that elastin is more disordered than other intrinsically disordered proteins. Furthermore, no changes in carbonyl backbone ordering took place with stretch. The backbone of elastin is highly disorder relaxed and stretched.

Novel thermomechanical methods were utilized to determine the essential thermodynamic parameters, ΔG, ΔH, ΔS ΔC_P and ΔU that are associated with elastin stretch and recoil. Complete reversibility of the stretch and recoil cycle was confirmed. Rather than using calorimetry, complete state functions, $l(F,T)$, were determined from which the thermodynamic parameters were obtained using Maxwell relations. The energetics of recoil in elastin are substantially different from the expected energetics of recoil in an ideal entropic elastomer. Rubber, for example, is approximately ideal indicating different recoil mechanisms in these two elastomers. Unlike most materials, both elastin and rubber shrink when warmed, however, the shrinkage of elastin upon warming is significantly larger than rubber. The compaction of elastin in the presence of PEG, sulfate or high concentrations of perchlorate anticipated by the 2Q experiments is confirmed and linked with the increase

in stiffness observed as a decrease in fiber length, volume and an increase in the spring constants when temperature is increased, or the solute is added. A signature feature of the hydrophobic effect is its temperature dependence. The entropic driving force of the hydrophobic effect is negligible above ~ 45 °C in proteins and these experiments show that the compaction of elastin, i.e., the temperature induced shortening of an elastin fiber, levels to a constant value at this temperature.

An unresolved difference in the recoil mechanism of elastin between P.J. Flory, the preeminent polymer chemist of the 20th century, and the biologists, Torkel Weis-Fogh and John Gosline, has persisted. Flory argued that elastin is like rubber and recoil is driven by an increase in polymer disorder. Weis-Fogh and Gosline argued that the large amount of heat evolved upon elastin stretch leads to a decrease in the internal energy, and this is a characteristic of the hydrophobic effect and indicates that recoil is driven by the hydrophobic effect. Flory pointed out that Gosline incorrectly based his calculation on defining the stretch work at constant temperature and pressure as the change in Helmholtz free energy (ΔA) when, in fact, this was the change in the Gibbs free energy (ΔG) and, consequently, the contribution of volume change to the change in the internal energy change had been neglected. By measuring the increase in volume with stretch, my work confirms that the internal energy still significantly decreases with stretch, in agreement with Gosline's results that support the idea that the hydrophobic effect is the main contributor to elastin recoil. I have also found, in agreement with Flory, that the decrease in internal energy and volume change are significantly decreased when 30% polyethylene glycol (PEG) was added. However, Flory did not consider the effect of glycol on elastin's elasticity. PEG, a crowding agent, increases hydrophobic protein:protein interactions that

causes fiber compaction and increase the stiffness of the fiber. The low stiffness of elastin is a key property in cardiac function. Increases in arterial stiffness, as results from aging, inevitably results in hypertension.

The one order of magnitude increases in ^2H_2O ordering with stretch coupled with no changes in carbonyl backbone ordering of elastin, and the unique energetics of elastin recoil confirm that the hydrophobic effect is the key player in driving elastin recoil.

REFERENCES

1.   Vrhovski, B.; Weiss, A., Biochemistry of tropoelastin.(1998) Eur. *J. Biochem 258*, 1-18.

2.   Sandberg, L. B.; Weissman, N.; Smith, D. W., The purification and partial characterization of a soluble elastin-like protein from copper-deficient porcine aorta. *Biochemistry* **1969,** *8* (7), 2940-5.

3.   Mithieux, S. M.; Weiss, A. S., Elastin. In *Fibrous Proteins: Coiled-Coils, Collagen and Elastomers*, Academic Press: 2005; Vol. Volume 70, pp 437-461.

4.   Debelle, L.; Tamburro, A. M., Elastin: molecular description and function. *Int J Biochem Cell Biol* **1999,** *31* (2), 261-72.

5.   Lucero, H. A.; Kagan, H. M., Lysyl oxidase: an oxidative enzyme and effector of cell function. *Cell Mol Life Sci* **2006,** *63* (19-20), 2304-16.

6.   Schrader, C. U.; Heinz, A.; Majovsky, P.; Karaman Mayack, B.; Brinckmann, J.; Sippl, W.; Schmelzer, C. E. H., Elastin is heterogeneously cross-linked. *J Biol Chem* **2018,** *293* (39), 15107-15119.

7.   Hoeve, C. A. J.; Flory, P. J., The Elastic Properties of Elastin1,2. *Journal of the American Chemical Society* **2002,** *80* (24), 6523-6526.

8.   Weis-Fogh, T.; Anderson, S. O., New molecular model for the long-range elasticity of elastin. *Nature* **1970,** *227* (5259), 718-21.

9.   Hoeve, C. A.; Flory, P. J., The elastic properties of elastin. *Biopolymers* **1974,** *13* (4), 677-86.

10.   Urry, D. W., Venkatachalam, C.M., Long, M.M., Prasad, K.U., Dynamic β-spirals and a librational entropy mechanism of elasticity. In *Conformation in biology*, Srinivasan, R., Sarma, R.H., Ed. Adenine Press: Guilderland, NY, 1982; pp 11-27.

11.   Urry, D. W.; Cunningham, W. D.; Ohnishi, T., Studies on the conformation and interactions of elastin. Proton magnetic resonance of the repeating pentapeptide. *Biochemistry* **1974,** *13* (3), 609-16.

12.   Gray, W. R.; Sandberg, L. B.; Foster, J. A., Molecular model for elastin structure and function. *Nature* **1973,** *246* (5434), 461-6.

13.   Partridge, S. M.; Davis, H. F.; Adair, G. S., The chemistry of connective tissues. 2. Soluble proteins derived from partial hydrolysis of elastin. *Biochem J* **1955,** *61* (1), 11-21.

14.   Daamen, W. F.; Hafmans, T.; Veerkamp, J. H.; van Kuppevelt, T. H., Isolation of intact elastin fibers devoid of microfibrils. *Tissue Eng* **2005,** *11* (7-8), 1168-76.

15.   Hofmeister, F., Zur Lehre von der Wirkung der Salze. *Archiv für Experimentelle Pathologie und Pharmakologie* **1888,** *25* (1), 1-30.

16.   Kunz, W.; Henle, J.; Ninham, B. W., 'Zur Lehre von der Wirkung der Salze' (about the science of the effect of salts): Franz Hofmeister's historical papers. *Current Opinion in Colloid & Interface Science* **2004,** *9* (1), 19-37.

17.   *Specific Ion Effects*. WORLD SCIENTIFIC: 2009; p 348.

18.   Yang, L.; Fan, Y.; Gao, Y. Q., Differences of Cations and Anions: Their Hydration, Surface Adsorption, and Impact on Water Dynamics. *The Journal of Physical Chemistry B* **2011,** *115* (43), 12456-12465.

19.   Morita, T.; Westh, P.; Nishikawa, K.; Koga, Y., How Much Weaker Are the Effects of Cations than Those of Anions? The Effects of K+ and Cs+ on the Molecular Organization of Liquid H2O. *The Journal of Physical Chemistry B* **2014,** *118* (29), 8744-8749.

20.   Lund, M.; Vacha, R.; Jungwirth, P., Specific ion binding to macromolecules: effects of hydrophobicity and ion pairing. *Langmuir* **2008,** *24* (7), 3387-91.

21.   Flores, S. C.; Kherb, J.; Cremer, P. S., Direct and Reverse Hofmeister Effects on Interfacial Water Structure. *J Phys Chem C* **2012,** *116* (27), 14408-14413.

22.   Moghaddam, S. Z.; Thormann, E., The Hofmeister series: Specific ion effects in aqueous polymer solutions. *Journal of Colloid and Interface Science* **2019,** *555*, 615-635.

23.   Rembert, K. B.; Paterova, J.; Heyda, J.; Hilty, C.; Jungwirth, P.; Cremer, P. S., Molecular mechanisms of ion-specific effects on proteins. *J Am Chem Soc* **2012,** *134* (24), 10039-46.

24.   Cho, Y.; Zhang, Y.; Christensen, T.; Sagle, L. B.; Chilkoti, A.; Cremer, P. S., Effects of Hofmeister anions on the phase transition temperature of elastin-like polypeptides. *J Phys Chem B* **2008,** *112* (44), 13765-71.

25.   Zhang, Y.; Furyk, S.; Sagle, L. B.; Cho, Y.; Bergbreiter, D. E.; Cremer, P. S., Effects of Hofmeister Anions on the LCST of PNIPAM as a Function of Molecular Weight. *The Journal of Physical Chemistry C* **2007,** *111* (25), 8916-8924.

26.   Zhang, Y.; Cremer, P. S., Interactions between macromolecules and ions: The Hofmeister series. *Curr Opin Chem Biol* **2006,** *10* (6), 658-63.

27.   Zhang, Y.; Furyk, S.; Bergbreiter, D. E.; Cremer, P. S., Specific ion effects on the water solubility of macromolecules: PNIPAM and the Hofmeister series. *J Am Chem Soc* **2005,** *127* (41), 14505-10.

28.   Record, M. T., Jr.; Guinn, E.; Pegram, L.; Capp, M., Introductory lecture: interpreting and predicting Hofmeister salt ion and solute effects on biopolymer and model processes using the solute partitioning model. *Faraday discussions* **2013,** *160*, 9-120.

29.   Pegram, L. M.; Record, M. T., Using Surface Tension Data to Predict Differences in Surface and Bulk Concentrations of Nonelectrolytes in Water. *The Journal of Physical Chemistry C* **2009,** *113* (6), 2171-2174.

30.   Pegram, L. M.; Record, M. T., Thermodynamic Origin of Hofmeister Ion Effects. *The Journal of Physical Chemistry B* **2008,** *112* (31), 9428-9436.

31.   Pegram, L. M.; Record, M. T., Jr., Hofmeister salt effects on surface tension arise from partitioning of anions and cations between bulk water and the air-water interface. *J Phys Chem B* **2007,** *111* (19), 5411-7.

32.   Pegram, L. M.; Record, M. T., Jr., Quantifying accumulation or exclusion of H(+), HO(-), and Hofmeister salt ions near interfaces. *Chem Phys Lett* **2008,** *467* (1-3), 1-8.

33.   Heyda, J.; Dzubiella, J., Thermodynamic Description of Hofmeister Effects on the LCST of Thermosensitive Polymers. *The Journal of Physical Chemistry B* **2014,** *118* (37), 10979-10988.

34.   Heyda, J.; Muzdalo, A.; Dzubiella, J., Rationalizing Polymer Swelling and Collapse under Attractive Cosolvent Conditions. *Macromolecules* **2013,** *46* (3), 1231-1238.

35.   Gonzalez-Tello, P.; Camacho, F.; Blazquez, G., Density and Viscosity of Concentrated Aqueous Solutions of Polyethylene Glycol. *Journal of Chemical & Engineering Data* **2002,** *39* (3), 611-614.

36.   McPherson, A., Jr., The growth and preliminary investigation of protein and nucleic acid crystals for X-ray diffraction analysis. *Methods Biochem Anal* **1976,** *23* (0), 249-345.

37.   Finet, S.; Vivarès, D.; Bonneté, F.; Tardieu, A., Controlling Biomolecular Crystallization by Understanding the Distinct Effects of PEGs and Salts on Solubility. In *Methods in Enzymology*, Academic Press: 2003; Vol. Volume 368, pp 105-129.

38.   Asakura, S.; Oosawa, F., Interaction between particles suspended in solutions of macromolecules. *Journal of Polymer Science* **1958,** *33* (126), 183-192.

39.   Edmond, E.; Ogston, A. G., An approach to the study of phase separation in ternary aqueous systems. *Biochemical Journal* **1968,** *109* (4), 569-576.

40.   Atha, D. H.; Ingham, K. C., Mechanism of precipitation of proteins by polyethylene glycols. Analysis in terms of excluded volume. *J Biol Chem* **1981,** *256* (23), 12108-17.

41.   Casassa, E. F.; Eisenberg, H., Thermodynamic Analysis of Multicomponent Solutions. *Adv Protein Chem* **1964,** *19*, 287-395.

42.   Lee, J. C.; Lee, L. L. Y., Preferential Solvent Interactions between Proteins and Polyethylene Glycols. *Journal of Biological Chemistry* **1981,** *256* (2), 625-631.

43.   Lee, J. C.; Lee, L. L., Interaction of calf brain tubulin with poly(ethylene glycols). *Biochemistry* **1979,** *18* (24), 5518-26.

44.   Arakawa, T.; Timasheff, S. N., Mechanism of poly(ethylene glycol) interaction with proteins. *Biochemistry* **1985,** *24* (24), 6756-62.

45.   Bhat, R.; Timasheff, S. N., Steric exclusion is the principal source of the preferential hydration of proteins in the presence of polyethylene glycols. *Protein Science* **1992,** *1* (9), 1133-1143.

46.   Bloustine, J.; Virmani, T.; Thurston, G. M.; Fraden, S., Light scattering and phase behavior of lysozyme-poly(ethylene glycol) mixtures. *Phys Rev Lett* **2006,** *96* (8), 087803.

47.   Tubio, G.; Nerli, B.; Pico, G., Relationship between the protein surface hydrophobicity and its partitioning behaviour in aqueous two-phase systems of polyethyleneglycol-dextran. *J Chromatogr B Analyt Technol Biomed Life Sci* **2004,** *799* (2), 293-301.

48.   Winzor, D. J.; Wills, P. R., Molecular crowding effects of linear polymers in protein solutions. *Biophysical Chemistry* **2006,** *119* (2), 186-195.

49.   Némethy, G.; Scheraga, H. A., Structure of Water and Hydrophobic Bonding in Proteins. IV. The Thermodynamic Properties of Liquid Deuterium Oxide. *The Journal of Chemical Physics* **1964,** *41* (3), 680-689.

50.   Hardy, R. C.; Cottington, R. L., Viscosity of deuterium oxide and water in the range 5 to 125 C. *Journal of Research of the National Bureau of Standards* **1949,** *42* (6).

51.   Soper, A. K.; Benmore, C. J., Quantum Differences between Heavy and Light Water. *Phys Rev Lett* **2008,** *101* (6), 065502.

52.   Kresheck, G. C.; Schneider, H.; Scheraga, H. A., The effect of D2-O on the thermal stability of proteins. Thermodynamic parameters for the transfer of model compounds from H2-O to D2-O. *J Phys Chem* **1965,** *69* (9), 3132-44.

53.   Jarisz, T. A.; Jena, K. C.; Dixon, M. C.; Hore, D. K., Solvent Isotope Effect on Biomolecular Adsorption at Hydrophobic Surfaces. *J Phys Chem C* **2017,** *121* (31), 16879-16887.

54.   Sasisanker, P.; Oleinikova, A.; Weingartner, H.; Ravindra, R.; Winter, R., Solvation properties and stability of ribonuclease A in normal and deuterated water studied by dielectric relaxation and differential scanning/pressure perturbation calorimetry. *Physical Chemistry Chemical Physics* **2004,** *6* (8), 1899-1905.

55.   Hermans, J.; Scheraga, H. A., The thermally induced configurational change of ribonuclease in H2O and D2O. *Biochimica et Biophysica Acta* **1959,** *36* (2), 534-535.

56.   Parker, M. J.; Clarke, A. R., Amide backbone and water-related H/D isotope effects on the dynamics of a protein folding reaction. *Biochemistry* **1997,** *36* (19), 5786-94.

57.   Guzzi, R.; Sportelli, L.; La Rosa, C.; Milardi, D.; Grasso, D., Solvent isotope effects on azurin thermal unfolding. *J Phys Chem B* **1998,** *102* (6), 1021-1028.

58.   Lee, J. J.; Berns, D. S., Protein aggregation. The effect of deuterium oxide on large protein aggregates of C-phycocyanin. *Biochemical Journal* **1968,** *110* (3), 465-470.

59.   Cho, Y.; Sagle, L. B.; Iimura, S.; Zhang, Y.; Kherb, J.; Chilkoti, A.; Scholtz, J. M.; Cremer, P. S., Hydrogen bonding of beta-turn structure is stabilized in D(2)O. *J Am Chem Soc* **2009,** *131* (42), 15188-93.

60.   Greenland, K. N.; Carvajal, M.; Preston, J. M.; Ekblad, S.; Dean, W. L.; Chiang, J. Y.; Koder, R. L.; Wittebort, R. J., Order, Disorder, and Temperature-Driven Compaction in a Designed Elastin Protein. *J Phys Chem B* **2018,** *122* (10), 2725-2736.

61.   Moghaddam, S. Z.; Thormann, E., Hofmeister effect on thermo-responsive poly(propylene oxide) in H2O and D2O. *RSC Advances* **2016,** *6* (33), 27969-27973.

62.   Krivokhizhina, T. V.; Wittebort, R., 2Q NMR of ^2H_2O ordering at solid interfaces. *Journal of Magnetic Resonance* **2014,** *243*, 33-39.

63.   Sharf, Y.; Seo, Y.; Eliav, U.; Akselrod, S.; Navon, G., Mapping strain exerted on blood vessel walls using deuterium double-quantum-filtered MRI. *Proceedings of the National Academy of Sciences* **1998,** *95* (8), 4108-4112.

64.   Shinar, H.; Seo, Y.; Navon, G., Discrimination between the Different Compartments in Sciatic Nerve by2H Double-Quantum-Filtered NMR. *Journal of Magnetic Resonance* **1997,** *129* (1), 98-104.

65.   Eliav, U.; Navon, G., Multiple Quantum Filtered NMR Studies of the Interaction between Collagen and Water in the Tendon. *Journal of the American Chemical Society* **2002,** *124* (12), 3125-3132.

66.   Navon, G.; Eliav, U.; Demco, D. E.; Blumich, B., Study of order and dynamic processes in tendon by NMR and MRI. *J Magn Reson Imaging* **2007,** *25* (2), 362-80.

67.   Fechete, R.; Demco, D. E.; Blumich, B., Parameter maps of 1H residual dipolar couplings in tendon under mechanical load. *J. Magn. Reson.* **2003,** *165* (1), 9-17.

68.   Sun, C.; Boutis, G. S., Investigation of the dynamical properties of water in elastin by deuterium Double Quantum Filtered NMR. *J. Magn. Reson.* **2010,** *205* (1), 86-92.

69.   Sun, C.; Mitchell, O.; Huang, J.; Boutis, G. S., NMR studies of localized water and protein backbone dynamics in mechanically strained elastin. *J Phys Chem B* **2011,** *115* (47), 13935-42.

70.   Jerschow, A., From nuclear structure to the quadrupolar NMR interaction and high-resolution spectroscopy. *Prog Nucl Mag Res Sp* **2005,** *46* (1), 63-78.

71.   H., L. M., *spin dynamics: Basics of Nuclear Magnetic Resonance*. John Wiley & Sons Ltd: Chichester, West Sussex, England, 2008; p 714

72.   Krivokhizhina, T. V. APPLICATIONS OF SOLID STATE NMR TO CARDIOLIPIN AND ELASTIN. University of Louisville, Louisville, KY, 2012.

73.   Mecham, R. P., Methods in elastic tissue biology: elastin isolation and purification. *Methods* **2008,** *45* (1), 32-41.

74.   Hahn, E. L., Spin Echoes. *Physical Review* **1950,** *80* (4), 580-594.

75.   Zhang, Q. W.; Zhang, H.; Lakshmi, K. V.; Lee, D. K.; Bradley, C. H.; Wittebort, R. J., Double and Triple Resonance Circuits for High-Frequency Probes. *Journal of Magnetic Resonance* **1998,** *132* (1), 167-171.

76.   Waldstein, P.; Rabideau, S. W.; Jackson, J. A., Nuclear Magnetic Resonance of Single Crystals of D2O Ice. *The Journal of Chemical Physics* **1964,** *41* (11), 3407-3411.

77.   Oakenfull, D. G.; Fenwick, D. E., Hydrophobic interaction in deuterium oxide. *Australian Journal of Chemistry* **1975,** *28* (4), 715-720.

78.   Partridge, S. M., Diffusion of solutes in elastin fibres. *Biochimica et Biophysica Acta (BBA) - Protein Structure* **1967,** *140* (1), 132-141.

79.   Lillie, M. A.; Chalmers, G. W. G.; Gosline, J. M., Elastin dehydration through the liquid and the vapor phase: A comparison of osmotic stress models. *Biopolymers* **1996,** *39* (5), 627-639.

80.   Baldwin, R. L., How Hofmeister ion interactions affect protein stability. *Biophysical Journal* **1996,** *71* (4), 2056-2063.

81.   Lo Nostro, P.; Ninham, B. W., Hofmeister phenomena: an update on ion specificity in biology. *Chem Rev* **2012,** *112* (4), 2286-322.

82. Von Hippel, P. H.; Peticolas, V.; Schack, L.; Karlson, L., Model studies on the effects of neutral salts on the conformational stability of biological macromolecules. I. Ion binding to polyacrylamide and polystyrene columns. *Biochemistry* **1973,** *12* (7), 1256-64.

83. Nandi, P. K.; Robinson, D. R., The effects of salts on the free energy of the peptide group. *J Am Chem Soc* **1972,** *94* (4), 1299-308.

84. Gosline, J. M., Hydrophobic interaction and a model for the elasticity of elastin. *Biopolymers* **1978,** *17* (3), 677-95.

85. Urry, D. W.; Hugel, T.; Seitz, M.; Gaub, H. E.; Sheiba, L.; Dea, J.; Xu, J.; Parker, T., Elastin: a representative ideal protein elastomer. *Philos Trans R Soc Lond B Biol Sci* **2002,** *357* (1418), 169-84.

86. Pometun, M. S.; Chekmenev, E. Y.; Wittebort, R. J., Quantitative observation of backbone disorder in native elastin. *J Biol Chem* **2004,** *279* (9), 7982-7.

87. Torchia, D. A.; Piez, K. A., Mobility of elastin chains as determined by 13C nuclear magnetic resonance. *Journal of Molecular Biology* **1973,** *76* (3), 419-424.

88. Lyerla, J. R., Jr.; Torchia, D. A., Molecular mobility and structure of elastin deduced from the solvent and temperature dependence of 13C magnetic resonance relaxation data. *Biochemistry* **1975,** *14* (23), 5175-83.

89. Carr, H. Y.; Purcell, E. M., Effects of Diffusion on Free Precession in Nuclear Magnetic Resonance Experiments. *Physical Review* **1954,** *94* (3), 630-638.

90. Meiboom, S.; Gill, D., Modified Spin-Echo Method for Measuring Nuclear Relaxation Times. *Review of Scientific Instruments* **1958,** *29* (8), 688-691.

91. Raju, K.; Anwar, R. A., Primary Structures of Bovine Elastin-a, Elastin-B and Elastin-C Deduced from the Sequences of Cdna Clones. *Faseb J* **1987,** *46* (6), 1989-1989.

92. Kjaergaard, M.; Poulsen, F. M., Sequence correction of random coil chemical shifts: correlation between neighbor correction factors and changes in the Ramachandran distribution. *Journal of Biomolecular NMR* **2011,** *50* (2), 157-165.

93. Duncan, T. M., *Principal Components of Chemical Shift Tensors*. Farragut Press: Madison, WI, 1997.

94. Abragam, A., *The Principles of Nuclear Magnetism*. Oxford University Press: Oxford, England, 1961.

95. Allard, P.; Härd, T., NMR Relaxation Mechanisms for Backbone Carbonyl Carbons in a13C,15N-Labeled Protein. *Journal of Magnetic Resonance* **1997,** *126* (1), 48-57.

96. Carvajal, M. F. C. A.; Preston, J. M.; Jamhawi, N. M.; Sabo, T. M.; Bhattacharya, S.; Aramini, J. M.; Wittebort, R. J.; Koder, R. L., Dynamics in Natural and Designed Elastins and Their Relation to Elastic Fiber Structure and Recoil. *bioRxiv* **2021**, 2020.07.14.202523.

97. Clore, G. M.; Szabo, A.; Bax, A.; Kay, L. E.; Driscoll, P. C.; Gronenborn, A. M., Deviations from the simple two-parameter model-free approach to the interpretation of nitrogen-15 nuclear magnetic relaxation of proteins. *Journal of the American Chemical Society* **2002,** *112* (12), 4989-4991.

98. Lipari, G.; Szabo, A., Model-free approach to the interpretation of nuclear magnetic resonance relaxation in macromolecules. 2. Analysis of experimental results. *Journal of the American Chemical Society* **2002,** *104* (17), 4559-4570.

99.   Lipari, G.; Szabo, A., Model-free approach to the interpretation of nuclear magnetic resonance relaxation in macromolecules. 1. Theory and range of validity. *Journal of the American Chemical Society* **2002,** *104* (17), 4546-4559.

100.   Perry, A.; Stypa, M. P.; Tenn, B. K.; Kumashiro, K. K., Solid-State 13C NMR Reveals Effects of Temperature and Hydrationon Elastin. *Biophysical Journal* **2002,** *82* (2), 1086-1095.

101.   Perry, A.; Stypa, M. P.; Foster, J. A.; Kumashiro, K. K., Observation of the glycines in elastin using (13)C and (15)N solid-state NMR spectroscopy and isotopic labeling. *J Am Chem Soc* **2002,** *124* (24), 6832-3.

102.   Gosline, J. M., The temperature-dependent swelling of elastin. *Biopolymers* **1978,** *17* (3), 697-707.

103.   Anthony, R. L.; Caston, R. H.; Guth, E., Equations of state for natural and synthetic rubber-like materials. I. Unaccelerated natural soft rubber. *The Journal of Physical Chemistry* **2002,** *46* (8), 826-840.

104.   Kauzmann, W., Some Factors in the Interpretation of Protein Denaturation. In *Advances in Protein Chemistry Volume 14*, Anfinsen, C. B.; Anson, M. L.; Bailey, K.; Edsall, J. T., Eds. Academic Press: 1959; Vol. 14, pp 1-63.

105.   Tanford, C., Contribution of Hydrophobic Interactions to the Stability of the Globular Conformation of Proteins. *Journal of the American Chemical Society* **2002,** *84* (22), 4240-4247.

106.   Gosline, J. M., The elastic properties of rubber-like proteins and highly extensible tissues. *Symp Soc Exp Biol* **1980,** *34* (3), 332-57.

107.   Roundy, D.; Rogers, M., Exploring the thermodynamics of a rubber band. *American Journal of Physics* **2013,** *81* (1), 20-23.

108.   Baldwin, R. L., Temperature dependence of the hydrophobic interaction in protein folding. *Proceedings of the National Academy of Sciences* **1986,** *83* (21), 8069.

109.   Vrhovski, B.;   Jensen, S.; Weiss, A. S., Coacervation Characteristics of Recombinant Human Tropoelastin. *European Journal of Biochemistry* **1997,** *250* (1), 92-98.

110.   Tanford, C., *The hydrophobic effect: formation of micelles and biological membranes*. J. Wiley.: New York, 1973.

111.   Chudoba, R.;   Heyda, J.; Dzubiella, J., Tuning the collapse transition of weakly charged polymers by ion-specific screening and adsorption. *Soft Matter* **2018,** *14* (47), 9631-9642.

112.   Zhang, Y.; Cremer, P. S., Chemistry of Hofmeister Anions and Osmolytes. *Annual Review of Physical Chemistry* **2010,** *61* (1), 63-83.

113.   Soskel, N. T.; Sandburg, L. B., A comparison of six methods of extracting elastin residue from hamster lungs. *Exp Lung Res* **1983,** *4* (2), 109-19.

APPENDIX A

All studied solutions show a decrease in the slope of $l(F)$ with the increase in temperature with the 30% (w/w) 20 kDa PEG solution shows the minimum slope and almost constant within the studied temperatures indicating an increase in the fiber stiffness with temperature, (Figure A.1).

The length decreases substantially in all solutions as a function of temperature with the 30% 20 kDa PEG solution shows almost constant length within the increased in temperatures at the studied forces, (Figure A.2).
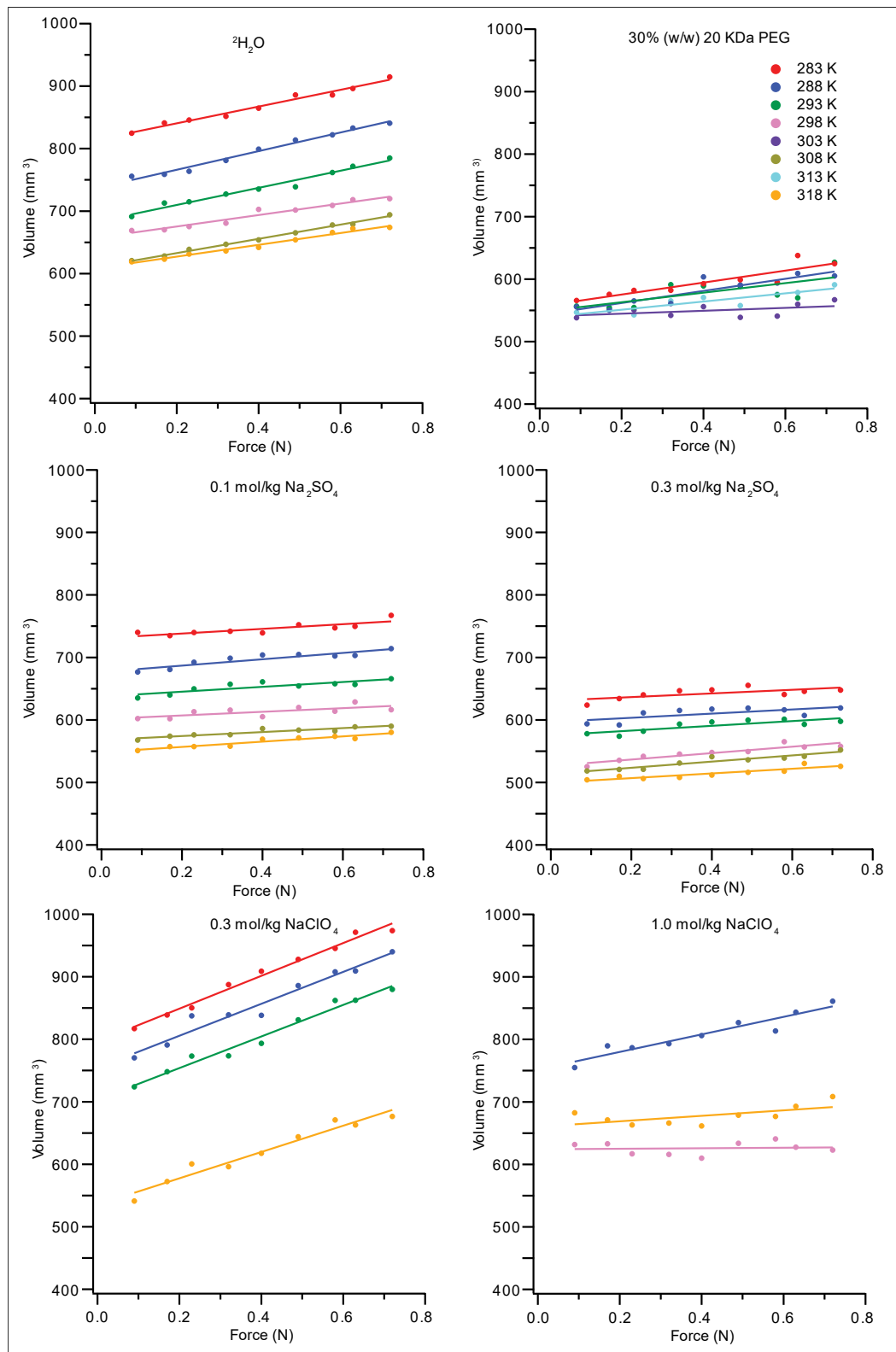
Figure A.1. The length of the hydrated elastin fiber as a function of force at different temperatures in the examined solutions.
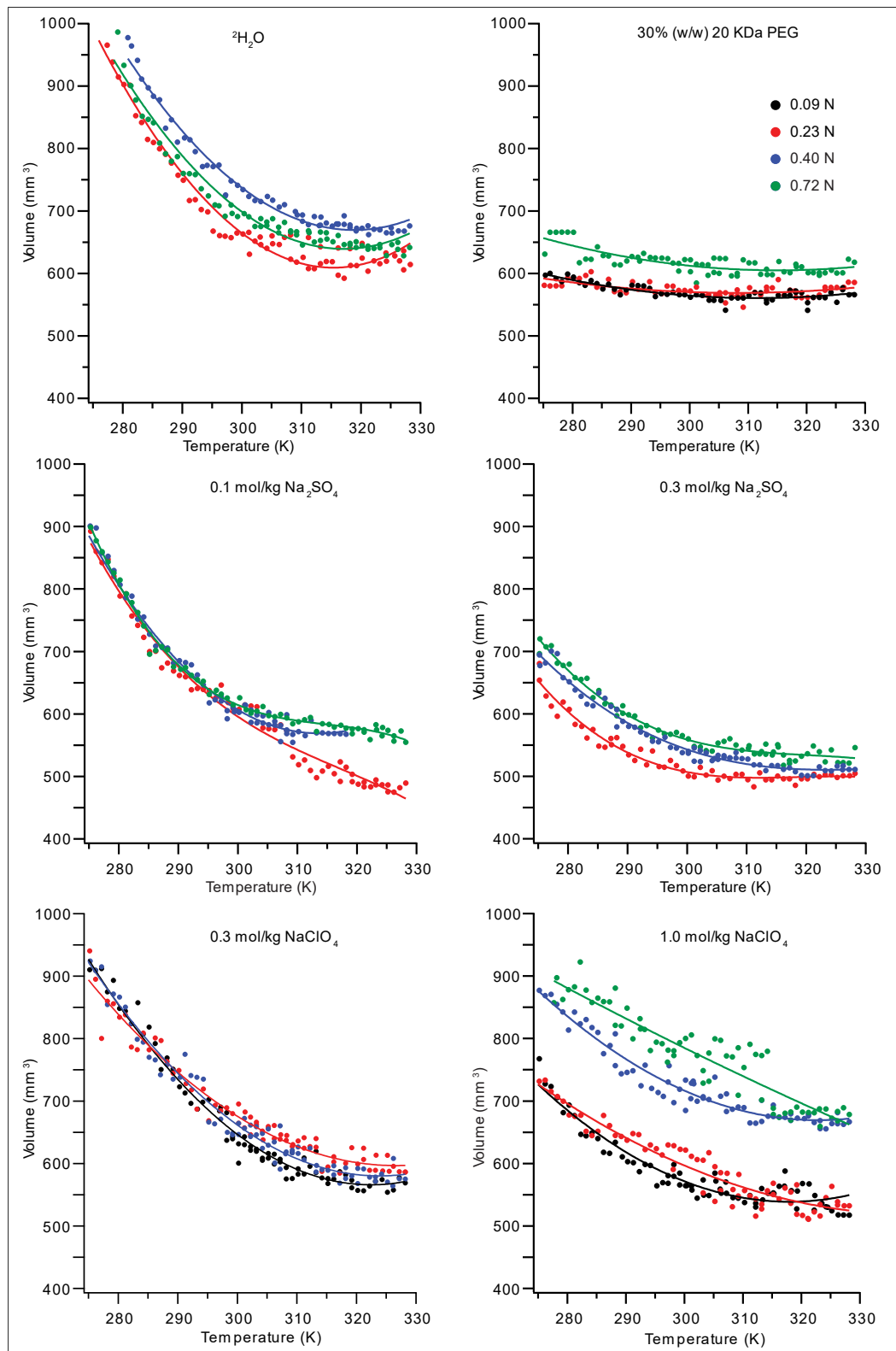
Figure A.2. The length of the hydrated elastin fiber as a function of temperature at different forces in the examined solutions.

Table A.1. Linear fit slope (b) of l(F) (mm/N) for all investigated solutions at different temperatures.

Temperature (K)	^1H_2O	^2H_2O	0.1 mol/kg Na$_2$SO$_4$	0.3 mol/kg Na$_2$SO$_4$	0.3 mol/kg NaClO$_4$	1.0 mol/kg NaClO$_4$	15% PEG	30% PEG
278	20.6 ± 0.1	ND	ND	ND	ND	ND	ND	ND
283	20.2 ± 0.1	19.7 ± 0.1	19.6 ± 0.1	18. 7 ± 0.1	19.5 ± 0.2	18.7 ± 0.5	18.4 ± 0.1	16.6 ± 0.2
288	19.6 ± 0.1	18.8 ± 0.1	18.9 ± 0.1	18.2 ± 0.1	19.3 ± 0.1	18.2 ± 0.4	18.1 ± 0.1	16.6 ± 0.1
293	19.0 ± 0.1	18.2 ± 0.1	18.4 ± 0.1	17.8 ± 0.1	18.7 ± 0.1	17.7 ± 0.1	17.6 ± 0.1	16.5 ± 0.2
298	18.4 ± 0.1	18.0 ± 0.1	17.9 ± 0.1	17.4 ± 0.1	18.5 ± 0.2	17.1 ± 0.2	ND	ND
303	17.8 ± 0.1	ND	ND	ND	ND	ND	16.9 ± 0.1	16.2 ± 0.1
308	17.4 ± 0.1	17.2 ± 0.1	17.2 ± 0.1	16.8 ± 0.1	18.0 ± 0.3	17.1 ± 0.1	ND	ND
313	ND	ND	ND	ND	ND	ND	16.2 ± 0.1	15.8 ± 0.2
318	16.8 ± 0.1	16.5± 0.1	16.5 ± 0.1	16.2 ± 0.1	17.3 ± 0.2	16.5 ± 0.1	ND	ND

ND: Not Determined

Table A.2. Linear fit intercept (a) of l(F) (mm), relaxed unstretched fiber length, for all investigated solutions at different temperatures.

Temperature (K)	^1H_2O	^2H_2O	0.1 mol/kg Na_2SO_4	0.3 mol/kg Na_2SO_4	0.3 mol/kg $NaClO_4$	1.0 mol/kg $NaClO_4$	15% PEG	30% PEG
278	80.16 ± 0.06	ND	ND	ND	ND	ND	ND	ND
283	76.96 ± 0.04	75.38 ± 0.05	73.79 ± 0.04	70.55 ± 0.05	78.72 ± 0.11	76.40 ± 0.24	72.67 ± 0.05	68.06 ± 0.08
288	74.75 ± 0.04	73.03 ± 0.05	71.91 ± 0.05	69.49 ± 0.06	76.80 ± 0.06	75.22 ± 0.20	71.50 ± 0.05	67.83 ± 0.07
293	72.80 ± 0.04	71.31 ± 0.05	70.52 ± 0.04	68.60 ± 0.06	75.20 ± 0.06	74.33 ± 0.07	70.29 ± 0.06	67.65 ± 0.07
298	71.26 ± 0.04	71.09 ± 0.05	69.56 ± 0.05	67.57 ± 0.06	73.86 ± 0.09	73.48 ± 0.11	ND	ND
303	70.27 ± 0.05	ND	ND	ND	ND	ND	69.30 ± 0.06	67.38 ± 0.06
308	69.64 ± 0.05	69.54 ± 0.05	68.29 ± 0.05	66.88 ± 0.05	72.07 ± 0.14	72.38 ± 0.04	ND	ND
313	ND	ND	ND	ND	ND	ND	68.65 ± 0.06	67.39 ± 0.07
318	68.68 ± 0.05	68.82 ± 0.06	67.60 ± 0.05	66.49 ± 0.06	70.92 ± 0.07	71.80 ± 0.04	ND	ND

Table A.3. Young's modulus (MPa) for all investigated solutions at different temperatures.

Temperature (K)	[1]H_2O	[2]H_2O	0.1 mol/kg Na_2SO_4	0.3 mol/kg Na_2SO_4	0.3 mol/kg $NaClO_4$	1.0 mol/kg $NaClO_4$	15% PEG	30% PEG
283	0.60 ± 0.01	0.60 ± 0.01	0.59 ± 0.01	0.59 ± 0.01	0.63 ± 0.01	0.64 ± 0.01	0.62 ± 0.01	0.64 ± 0.01
288	0.60 ± 0.01	0.61 ± 0.01	0.60 ± 0.01	0.60 ± 0.01	0.63 ± 0.01	0.65 ± 0.01	0.62 ± 0.01	0.64 ± 0.01
293	0.60 ± 0.01	0.61 ± 0.01	0.60 ± 0.01	0.60 ± 0.01	0.63 ± 0.01	0.66 ± 0.01	0.63 ± 0.01	0.64 ± 0.01
298	0.61 ± 0.01	0.62 ± 0.01	0.61 ± 0.01	0.61 ± 0.01	0.62 ± 0.01	0.67 ± 0.01	ND	ND
303	0.62 ± 0.01	ND	ND	ND	ND	ND	0.64 ± 0.01	0.65 ± 0.01
308	0.63 ± 0.01	0.63 ± 0.01	0.62 ± 0.01	0.63 ± 0.01	0.63 ± 0.01	0.66 ± 0.01	ND	ND
313	ND	ND	ND	ND	ND	ND	0.66 ± 0.01	0.67 ± 0.01
318	0.64 ± 0.01	0.65 ± 0.01	0.64 ± 0.01	0.65 ± 0.01	0.64 ± 0.01	0.68 ± 0.01	ND	ND

Table A.4. The thermodynamic parameters $\varDelta G$ (mJ), $\varDelta H$ (mJ), $T\varDelta S$ (mJ) and $\varDelta C_p$) and the relaxed length l_0(mm) for hydrated elastin fiber (0.24 g dry mass) in ^1H_2O, ^2H_2O and Na_2SO_4 at 20% versus Temperature.

T (K)	^1H_2O					^2H_2O					0.1 mol/kg Na_2SO_4					0.3 mol/kg Na_2SO_4				
	l_0	$\varDelta G$	$\varDelta H$	$T\varDelta S$	$\varDelta C_p$	l_0	$\varDelta G$	$\varDelta H$	$T\varDelta S$	$\varDelta C_p$	l_0	$\varDelta G$	$\varDelta H$	$T\varDelta S$	$\varDelta C_p$	l_0	$\varDelta G$	$\varDelta H$	$T\varDelta S$	$\varDelta C_p$
276	82	7	-156	-162	5	80	6	-176	-183	9	79	6	-150	-156	7	73	5	-84	-89	3
277	81	6	-150	-157	5	80	6	-167	-174	9	78	6	-144	-150	7	73	5	-81	-86	3
278	80	6	-145	-151	5	79	6	-159	-165	8	77	6	-137	-143	6	72	5	-77	-83	3
279	80	6	-140	-146	5	78	6	-151	-157	8	77	6	-131	-137	6	72	5	-74	-80	3
280	79	6	-135	-141	5	78	6	-143	-149	8	76	6	-125	-131	6	72	5	-71	-76	3
281	78	6	-130	-136	5	77	6	-136	-142	7	76	6	-119	-125	6	71	5	-68	-73	3
282	78	6	-125	-131	5	76	6	-128	-134	7	75	6	-113	-119	6	71	5	-65	-70	3
283	77	6	-120	-126	5	76	6	-121	-127	7	74	6	-108	-114	5	71	5	-62	-68	3
284	77	6	-116	-122	5	75	6	-115	-120	7	74	6	-103	-108	5	70	5	-60	-65	3
285	76	6	-111	-117	4	75	6	-108	-114	6	74	6	-97	-103	5	70	5	-57	-62	3
286	76	6	-107	-113	4	74	6	-102	-108	6	73	6	-92	-98	5	70	5	-54	-59	3
287	75	6	-102	-108	4	74	6	-96	-101	6	73	5	-88	-93	5	70	5	-52	-57	3

288	75	6	-98	-104	4	73	6	-90	-96	6	72	5	-83	-88	5	69	5	-49	-54	2
289	74	6	-94	-100	4	73	6	-84	-90	5	72	5	-78	-84	4	69	5	-47	-52	2
290	74	6	-90	-96	4	73	5	-79	-85	5	72	5	-74	-79	4	69	5	-44	-49	2
291	74	6	-86	-92	4	72	5	-74	-79	5	71	5	-70	-75	4	69	5	-42	-47	2
292	73	6	-82	-88	4	72	5	-69	-75	5	71	5	-66	-71	4	69	5	-40	-45	2
293	73	6	-78	-84	4	72	5	-64	-70	5	71	5	-62	-67	4	68	5	-37	-43	2
294	73	6	-75	-80	4	71	5	-60	-65	4	70	5	-58	-63	4	68	5	-35	-40	2
295	72	6	-71	-77	4	71	5	-56	-61	4	70	5	-54	-60	4	68	5	-33	-38	2
296	72	6	-68	-73	3	71	5	-51	-57	4	70	5	-51	-56	3	68	5	-31	-36	2
297	72	6	-64	-70	3	71	5	-47	-53	4	70	5	-47	-53	3	68	5	-29	-34	2
298	71	6	-61	-67	3	70	5	-44	-49	4	70	5	-44	-50	3	68	5	-27	-33	2
299	71	6	-58	-63	3	70	5	-40	-46	3	69	5	-41	-46	3	68	5	-26	-31	2
300	71	6	-55	-60	3	70	5	-37	-42	3	69	5	-38	-43	3	67	5	-24	-29	2
301	71	6	-51	-57	3	70	5	-34	-39	3	69	5	-35	-41	3	67	5	-22	-27	2
302	71	5	-48	-54	3	70	5	-31	-36	3	69	5	-33	-38	3	67	5	-21	-26	2

303	70	5	-45	-51	3	70	5	-28	-33	3	69	5	-30	-35	2	67	5	-19	-24	1
304	70	5	-43	-48	3	70	5	-26	-31	2	69	5	-28	-33	2	67	5	-18	-23	1
305	70	5	-40	-45	3	69	5	-23	-29	2	69	5	-25	-31	2	67	5	-16	-22	1
306	70	5	-37	-43	3	69	5	-21	-26	2	68	5	-23	-29	2	67	5	-15	-20	1
307	70	6	-34	-40	3	69	5	-19	-25	2	68	5	-21	-27	2	67	5	-14	-19	1
308	70	6	-32	-37	3	69	5	-17	-23	2	68	5	-19	-25	2	67	5	-13	-18	1
309	69	6	-29	-35	2	69	5	-16	-21	1	68	5	-18	-23	2	67	5	-12	-17	1
310	69	6	-27	-32	2	69	5	-15	-20	1	68	5	-16	-22	1	67	5	-11	-16	1
311	69	6	-25	-30	2	69	5	-14	-19	1	68	5	-15	-20	1	67	5	-10	-15	1
312	69	6	-22	-28	2	69	5	-13	-18	1	68	5	-14	-19	1	67	5	-9	-14	1
313	69	6	-20	-26	2	69	5	-12	-18	0	68	5	-13	-18	1	67	5	-8	-13	1
314	69	6	-18	-23	2	69	6	-12	-17	0	68	5	-12	-17	1	67	5	-7	-13	1
315	69	6	-16	-21	2	69	6	-12	-17	0	68	5	-11	-16	1	67	5	-7	-12	1
316	69	6	-14	-19	2	69	6	-12	-18	0	68	5	-10	-16	0	67	5	-6	-12	0
317	69	6	-12	-18	2	69	6	-12	-18	-1	68	5	-10	-15	0	67	5	-6	-11	0

318	69	6	-10	-16	2	69	6	-13	-19	-1	68	6	-10	-15	0	67	5	-6	-11	0
319	69	6	-8	-14	2	69	6	-14	-20	-1	68	6	-10	-15	0	67	5	-5	-11	0
320	69	6	-7	-12	2	69	6	-15	-21	-1	68	6	-10	-15	0	67	5	-5	-11	0
321	69	6	-5	-11	2	69	6	-17	-22	-2	68	6	-10	-16	0	67	6	-5	-11	0
322	69	6	-4	-9	1	69	6	-19	-24	-2	68	6	-11	-16	-1	67	6	-5	-11	0
323	69	6	-2	-8	1	69	6	-21	-26	-2	68	6	-11	-17	-1	67	6	-5	-11	0
324	69	6	-1	-7	1	68	6	-23	-29	-3	68	6	-12	-18	-1	67	6	-6	-11	0
325	69	6	0	-6	1	68	6	-26	-31	-3	68	6	-13	-19	-1	67	6	-6	-12	0
326	69	6	1	-4	1	68	6	-29	-34	-3	68	6	-15	-20	-1	67	6	-7	-12	-1
327	69	6	2	-4	1	68	6	-32	-38	-3	68	6	-16	-22	-2	67	6	-7	-13	-1
328	69	6	3	-3	1	68	6	-35	-41	-4	68	6	-18	-24	-2	67	6	-8	-14	-1

Table A.5. The thermodynamic parameters (ΔG (mJ), ΔH (mJ), $T\Delta S$ (mJ) and ΔC_p) and the relaxed length l_0(mm) for hydrated elastin fiber (0.24 g dry mass) in 20 kDa PEG and $NaClO_4$ at 20% versus Temperature.

T (K)	15% PEG					30% PEG					0.3 mol/kg NaClO$_4$					1.0 mol/kg NaClO$_4$				
	l_0	ΔG	ΔH	TΔS	ΔC_p	l_0	ΔG	ΔH	TΔS	ΔC_p	l_0	ΔG	ΔH	TΔS	ΔC_p	l_0	ΔG	ΔH	TΔS	ΔC_p
276	76	6	-94	-100	3	69	6	-15	-20	1	82	7	-126	-133	4	79	6	-85	-92	3
277	75	6	-90	-96	3	69	6	-14	-20	1	82	7	-122	-129	4	78	6	-82	-89	3
278	75	6	-87	-93	3	69	5	-13	-19	1	81	7	-118	-125	4	78	6	-79	-86	3
279	75	6	-84	-90	3	69	5	-13	-18	1	81	7	-115	-121	4	78	6	-77	-83	3
280	74	6	-80	-86	3	68	5	-12	-18	1	80	7	-111	-117	4	77	6	-74	-80	3
281	74	6	-77	-83	3	68	5	-12	-17	1	80	6	-107	-114	4	77	6	-71	-78	3
282	74	6	-74	-80	3	68	5	-11	-17	1	79	6	-104	-110	3	77	6	-69	-75	3
283	73	6	-71	-77	3	68	5	-11	-16	1	79	6	-100	-107	3	77	6	-66	-73	2
284	73	6	-68	-74	3	68	5	-10	-16	1	78	6	-97	-103	3	76	6	-64	-70	2
285	73	6	-66	-71	3	68	5	-10	-15	1	78	6	-94	-100	3	76	6	-62	-68	2
286	72	6	-63	-69	3	68	5	-9	-15	0	78	6	-91	-97	3	76	6	-59	-65	2
287	72	6	-60	-66	3	68	5	-9	-14	0	77	6	-87	-94	3	75	6	-57	-63	2

288	72	6	-58	-63	3	68	5	-8	-14	0	77	6	-84	-90	3	75	6	-55	-61	2
289	72	6	-55	-61	3	68	5	-8	-13	0	76	6	-81	-87	3	75	6	-53	-59	2
290	71	6	-52	-58	2	68	5	-7	-13	0	76	6	-78	-84	3	75	6	-50	-57	2
291	71	6	-50	-56	2	68	5	-7	-12	0	76	6	-76	-82	3	75	6	-48	-55	2
292	71	6	-48	-53	2	68	5	-6	-12	0	75	6	-73	-79	3	74	6	-46	-53	2
293	71	6	-45	-51	2	68	5	-6	-12	0	75	6	-70	-76	3	74	6	-45	-51	2
294	71	6	-43	-49	2	68	5	-6	-11	0	75	6	-67	-73	3	74	6	-43	-49	2
295	70	6	-41	-47	2	68	5	-5	-11	0	75	6	-65	-71	3	74	6	-41	-47	2
296	70	6	-39	-44	2	68	5	-5	-10	0	74	6	-62	-68	3	74	6	-39	-45	2
297	70	6	-37	-42	2	68	5	-4	-10	0	74	6	-60	-65	2	73	6	-37	-44	2
298	70	6	-35	-40	2	68	5	-4	-9	0	74	6	-57	-63	2	73	6	-36	-42	2
299	70	6	-33	-38	2	68	6	-3	-9	0	74	6	-55	-61	2	73	6	-34	-40	2
300	70	6	-31	-37	2	68	6	-3	-8	0	73	6	-52	-58	2	73	6	-33	-39	1
301	70	6	-29	-35	2	67	6	-2	-8	0	73	6	-50	-56	2	73	6	-31	-37	1
302	69	6	-27	-33	2	67	6	-2	-7	0	73	6	-48	-54	2	73	6	-30	-36	1

303	69	6	-26	-31	2	67	6	-1	-7	0	73	6	-46	-52	2	73	6	-28	-35	1
304	69	6	-24	-30	2	67	6	-1	-6	0	73	6	-44	-50	2	73	6	-27	-33	1
305	69	6	-23	-28	2	67	6	-1	-6	0	72	6	-42	-47	2	73	6	-26	-32	1
306	69	6	-21	-27	1	67	6	0	-6	0	72	6	-40	-46	2	72	6	-25	-31	1
307	69	6	-20	-25	1	67	6	0	-5	0	72	6	-38	-44	2	72	6	-24	-30	1
308	69	6	-18	-24	1	67	6	1	-5	0	72	6	-36	-42	2	72	6	-23	-29	1
309	69	6	-17	-23	1	67	6	1	-4	0	72	6	-34	-40	2	72	6	-22	-28	1
310	69	6	-16	-21	1	67	6	2	-4	0	72	6	-32	-38	2	72	6	-21	-27	1
311	69	6	-15	-20	1	67	6	2	-4	0	71	6	-31	-37	2	72	6	-20	-26	1
312	69	6	-14	-19	1	67	6	2	-3	0	71	6	-29	-35	2	72	6	-19	-25	1
313	69	6	-13	-18	1	67	6	3	-3	0	71	6	-28	-33	2	72	6	-18	-25	1
314	69	6	-12	-17	1	67	6	3	-2	0	71	6	-26	-32	1	72	6	-18	-24	1
315	69	6	-11	-17	1	67	6	4	-2	0	71	6	-25	-30	1	72	6	-17	-23	1
316	69	6	-10	-16	1	67	6	4	-2	0	71	6	-23	-29	1	72	6	-17	-23	0
317	69	6	-9	-15	1	67	6	4	-1	0	71	6	-22	-28	1	72	6	-16	-22	0

318	69	6	-9	-14	1	67	6	5	-1	0	71	6	-21	-26	1	72	6	-16	-22	0
319	69	6	-8	-14	1	67	6	5	0	0	71	6	-19	-25	1	72	6	-16	-22	0
320	68	6	-8	-13	0	67	6	6	0	0	71	6	-18	-24	1	71	6	-15	-22	0
321	68	6	-7	-13	0	67	6	6	0	0	71	6	-17	-23	1	71	6	-15	-22	0
322	68	6	-7	-13	0	67	6	6	1	0	71	6	-16	-22	1	71	6	-15	-22	0
323	68	6	-7	-13	0	67	6	7	1	0	70	6	-15	-21	1	71	6	-15	-22	0
324	68	6	-7	-13	0	67	6	7	1	0	70	6	-14	-20	1	71	6	-15	-22	0
325	68	6	-7	-13	0	67	6	7	2	0	70	6	-14	-19	1	71	6	-16	-22	0
326	68	6	-7	-13	0	67	6	8	2	0	70	6	-13	-19	1	71	6	-16	-22	0
327	68	6	-7	-13	0	68	6	8	2	0	70	6	-12	-18	1	71	6	-16	-23	0
328	68	6	-7	-13	0	68	6	8	3	0	70	6	-12	-18	1	71	6	-17	-23	0

Table A.6. The thermodynamic parameters: ΔG (mJ), ΔH (mJ) and $T\Delta S$ (mJ) for hydrated elastin fiber (0.24 g dry mass) in ^1H_2O, ^2H_2O and Na_2SO_4 at 298 K versus strain.

strain%	^1H_2O			^2H_2O			0.1 mol/kg Na_2SO_4			0.3 mol/kg Na_2SO_4		
	ΔG	ΔH	$T\Delta S$	ΔG	ΔH	$T\Delta S$	ΔG	ΔH	$T\Delta S$	ΔG	ΔH	$T\Delta S$
1	0.01	-3	-3	0.01	-2	-2	0.01	-2	-2	0.01	-1	-1
2	0.06	-6	-6	0.05	-4	-4	0.05	-4	-4	0.05	-3	-3
3	0.12	-9	-9	0.12	-6	-6	0.12	-6	-7	0.12	-4	-4
4	0.22	-12	-12	0.21	-8	-9	0.21	-9	-9	0.20	-5	-5
5	0.35	-15	-15	0.33	-11	-11	0.33	-11	-11	0.32	-7	-7
6	0.50	-18	-18	0.48	-13	-13	0.47	-13	-13	0.46	-8	-8
7	0.68	-21	-22	0.65	-15	-16	0.65	-15	-16	0.63	-9	-10
8	0.89	-24	-25	0.86	-17	-18	0.84	-17	-18	0.82	-11	-11
9	1.12	-27	-28	1.08	-19	-20	1.07	-20	-21	1.04	-12	-13
10	1.38	-30	-31	1.34	-21	-23	1.32	-22	-23	1.28	-13	-15
11	1.67	-33	-35	1.62	-24	-25	1.59	-24	-26	1.55	-15	-16
12	1.99	-36	-38	1.92	-26	-28	1.90	-26	-28	1.84	-16	-18

13	2.34	-39	-41	2.26	-28	-30	2.23	-28	-31	2.16	-18	-20
14	2.71	-42	-45	2.62	-30	-33	2.58	-31	-33	2.51	-19	-21
15	3.11	-45	-48	3.01	-33	-36	2.96	-33	-36	2.88	-20	-23
16	3.54	-48	-52	3.42	-35	-38	3.37	-35	-39	3.27	-22	-25
17	4.00	-52	-56	3.86	-37	-41	3.81	-37	-41	3.70	-23	-27
18	4.48	-55	-59	4.33	-39	-44	4.27	-40	-44	4.14	-25	-29
19	4.99	-58	-63	4.82	-41	-46	4.76	-42	-47	4.62	-26	-31
20	5.53	-61	-67	5.34	-44	-49	5.27	-44	-50	5.12	-27	-33
21	6.10	-64	-70	5.89	-46	-52	5.81	-47	-52	5.64	-29	-35
22	6.69	-67	-74	6.47	-48	-55	6.38	-49	-55	6.19	-30	-37
23	7.32	-71	-78	7.07	-51	-58	6.97	-51	-58	6.77	-32	-39
24	7.97	-74	-82	7.70	-53	-61	7.59	-53	-61	7.37	-33	-41
25	8.64	-77	-86	8.35	-55	-64	8.23	-56	-64	7.99	-35	-43
26	9.35	-80	-90	9.03	-57	-67	8.91	-58	-67	8.65	-36	-45
27	10.08	-83	-93	9.74	-60	-70	9.60	-60	-70	9.33	-38	-47

28	10.84	-87	-97	10.48	-62	-73	10.33	-63	-73	10.03	-39	-49
29	11.63	-90	-102	11.24	-64	-76	11.08	-65	-76	10.76	-41	-52
30	12.45	-93	-106	12.03	-67	-79	11.86	-68	-79	11.51	-42	-54
31	13.29	-96	-110	12.84	-69	-82	12.66	-70	-83	12.29	-44	-56
32	14.16	-100	-114	13.68	-71	-85	13.49	-72	-86	13.10	-45	-58
33	15.06	-103	-118	14.55	-74	-88	14.35	-75	-89	13.93	-47	-61
34	15.99	-106	-122	15.45	-76	-92	15.23	-77	-92	14.79	-48	-63
35	16.94	-110	-127	16.37	-79	-95	16.14	-80	-96	15.67	-50	-66
36	17.92	-113	-131	17.32	-81	-98	17.07	-82	-99	16.58	-52	-68
37	18.93	-116	-135	18.29	-83	-102	18.04	-84	-102	17.51	-53	-71
38	19.97	-120	-140	19.30	-86	-105	19.02	-87	-106	18.47	-55	-73
39	21.04	-123	-144	20.32	-88	-109	20.04	-89	-109	19.46	-56	-76
40	22.13	-126	-149	21.38	-91	-112	21.08	-92	-113	20.47	-58	-78
41	23.25	-130	-153	22.46	-93	-116	22.15	-94	-116	21.50	-59	-81
42	24.40	-133	-158	23.57	-95	-119	23.24	-97	-120	22.56	-61	-84

43	25.57	-137	-162	24.71	-98	-123	24.36	-99	-123	23.65	-63	-86
44	26.78	-140	-167	25.87	-100	-126	25.51	-102	-127	24.76	-64	-89
45	28.01	-143	-171	27.06	-103	-130	26.68	-104	-131	25.90	-66	-92
46	29.26	-147	-176	28.27	-105	-134	27.88	-107	-134	27.07	-67	-95
47	30.55	-150	-181	29.52	-108	-137	29.10	-109	-138	28.26	-69	-97
48	31.86	-154	-186	30.79	-110	-141	30.35	-112	-142	29.47	-71	-100
49	33.21	-157	-190	32.08	-113	-145	31.63	-114	-146	30.71	-72	-103
50	34.58	-161	-195	33.41	-115	-149	32.94	-117	-150	31.98	-74	-106

Table A.7. The thermodynamic parameters: ΔG (mJ), ΔH (mJ) and $T\Delta S$ (mJ) for hydrated elastin fiber (0.24 g dry mass) in 20 kDa PEG and NaClO$_4$ at 298 K versus strain.

strain%	15% PEG			30% PEG			0.3 mol/kg NaClO$_4$			1.0 mol/kg NaClO$_4$		
	ΔG	ΔH	$T\Delta S$	ΔG	ΔH	$T\Delta S$	ΔG	ΔH	$T\Delta S$	ΔG	ΔH	$T\Delta S$
1	0.01	-2	-2	0.01	0	0	0.01	-3	-3	0.02	-2	-2
2	0.06	-3	-3	0.05	-1	-1	0.06	-6	-6	0.06	-4	-4
3	0.13	-5	-5	0.12	-1	-1	0.13	-9	-9	0.14	-5	-5
4	0.23	-7	-7	0.22	-1	-1	0.23	-11	-12	0.24	-7	-7
5	0.35	-9	-9	0.34	-1	-2	0.37	-14	-15	0.38	-9	-9
6	0.51	-10	-11	0.49	-2	-2	0.53	-17	-18	0.55	-11	-11
7	0.69	-12	-13	0.67	-2	-3	0.72	-20	-21	0.74	-12	-13
8	0.90	-14	-15	0.88	-2	-3	0.93	-23	-24	0.97	-14	-15
9	1.14	-15	-17	1.11	-2	-4	1.18	-26	-27	1.23	-16	-17
10	1.41	-17	-19	1.37	-3	-4	1.46	-29	-30	1.51	-18	-19
11	1.71	-19	-21	1.66	-3	-4	1.77	-31	-33	1.83	-20	-21
12	2.03	-21	-23	1.98	-3	-5	2.10	-34	-36	2.18	-21	-24

13	2.38	-22	-25	2.32	-3	-5	2.47	-37	-40	2.56	-23	-26
14	2.76	-24	-27	2.69	-3	-6	2.86	-40	-43	2.97	-25	-28
15	3.17	-26	-29	3.09	-3	-6	3.29	-43	-46	3.41	-27	-30
16	3.61	-28	-31	3.52	-3	-7	3.74	-46	-49	3.88	-29	-32
17	4.07	-29	-34	3.97	-4	-7	4.22	-49	-53	4.38	-30	-35
18	4.57	-31	-36	4.45	-4	-8	4.73	-51	-56	4.91	-32	-37
19	5.09	-33	-38	4.96	-4	-9	5.27	-54	-60	5.47	-34	-39
20	5.64	-35	-40	5.50	-4	-9	5.84	-57	-63	6.06	-36	-42
21	6.22	-37	-43	6.06	-4	-10	6.44	-60	-66	6.68	-38	-44
22	6.82	-38	-45	6.65	-4	-10	7.07	-63	-70	7.33	-39	-47
23	7.46	-40	-48	7.27	-4	-11	7.73	-66	-73	8.01	-41	-49
24	8.12	-42	-50	7.92	-4	-12	8.41	-69	-77	8.72	-43	-52
25	8.81	-44	-52	8.59	-4	-12	9.13	-71	-81	9.46	-45	-54
26	9.53	-45	-55	9.29	-4	-13	9.87	-74	-84	10.23	-47	-57
27	10.28	-47	-57	10.02	-4	-14	10.65	-77	-88	11.04	-49	-60

28	11.05	-49	-60	10.78	-3	-14	11.45	-80	-91	11.87	-50	-62
29	11.85	-51	-63	11.56	-3	-15	12.28	-83	-95	12.73	-52	-65
30	12.69	-53	-65	12.37	-3	-16	13.15	-86	-99	13.63	-54	-68
31	13.55	-54	-68	13.21	-3	-16	14.04	-88	-103	14.55	-56	-70
32	14.43	-56	-71	14.08	-3	-17	14.96	-91	-106	15.50	-58	-73
33	15.35	-58	-73	14.97	-3	-18	15.91	-94	-110	16.49	-59	-76
34	16.29	-60	-76	15.89	-3	-19	16.89	-97	-114	17.50	-61	-79
35	17.27	-62	-79	16.84	-2	-19	17.89	-100	-118	18.55	-63	-82
36	18.27	-63	-82	17.82	-2	-20	18.93	-103	-122	19.62	-65	-85
37	19.30	-65	-85	18.82	-2	-21	20.00	-106	-126	20.73	-67	-88
38	20.35	-67	-87	19.85	-2	-22	21.09	-108	-129	21.86	-69	-91
39	21.44	-69	-90	20.91	-2	-22	22.22	-111	-133	23.03	-71	-94
40	22.55	-71	-93	22.00	-1	-23	23.37	-114	-137	24.22	-72	-97
41	23.70	-73	-96	23.11	-1	-24	24.56	-117	-141	25.45	-74	-100
42	24.87	-74	-99	24.25	-1	-25	25.77	-120	-145	26.71	-76	-103

43	26.06	-76	-102	25.42	0	-26	27.01	-123	-150	27.99	-78	-106
44	27.29	-78	-105	26.61	0	-27	28.28	-125	-154	29.31	-80	-109
45	28.54	-80	-109	27.84	0	-28	29.58	-128	-158	30.66	-82	-112
46	29.83	-82	-112	29.09	1	-28	30.91	-131	-162	32.04	-83	-116
47	31.14	-84	-115	30.37	1	-29	32.27	-134	-166	33.44	-85	-119
48	32.48	-86	-118	31.67	1	-30	33.66	-137	-170	34.88	-87	-122
49	33.84	-87	-121	33.01	2	-31	35.07	-140	-175	36.35	-89	-125
50	35.24	-89	-124	34.37	2	-32	36.52	-142	-179	37.85	-91	-129

Table A.8. The change in heat capacity (ΔC_p in mJ/K) for the hydrated elastin fiber (0.24 g dry mass) in ^1H_2O, ^2H_2O, Na_2SO_4, 20 kDa PEG and $NaClO_4$ at 298 K versus strain.

strain	$^1H_2$	$^2H_2$	0.1 mol/kg	0.3 mol/kg	15%	30%	0.3 mol/kg	1.0 mol/kg
%	O	O	Na_2SO_4	Na_2SO_4	PEG	PEG	$NaClO_4$	$NaClO_4$
1%	0.17	0.18	0.16	0.09	0.10	0.02	0.12	0.08
5%	0.83	0.92	0.80	0.47	0.50	0.12	0.61	0.41
10%	1.66	1.83	1.60	0.92	0.99	0.23	1.21	0.82
15%	2.48	2.73	2.38	1.38	1.48	0.35	1.81	1.21
20%	3.29	3.63	3.17	1.82	1.97	0.46	2.41	1.61
25%	4.10	4.52	3.94	2.26	2.44	0.57	3.00	2.00
30%	4.90	5.40	4.71	2.70	2.91	0.68	3.58	2.38
35%	5.69	6.28	5.47	3.12	3.38	0.79	4.16	2.76
40%	6.47	7.15	6.23	3.55	3.84	0.90	4.74	3.13
45%	7.25	8.02	6.98	3.96	4.30	1.01	5.31	3.49
50%	8.02	8.87	7.72	4.37	4.75	1.12	5.87	3.85

The energetics of stretch: ΔG_T, ΔH_T, $T\Delta S_T$ and ΔC_p were determined as a function of temperature at constant strain 20%, (Figure A.3 and Figure A.4).
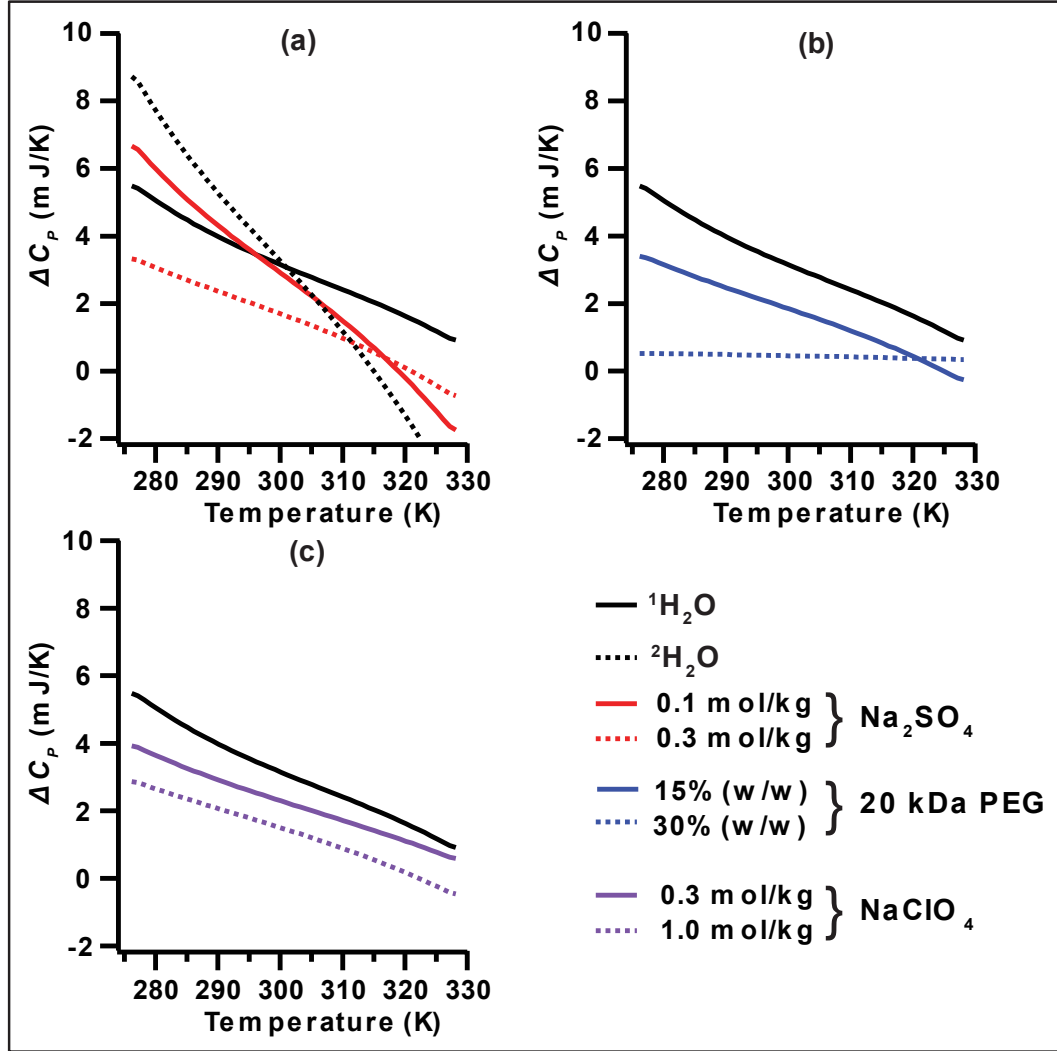

Figure A.3. The heat capacity change of stretching hydrated elastin (0.24 g dry mass) by 20% as a function of temperature in in all studied solutions in comparison to ^1H_2O.

ΔC_p, like in water, decreases linearly in all investigated solutions. Solutions that increase the compaction of elastin fiber; ^2H_2O, sulfate and high concentration perchlorate, decrease the change in ΔC_p until reaches about zero in the high concentration PEG solution Because of the decrease hydrophobic hydration that accompany these solutions.
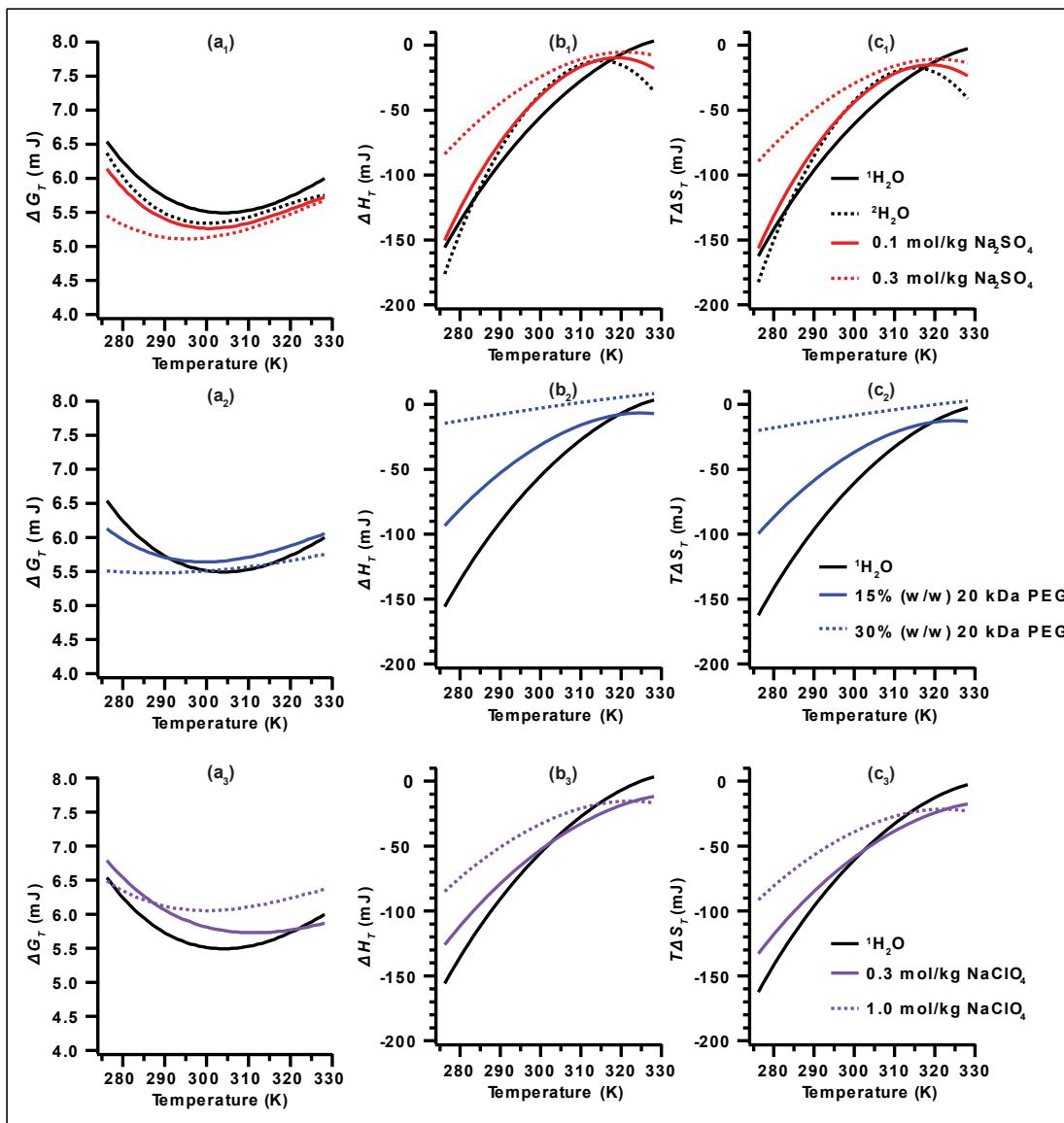
150

Figure A.4. Energetics of stretching hydrated elastin (0.24 g dry mass) by 20% (ΔG_T, ΔH_T and $T\Delta S_T$) as a function of temperature in all studied solutions in comparison to ^1H_2O.

ΔG_T is small (5.3 – 6.8) mJ and decreases slightly with the increase in temperature in all solutions. Both the entropic ($T\Delta S_T$) component and the enthalpic (ΔH_T) component are negative. However, the magnitude of $T\Delta S_T$ is always greater than ΔH_T. In resemblance to the coacervation process discussed before in the ^1H_2O results, both ΔH_T and $T\Delta S_T$ increase with the increase in temperature, i.e., become less negative. The magnitude of both

ΔH_T and $T\Delta S_T$ decreases as the fiber become more compact in ^2H_2O, sulfate and high concentration perchlorate hydrating solutions.

The volume as a function of both force, (Figure A.5), and temperature, (Figure A.6), were measured when the elastin fiber was hydrated in the studied solutions in the same mannar as in deionized water ^1H_2O. The fiber shape is rectangular prism to a good estimation and so its volume = length $\times$ width $\times$ thickness. The fiber length and width were measured directly from the photos, whereas the thickness was calculated assuming the change in thickness is proportional to that in width using the dry dimensions as reference.
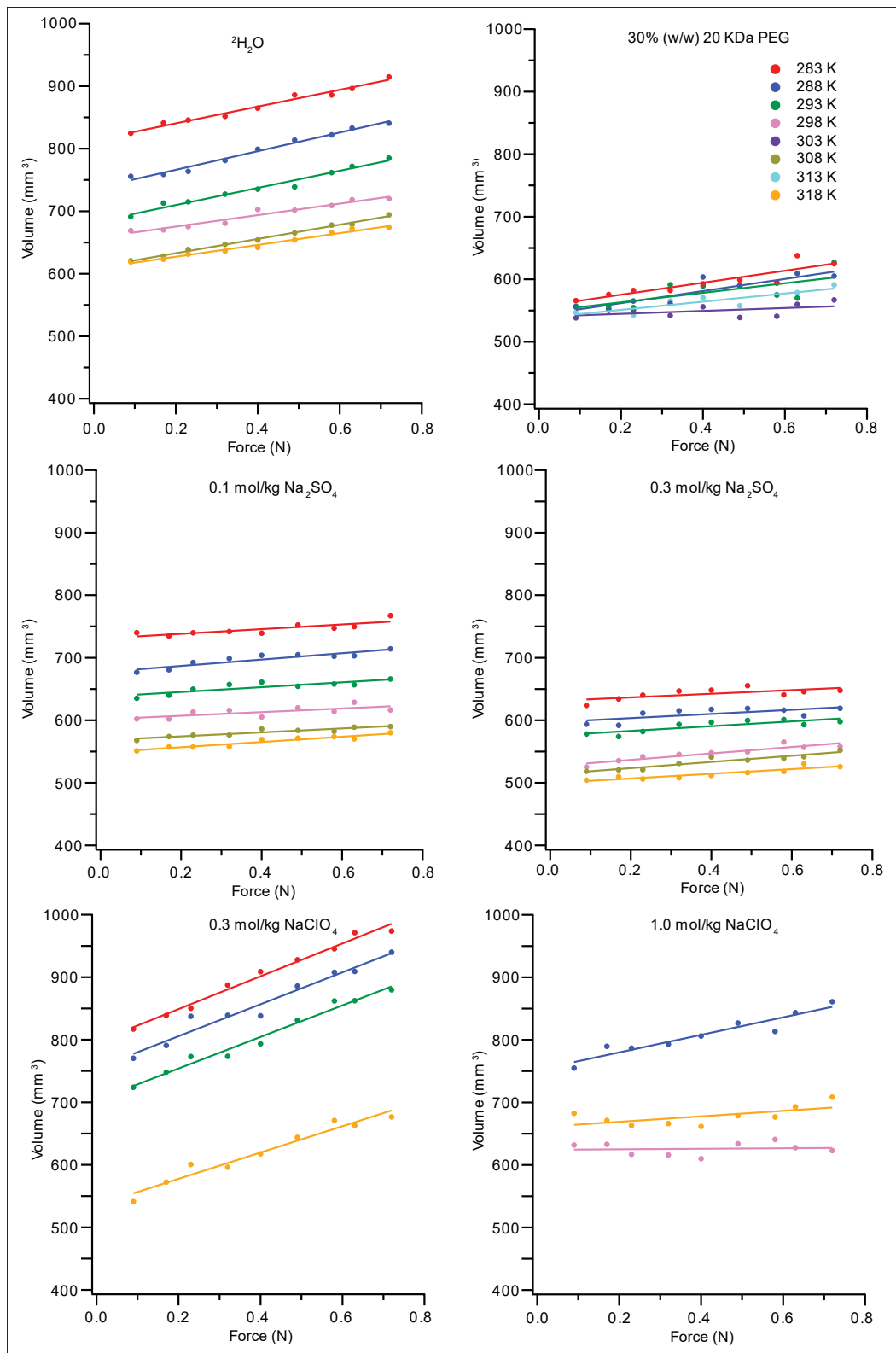
Figure A.5. The volume of the hydrated elastin fiber as a function of force at different temperatures in the studied solutions.
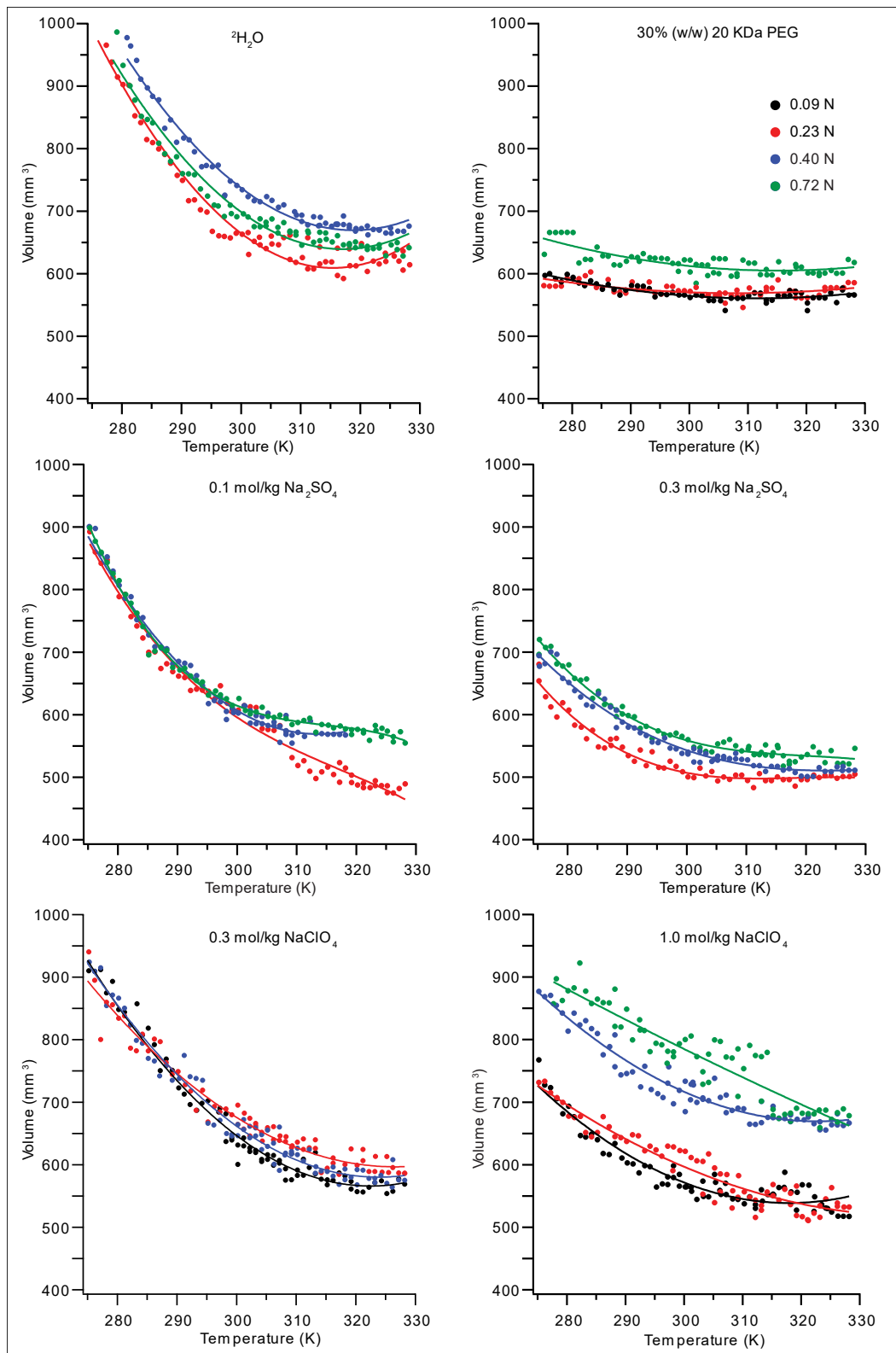
Figure A.6. The volume of the hydrated elastin fiber as a function of temperature at different forces in the examined solutions.

CURRICULUM VITAE

Nour M. Jamhawi

Department of Chemistry | University of Louisville

2320 South Brook St | Louisville, KY, 40292

n.jamhawi@louisville.edu

EDUCATION

Ph.D., Chemistry/ Physical biochemistry   Expected April 2021

University of Louisville (UofL), Louisville, Ky, USA.

Dissertation: Investigations of Elastin Recoil on molecular and Macroscopic levels

M.Sc., Chemistry/ Physical biochemistry   August 2018

University of Louisville, Louisville (UofL), Ky, USA.

M.Sc., Medicinal Chemistry and Pharmacognosy   March 2010

Jordan University of Science and Technology (JUST), Irbid, Jordan.

Thesis: Synthesis and Study of the Hydrolysis kinetics of Monobasic and Dibasic Aminoalkylesters of Ketorolac.

B.Sc., Pharmacy   February 2004

Jordan University of Science and Technology (JUST), Irbid, Jordan.

WORK EXPERIENCE

Head of Inpatient Pharmacy,   August 2011 – June 2014

King Abdulla University Hospital (KAUH), Irbid, Jordan

Inpatient Pharmacist,   June 2005 – August 2011

King Abdulla University Hospital (KAUH), Irbid, Jordan

RESEARCH SKILLS

Physical Biochemistry laboratory   August 2014– Now

Advisor: Dr. Richard J. Wittebort   UofL, Louisville, Ky, USA

- Running solid state NMR experiments to study the weakly ordered water in elastin using double quantum pulse sequence.
- Running thermomechanical experiments in a homebuilt apparatus analogous in principle to the dynamic mechanical analyzer (DMA) to calculate the free energy and entropy of elastin recoil.
- Data analysis using different software including, NMRpipe, Igor, ImajeJ, MATLAB and others based on need.

Medicinal Chemistry laboratory   August 2006 – March 2010

Advisor: Dr. Amjad M. Qandil   JUST, Irbid, Jordan

- Synthesis of different esters of the non-steroidal drug Ketorolac, purification and characterization of the products using IR and NMR.
- Studying the stability of the products in different conditions using HPLC techniques.
- Data analysis using different software including Kaleidagraph.

PUBLICATIONS

- Amjad M. Qandil, Nour M. Jamhawi, Bassam M. Tashtoush, Ahmad M. Al-Ajlouni, Nasir M Idkaidek & Aiman A. Obaidat (2013) The hydrolysis kinetics of monobasic and dibasic aminoalkyl esters of ketorolac, Drug Development and Industrial Pharmacy, 39:9, 1346-1356, DOI: 10.3109/03639045.2012.712535

- Carvajal, M. F. C. A.; Preston, J. M.; Jamhawi, N. M.; Sabo, T. M.; Bhattacharya, S.; Aramini, J. M.; Wittebort, R. J.; Koder, R. L., (2021) Dynamics in Natural and Designed Elastins and Their Relation to Elastic Fiber Structure and Recoil. bioRxiv 2021, DOI: 10.1101/2020.07.14.202523

- Jamhawi, N. M. and Wittebort, R. J, "Investigations of the surface ^2H_2O on elastin fibers using 2Q NMR" (Manuscript in preparation)

- Jamhawi, N. M. and Wittebort, R. J, "Thermomechanical study of elastin recoil" (Manuscript in preparation)

CONFERENCE PARTICIPATION

- <u>Nour Jamhawi</u>, Tatiana Krivokhizhina and Richard Wittebort, Hydrophobic Effect a Key player in the Elasticity Mechanism of Elastin. Poster presentation at the 2nd Annual NMR Gateway meeting, Ohio state university, coulombs, OH, 4th November 2017.

- <u>Nour Jamhawi</u> and Richard Wittebort, Elastin's Mechanism of Elasticity. Poster presentation at the 10th European Elastin Meeting, Radboud UMC, Nijmegen, Netherlands, 14-16th June 2018.

- <u>Nour Jamhawi</u> and Richard Wittebort, MQ NMR & Thermomechanics, Elastin's Elasticity. Poster presentation at the 32nd Gibbs Society of Biological Thermodynamics, Touch of Nature Conference Center, Cardonale, IL, 6-9th October 2018.

TEACHING EXPERIENCE

Teacher Assistant,   August 2014 – present.

University of Louisville (UofL), Louisville, Ky, USA.

- Chemistry 201 (General Chemistry)
- Chemistry 202 (General Chemistry)
- Chemistry 105 (Chemistry for Health Professionals)
- Assisted in mentoring for undergraduate projects (2 undergraduate students)

PROFESSIONAL MEMBERSHIP

Biophysical Society   2018 – Now